ERROR PERFORMANCE OF DPSK SIGNALS IN FREQUENCY-SELECTIVE RAYLEIGH FADING CHANNELS

by

Weiwan Liu

B.E.E. Shanghai Jiao Tong University, Shanghai, China, 1989

A THESIS SUBMITTED IN PARTIAL FULFILLMENT
OF THE REQUIREMENTS FOR THE DEGREE OF
MASTER OF APPLIED SCIENCE

in the School
of
Engineering Science

SIMON FRASER UNIVERSITY
October 1993

APPROVAL

Name:	Weiwan Liu
Degree:	Master of Applied Science
Title of thesis:	**Error Performance of DPSK Signals in Frequency-selective Rayleigh Fading Channels**

Examining Committee: Dr. Jacques Vaisey, Chairman

Dr. Paul Ho, Senior Supervisor

Dr. John Bird, Supervisor

Dr. James Cavers, Examiner

Date Approved: October 7, 1993

PARTIAL COPYRIGHT LICENSE

I hereby grant to Simon Fraser University the right to lend my thesis, project or extended essay (the title of which is shown below) to users of the Simon Fraser University Library, and to make partial or single copies only for such users or in response to a request from the library of any other university, or other educational institution, on its own behalf or for one of its users. I further agree that permission for multiple copying of this work for scholarly purposes may be granted by me or the Dean of Graduate Studies. It is understood that copying or publication of this work for financial gain shall not be allowed without my written permission.

Title of Thesis/Project/Extended Essay

"Error Performance of DPSK Signals in Frequency-Selective Rayleigh Fading Channels"

Author:

_____
(signature)

Weiwan LIU
(name)

October 12, 1993
(date)

ABSTRACT

The emerging digital cellular system in North America is a narrow band TDMA system with $\frac{\pi}{4}$-QPSK as modulation scheme. The digital cellular channel exhibits frequency-selective Rayleigh fading phenomena. This thesis studies the error performance of conventional differential detection and multisymbol differential detection of QPSK signals in a 2-ray frequency selective Rayleigh fading channel with additive white Gaussian noise. We investigate the performance of the conventional differential detector (CDD) but find that it breaks down under some channel conditions. Then we suggest using multisymbol differential detector (MSDD) and discover that its bit error rate (BER) can be controlled below 10^{-2} under almost all the channel conditions as long as proper transmitted pulses are adopted. It is found that channel coding helps to improve the error performance when the BER of the corresponding uncoded systems is at least below 10^{-1}. We also provide proofs to the validity of the piece-wise-constant assumption in differential detection using analytical derivation and numerical results under practical channel conditions.

To my wife, my parents and my sister for their support during the past two years

ACKNOWLEDGMENT

I would like to express my gratitude to Dr. Paul Ho for suggesting the subject of the thesis and supervising me helpfully and patiently throughout the course of the research. I would like to thank Dr. Jim Cavers for helpful discussion and advice. Also thank Dr. Jiantian Wu and Mr. Fenghua Liu for their kindly help. Financial support from the Natural Science and Engineering Research Council is gratefully acknowledged.

Contents

List of Figures

ABBREVIATIONS

AWGN	Additive white Gaussian noise
BPSK	Binary phase shift keying
CCITT	International Telephone and Telephone Consultative Committee
CDD	Conventional Differential Detector
CSI	Channel state information
dB	Decibel
DF	Decision Feedback
DPSK	Differential phase shift keying
FEC	Forward error correction
FIR	Finite Impulse Response
Hz	Hertz
IEEE	Institute of Electrical and Electronic Engineers
i.i.d.	independent and identically distributed
ISI	Intersymbol Interference
kHz	kiloHertz
MHz	Mega Hertz
MPSK	M-ary phase shift keying

MSDD	Multisymbol Differential Detector
PSK	Phase shift keying
rms	Root mean square
RPpoles	Poles on the right-half of the complex s-plane
SNR	Singal to noise ratio
TDMA	Time-Division Multiplexing Access
TCM	Trellis coded modulation

VARIABLES AND FUNCTIONS

A	Pulse amplitude
c	Speed of light
C	Vector containing data QPSK symbols in the N received samples
C'	Vector containing desired data QPSK symbols in the five received samples
c_k	k^{th} data PSK symbol
$c(\bullet,\bullet)$	Equivalent impulse response of channel
c.i.	95 % confidence interval
D	Difference between two decoding metrics
d_K	Difference between the transmitted PSK symbol c_k and the estimated PSK symbol $\hat{c_K}$
$E[\bullet]$	Statistical average
$\frac{E_b}{N_o}$	Received bit signal to noise ratio
$\frac{E_s}{N_o}$	Received symbol signal to noise ratio
f	Frequency
f_c	Carrier frequency
f_D	Maximum Doppler frequency
f_DT	Normalized maximum Doppler frequency or fade rate

g(t), h(t)	Flat fading process
$G(\tau_1)$	Power-delay profile
$J_o(\bullet)$	Zero-order Bessel function
L	The length of **Y**
$\mathbf{L_1}$	The number of data QPSK symbols before c_k in **C**
M(C)	Decoding metric related to vector **C**
M_1	The number of previous symbols before x_k contained in the received sample y_k
M_2	The number of future symbols after x_k contained in the received sample y_k
N	Number of received samples used in MSDD
N_1	Number of received samples in front of y_k in **Y**
$n_w(t)$	Channel additive white Gaussian noise
p(t)	Impulse response of a transmitter pulse shaping filter
P(f)	Fourier transform of p(t)
$P(c_k \rightarrow \hat{c_k})$	Pairwise error probability
P_b	Bit error rate
q(t)	Impulse response of the combination of the transmitter and receiver pulse shaping filter
Q(f)	Fourier transform of q(t)
r(t)	Received signal
t	Time
$\frac{1}{T}$	Transmitted symbol rate
U_k	Vector containing the fading gains in the k^{th} received sample
u_{nk}	Fading gain on the n^{th} transmitted PSK symbol at $t = kT$

v	Vehicle speed
$\mathbf{X}$	Vector containing transmitted QPSK symbols in the N received samples
x(t)	Baseband equivalent transmitted signal
x_k	k^{th} transmitted QPSK symbol
y(t)	Output of the matched filter
$\mathbf{Y}$	N-received-sample vector
y_k	k^{th} received sample
$z_{m,n}$	Product of data PSK symbols from c_m to c_n
α	Power split ratio in the two-ray channel model
β	Roll-off parameter of a raised-cosine pulse
$\phi_g(\bullet)$, $\phi_h(\bullet)$	Autocorrelation functions of flat fading process
$\phi_{mn}(i,j)$	Correlation between fading gains u_{im} and u_{jn}
$\mathbf{\Phi_{yy}(C)}$	Covariance matrix of $\mathbf{Y}$ related to $\mathbf{C}$
ρ	Normalized relative delay in the two-ray channel model
σ_g^2, σ_h^2	Variance of flat fading process
σ_k^2	Variance of k^{th} received sample y_k
σ_{k-1}^2	Variance of $(k-1)^{th}$ received sample y_{k-1}
$\sigma_{k,k-1}^2$	Covariance of k^{th} and $(k-1)^{th}$ received sample
Γ	Symbol signal to noise ratio

Chapter 1

Introduction

Mobile radio communication has a long history beginning with early maritime use for disaster and safety communications. However, progress in mobile radio communications for public use has lagged behind until the last twenty years. In recent years, the technique of high-density geographical co-channel, that is cellular, has enabled the reuse of channels thus helping achieve efficient spectrum utilization for accommodation of large demands, and the advanced very large scale integration (VLSI) technology has greatly assisted the development of mobile communications.

The usual digital cellular system works in the range of frequency from 400-900 MHz, depending on different countries in the world. In Europe, for instance in Germany, the fully cellular radiotelephone set up by Siemens company works in the 450 MHz range. In the USA, however, the allocation of 115 MHz of spectrum is in the range between 806-947 MHz among several land mobile radio services. Radio communication is carried out with a channel spacing of 30 kHz.

The digital cellular systems transmit signals over mobile channels. At the receiver, differential detection is widely used to detect the transmitted information. Compared with the additive white Gaussian noise (AWGN) channel, there are multiplicative random fading gains in the received signals after being transmitted over mobile channels. Therefore quality of communication is generally worse than that in the pure AWGN channel. Due to the limited bandwidth of each channel and the presences of multiple propagation paths, different frequency components of the transmitted signal are subject to different fading effects. Thus there exists intersymbol interference (ISI) in the received samples, which make the communication system suffer more. The subject of this thesis is the analyses and evaluation of the error performance of differential detection in communication systems and to improve it using different techniques in the frequency-selective Rayleigh fading channel.

In the following sections, we will go over some terminologies commonly used in mobile communications, then carry on the literature review, and finally give a brief description of contribution and organization.

1.1 Background and Literature Review

In a mobile radio channel, there are three main factors which have significant effects on the performance of a communication system: 1) **fading**, due to **multipath**; 2) **Doppler effect**, due to time variation of the channel; 3) **Selectivity**, due to

bandwidth of the channel. We will describe these phenomena briefly in the following subsection.

1.1.1 Some Common Terminologies in Mobile Communication

Before proceeding, let us explain some common terminologies.

To understand the concept of **multipath** in mobile communications, refer to Figure 1.1 (a). At the transmitter, we send an extremely short pulse. Then at the receiver we can receive a train of pulses due to many transmitting paths between the transmitter and the receiver. In most cases, as discussed in [1], the equivalent amplitude and phase fluctuations of the sum of received signals have the same statistical characters as those of narrow-band AWGN, and the corresponding envelope is Rayleigh-distributed, so the transmitting channel is called **Rayleigh fading channel**.

Owing to its time variation, its limited bandwidth and the multipath effect, the channel exhibits time- and frequency-selective behavior. The **time-selective** channel has so called **Doppler effects**. Due to the relative motion between the transmitter and the receiver, there are additional frequency components contributed to the power spectrum of the transmitted signals so that the spectrum is broaden. The doppler frequency shift depends on how fast the mobile vehicle goes. For example, the maximum Doppler frequency is approximately 6.7 Hz if a car travels at the speed of 10 km per

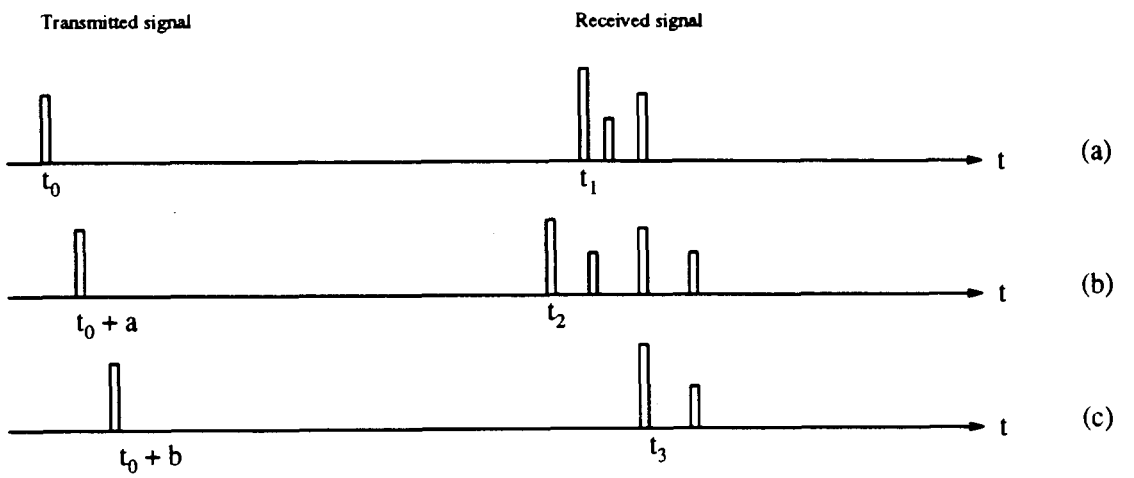

Figure 1.1: Examples of the responses of a time-variant multipath channel to a very narrow pulse.

hour while the maximum Doppler frequency is approximately 80 Hz at the speed of 100 km per hour. A formula is shown in Chapter 2 to calculate the maximum Doppler frequency. Consequently the fading gains of received signals at different instants are not fully correlated any more and we also refer to it as the **dynamic** channel. The phenomena is that if we repeat the experiment of sending an extremely short pulse, we would observe changes in the received pulse train, which include changes in the sizes of the individual pulses, in the relative delays among the pulses, and in the number of pulses observed in the received pulse train as shown in Figure 1.1 (a), (b) and (c).

To the contrary, the so called **time-flat** fading channel, or **static** fading channel may be represented as random but time-invariant when the doppler frequency shift is zero, or say the vehicle is at rest. The fading gains of the received signal are random but fully correlated, that is the gain of the first received signal is a random number and the gains of the successive signals are almost the same as the first one. This is a kind of classic fading channel and its behavior has been studied in details, see [1].

In frequency **non-selective** Rayleigh fading channels, or **flat** Rayleigh fading channels, the coherent bandwidth of the channel is larger than that of transmitted signals, thus the amplitude and phase fluctuations of the response to a sinusoid, observed at the receiver, are the *same* for any excitation frequency component. On the other hand, in the **frequency-selective** Rayleigh fading channel the different frequency components of the transmitted signals are subject to different fading effects. For example, when two sinusoids with frequency separation greater than the bandwidth of the channel are sent through the channel, they are affected differently. As we

know, the transmitted signal usually contains many sinusoid components of various frequencies, therefore it is severely distorted by the channel.

In this thesis, the emphasis will be on the **dynamic** and **frequency-selective** Rayleigh fading channel although the **flat** or **static** fading channel will be treated as a special case. In the following, we begin our literature review for **flat** fading channel.

1.1.2 Literature Review

In recent years, mobile communication has been a very popular subject in Communication Engineering. In order to use the bandwidth efficiently, people have designed a number of digital modulation schemes as well as detection methods for the mobile radio channel. For example, for phase-shift keying (PSK) modulation, the two common detection schemes are pilot symbol assisted modulation (PSAM) and differential detection (DD). As for PSAM, the system has to insert a known symbol periodically into the transmitted sequence so that the fading distortion, or channel state information (CSI), can be estimated at the receiver. Thus the effective transmitting bandwidth will be reduced and complexity of the system is high. However, PSAM provides better error performance due to better channel estimate, compared with DD. In the case of DD, the detector uses only successive received samples as reference to make decisions. Since it requires very little information about the channel, the DD is simpler to implement. The advantages of DD are summarized as follows:

- Easy and economical realization;

- No expansion of bandwidth for channel state estimation;
- Very little delay in detection.

Various schemes have also been designed to enhance the performance of DD, see [2], [3], [4], [5], and [6], such as Trellis Coding Modulation (TCM), in [2] and [3], Multi-symbol differential detection in [6], etc.. Unfortunately, these studies only concentrate on the additive white Gaussian noise (AWGN) channel and the **flat** fading channels.

As we mentioned earlier, digital cellular systems in North America are narrow band TDMA systems working in the ultra high frequency (UHF) band. Much work has already been done to characterize UHF mobile radio channels by researchers world wide. They demonstrate that the digital cellular channel exhibits the frequency-selective fading behavior. Zogg [13] provides multipath profiles measured between a base and mobile in many types of terrain. For example in hilly terrain, Zogg indicates that signal components typically arrive 10 to 25 us after the direct signal and have amplitudes 10 to 20 dB weaker than the direct signal. Building facades induce multipath signals which have excess delays of less than 10 us and amplitudes 10 dB below the direct signal. In mountainous regions, significant multipath have amplitudes within 10 dB of the direct signal at excess delays of 20 us or more. Summarizing the research and measurements in recent years, Telecommunications Industry Association (TIA) characterize the digital cellular channel as a frequency-selective Rayleigh fading channel. The North American digital cellular system document IS 54 indicates that a 2-ray channel model is a reasonably good model for the reality.

The study of the frequency-selective Rayleigh fading channel began as early as 1960s. P.A. Bello, B.C. Nelin, C.C. Bailey and M.B. Pursley studied in details the performance of communication systems transmitting binary signals over the frequency-selective Rayleigh fading channel, see [7] [8], [9], [10], and [11]. They considered the dependence of the error probability on the shapes of the data-pulse waveform used in the differential binary phase-shift keying (DBPSK) signals and on the different frequency spectrums in the channel models.

The analysis and results mentioned above in [7] - [11] for the frequency-selective Rayleigh fading channel are applicable for binary signaling only. In order to accomodate the projected ten-fold increase in users and the need for data as well as voice transmission, M-ary digital modulation and speech coding techniques are used to exploit digital communications efficiencies. According to current standards for cellular mobile radio system for North America [12], the digital modulation method chosen is a modified version of differential Quadrature Phase Shift Keying (PSK) scheme with differentially coherent detection, known as $\frac{\pi}{4}$-DQPSK.

This thesis focuses on studying the DD of QPSK signals in the frequency-selective Rayleigh fading represented by a 2-ray channel model. It shows the effects of different statistical channel parameters on the performance of conventional differential detection. It is found that the DD works well when the delay between the two rays is small as long as a suitable transmitted pulse is chosen. It also shows that the piece-wise-constant assumption of fading gain on the transmitted signal is valid and accurate for the DD.

As we will see, conventional differential detection does not work well all the time. As the delay spread becomes larger, ISI is the main factor which makes performance deteriorate rapidly. It is shown in the thesis that even channel coding does not help when the delay spread is large, say, more than half a symbol interval. Therefore various techniques are suggested to combat ISI. In [14], Noneaker and Pursley use diversity to improve the performance of DD in the doubly selective (time selective and frequency selective) rayleigh fading channel. It works well at low delay spread, say 0.1. In [15] Cavers suggests that PSAM works better than DD when the delay is small, at the expense of a small expansion of bandwidth for using pilot symbol.

Generally if ISI is mentioned, people consider **equalization**. Today, **"equalizer" is used to describe any device or signal processing algorithm that is designed to deal with intersymbol interference** [1]. Until now, no paper is found to apply equalization to solve ISI in the DD in a frequency-selective Rayleigh fading channel. There are many papers which implement equalization in coherent PSK detection [22]. Linear equalizers experience noise enhancement in channels with severe frequency-selective fading, and therefore cannot be used. Nonlinear equalizers utilize decisions to either cancel the interference or enhance the signal. In [22], Baum, Borth and Mueller consider Decision feedback equalizer (DFE) as well as maximum likelihood sequence estimator(MLSE). It is found that adaptive DFE with the rapidly adapting algorithm can track the fast fading channel but with some error propagation problems. MLSE equalizers works better than DFE but its complexity is higher.

We propose in this thesis the use of multi-symbol differential detection with decision feedback (DF) to improve the performance of differential detection in the frequency-selective Rayleigh fading channel. Compared with coherent PSK detection, DD is easier to implement since it does not need much information about the channel. It makes decisions mostly by using received samples and without expansion of bandwidth so it is cheaper to implement. Divsalar and Simon [18] used the maximum likelihood sequence estimation technique to analyze the performance of multiple-symbol differential detection for uncoded MPSK signals in the AWGN channel. They demonstrated that the amount of improvement over conventional DPSK depends on the number of phases and the number of additional symbol intervals added to the observation. The first investigation of multiple-symbol differential detection in the Rayleigh fading channel was shown in [19] where two or more differential detectors were jointly utilized to take advantage of the redundancy introduced by the differential encoder. Later on Ho and Fung show in [6] the true optimal multiple symbol differential detector for uncoded PSK modulation transmitted over flat and dynamic Rayleigh fading channels with AWGN. An exact expression for the pairwise error event probability of this detector is derived there. In addition, it is found that this decoding strategy is not very sensitive to the mismatch between fade rates of the channel fading process and the one used in decoding metrics.

In this thesis, sequence detection of differentially encoded PSK signals transmitted over a 2-ray frequency-selective Rayleigh fading channel is considered. The detector in our system is a multisymbol differential detector (MSDD) with decision feedback, processing N consecutive received samples and making a decision about the symbol in the middle ($N = 2$ for conventional differential detector). It was found that with

$N = 5$, if the statistical channel parameters are estimated correctly at the receiver, the performance of the decoder is superior to conventional differential detection, especially for the case of large delay between the two rays, say one symbol interval. We call this decoder as **matched decoder**. In nearly all cases that we examined, there are no noticeable irreducible error floors within the range of the investgated bit signal to noise ratio (SNR). The decoder can also provide satisfactory performance even when channels conditions are misinterpreted as long as a suitable transmitted pulse shape is chosen. We use the term **mismatched decoder** for the decoder using misinterpreted channel conditions. Of course, the smaller the mismatch is, the better the results are. The optimum 32-state convolution code combined with hard decision of the output from the MSDD gives us good results. Assuming certain channel conditions, BER goes down to 10^{-4} for most matched and mismatch cases at $SNR = 25dB$ even for fast fading channels. Since MSDD can combat ISI in the frequency-selective Rayleigh fading channel, it can be referred to as a kind of equalizer in the sense of the defination of equalizer on Page 554 in [1]

1.2 Contributions of The Thesis

The major contributions of this thesis are summarized as follows:

1. Examination of effects of channel parameters and transmitting pulses on the performance of the conventional differential detector (CDD) in a 2-ray frequency-selective Rayleigh fading channel.

2. Suggestion of the multisymbol differential detection as a possible way of combating ISI and improving the performance of differential detector in a 2-ray frequency-selective Rayleigh fading channel without expansion of bandwidth.

3. Relaxation of the piece-wise constant assumption of fading gains in Rayleigh fading channel, concluding that piece-wise-constant is a good assumption for differential detection in Rayleigh fading channel.

1.3 Thesis Outline

In Chapter 2, a general description of the system block diagram for the CDD and the MSDD is given; the assumptions made in this thesis are clearly stated; and application of the channel coding scheme is shown.

In Chapter 3, firstly we will analyze the performance of the CDD in a 2-ray frequency-selective Rayleigh fading channel. In the following sections we show the effects of various channel parameters and different transmitted pulses on its performance. The effect of optimal sampling time instants on its performance is also shown. In addition, we show the piece-wise-constant assumption usually used to model fading gain is a valid assumption to analyze the performance of differential detection.

In Chapter 4, the MSDD is proposed to improve the performance of differential detector. The performance of this decoder, under both matched and mismatched conditions, with rectangular and raised-cosine pulse, are presented.

In Chapter 5, convolutional coding schemes are applied in both the CDD and the MSDD. The comparison of the performance in the two cases is shown.

Finally, we draw conclusions of this study in Chapter 6.

Chapter 2

Introduction to Differential Detection of QPSK Signals in a Frequency-Selective Rayleigh Fading Channel

In this chapter, first we define the system notation and introduce the mobile communication system, then describe the structure of the conventional differential detector (CDD) and the multisymbol differential detector(MSDD), and finally the application of coding scheme in communication systems.

2.1 Assumptions and Notations

The following assumptions are made in the whole thesis unless otherwise specified. First, the channel is assumed to be a doubly (time and frequency) selective Rayleigh fading channel. Second, sampling the received signal at the integer timing is assumed in most part of this thesis, and the effect of sampling the received signal at optimal timing is discussed in Section 3.5 and Section 4.1.2.

This thesis uses $E[\bullet]$ to represent statistical average, $(\bullet)^*$ to represent complex conjugate, $(\bullet)^t$ to represent the transpose of a matrix or a vector, and $(\bullet)^\dagger$ to represent the Hermitian transpose of a matrix.

2.2 System and Channel Model

The System block diagram of the uncoded communication system used in the thesis is given in Figure 2.2 while the diagram of the coded one is treated in Section 2.4. Complex baseband notation is used throughout the thesis.

2.2.1 Transmitter

First, let's consider the structure of the transmitter, which is the upper part of Figure 2.2. A sequence of binary digits i_k from the source coder is fed into the transmitter. In the uncoded system, the data PSK symbol c_k is obtained after modulation and

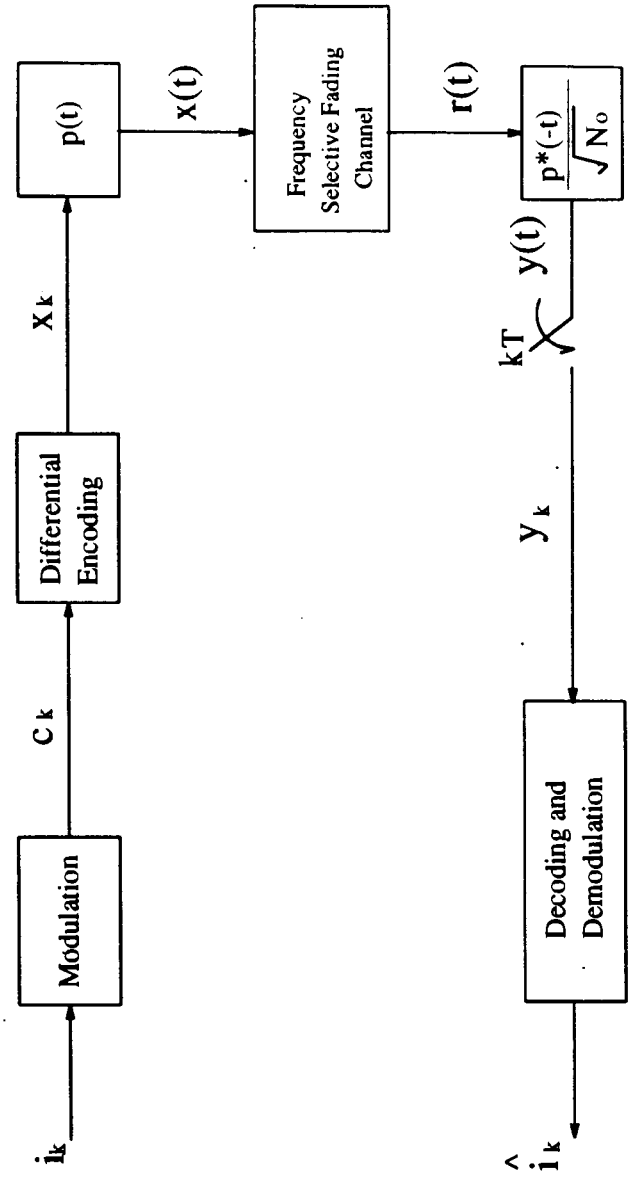

Figure 2.1: System block diagram for uncoded system

then sent into the differential encoder. The output is a sequence of transmitted PSK symbols x_k's. The emphasis is on QPSK throughout the thesis.

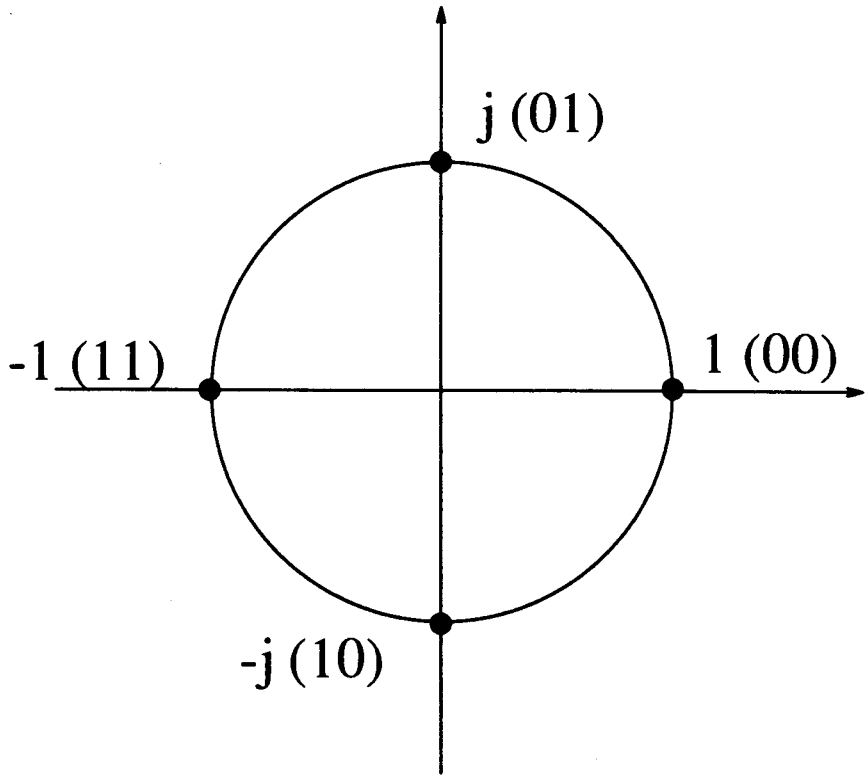

Figure 2.2: QPSK constellation

The constellation of QPSK is shown in Figure 2.2. Due to the differential encoding process, the k^{th} transmitted symbol x_k is related to the k^{th} data symbol c_k by the following equation:

$$x_k = c_k x_{k-1} \tag{2.1}$$

where both c_k and x_k are QPSK symbols chosen from the set $\{exp[\frac{j2\pi n}{4}], n = 0, 1, 2, 3$

}, or equivalently {1, j, -1, -j}. While the sequence of transmitted PSK symbols x_k is inputed to the pulse shaping filter, the transmitted signal x(t), the output of the pulse shaping filter, is transmitted over the channel.

Based on the above description, the baseband equivalent of the transmitted signal x(t) can be written as

$$x(t) = A\sum_n x_n p(t - nT) \tag{2.2}$$

where A is a constant, p(t) is the transmitted pulse, $\frac{1}{T}$ is the pulse rate. The pulse p(t) is a unit energy Nyquist's pulse, ie.

$$\int_{-\infty}^{\infty} |p(t)|^2 dt = 1 \tag{2.3}$$

Two kinds of pulse shaping filters are considered: rectangular pulse filter and square root raised-cosine pulse filter. Usually we are more interested in the impulse response q(t) of the combination of the transmitter and the receiver filters and its spectrum. If P(f) is the Fourier transform of p(t) and Q(f) is the Fourier transform of q(t), we know

$$q(t) = p(t) \otimes \frac{p^*(-t)}{\sqrt{N_o}} \tag{2.4}$$

$$Q(f) = \frac{|P(f)|^2}{\sqrt{N_o}} \tag{2.5}$$

where $\otimes$ represents convolution. The factor $\frac{1}{\sqrt{N_o}}$ in the matched filter is to normalize the variance of the additive white noise in the received sample to unity. In the case

that p(t) is a rectangular pulse, q(t) is

$$q(t) = \begin{cases} \frac{1}{\sqrt{N_o}}(1 - |t|/T) & \text{when } 0 \leq |t| \leq T \\ 0 & \text{elsewhere} \end{cases} \tag{2.6}$$

and its spectrum is

$$Q(f) = \frac{1}{\sqrt{N_o}} \frac{sin^2(\pi fT)}{(\pi f)^2 T} \tag{2.7}$$

while in case of square root raised-cosine pulse, q(t) is

$$q(t) = \frac{1}{\sqrt{N_o}} \frac{sin\pi t/T}{\pi t/T} \frac{cos\beta\pi t/T}{1 - 4\beta^2 t^2/T^2} \tag{2.8}$$

and its frequency response is

$$Q(f) = \begin{cases} \frac{T}{\sqrt{N_o}} & \text{when} 0 \leq |f| \leq (1-\beta)/2T \\ \frac{T}{2\sqrt{N_o}}[1 - sin\pi T(|f| - \frac{1}{2T})/\beta] & \text{when}(1-\beta)/2T \leq |f| \leq (1+\beta)/2T \\ 0 & \text{elsewhere} \end{cases} \tag{2.9}$$

2.2.2 The Frequency-Selective Rayleigh Fading Channel Model

Due to the multipath feature and the limited bandwidth of digital cellular channel, the transmitted signal x(t) suffers frequency-selective distortion. The digital cellular channel is considered to be a wide-sense stationary zero-mean complex Gaussian random process including the additive white Gaussian noise (AWGN) and can be treated

as time-variant system with an impulse response $c(\tau_1;t)$ plus the AWGN $n_w(t)$. This means the received signal is

$$r(t) = \int_{-\infty}^{\infty} c(\tau_1;t)x(t-\tau_1)d\tau_1 + n_w(t) \tag{2.10}$$

Proakis in [1] indicates that in most transmission media the attenuation and phase shift of the channel associated with path delay τ_1 is uncorrelated with those associated with path delay τ_2, thus the autocorrelation function of $c(\tau;t)$ can be defined as

$$\begin{aligned} \phi_c(\tau_1,\tau_2;\lambda_1-\lambda_2) &= \frac{1}{2}E[c^*(\tau_1;\lambda_1)c(\tau_2;\lambda_2)] \\ &= J_o[2\pi f_D(\lambda_1-\lambda_2)]G(\tau_1)\delta(\tau_1-\tau_2) \end{aligned} \tag{2.11}$$

where $J_o[\bullet]$ is the zero-order Bessel function, and

$$f_D = \frac{f_c v}{c} \tag{2.12}$$

is the maximum Doppler frequency at a mobile vehicle speed of v. Here f_c is the carrier frequency and c is the speed of light. For example, if the car travels at a speed of $v = 120$ km/hour and if the carrier frequency is $f_c = 900$ MHz, the corresponding maximum Doppler frequency f_D is 100 Hz. **In this thesis, we are going to study the range of f_D from 0 Hz to 100 Hz, which corresponds to the speed of the vehicle from rest to 120 km/hour.** The fade rate is more commonly used which is defined as $f_D T$, where T is the pulse duration and $\frac{1}{T}$ is the pulse rate. According to IS 54, the pulse rate is $\frac{1}{T} = 24$ kHz, therefore **the fade rate $f_D T$ varies from 0**

to 0.004. $G(\tau_1)$ is the power-delay profile. In the case of the **flat** fading channel, the power-delay profile is simply

$$G(\tau_1) = \sigma_g^2 \delta(\tau_1) \tag{2.13}$$

where σ_g^2 is the variance of the flat fading process.

Example

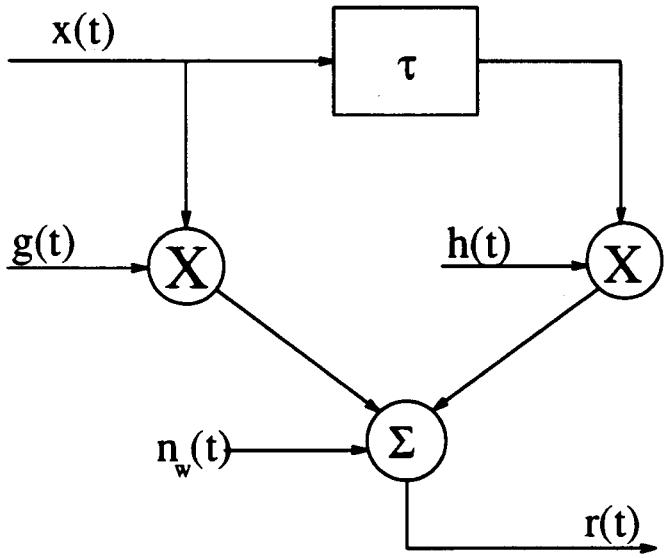

Figure 2.3: Two-ray channel model

As indicated in Chapter 1, a two-ray channel model is generally adopted to describe the frequency-selective fading channel and it is shown in Figure 2.3. As we can see,

x(t) arrives at the receiver through two rays. There is a flat fading process in each ray, but the combination of the two represents the frequency-selective fading process. The relative delay τ between the two paths is comparable with the pulse duration T, and therefore is not negligible. Mathematically the impulse channel response $c(\tau_1; t)$ and then the received signal r(t) can be written as :

$$c(\tau_1; t) = g(t)\delta(\tau_1) + h(t)\delta(\tau_1 - \tau) \tag{2.14}$$

$$r(t) = g(t)x(t) + h(t)x(t-\tau) + n_w(t) \tag{2.15}$$

The process $n_w(t)$ in (2.15) is additive white Gaussian noise (AWGN) in the channel and it has a two-sided power spectral density of N_o. On the other hand, both g(t) and h(t) represent the effect of flat fading. Their autocorrelation functions are

$$\begin{aligned} \phi_g(\lambda) &= \frac{1}{2}E[g(t)g(t-\lambda)^*] \\ &= \sigma_g^2 J_o(2\pi f_D \lambda) \end{aligned} \tag{2.16}$$

and

$$\begin{aligned} \phi_h(\lambda) &= \frac{1}{2}E[h(t)h(t-\lambda)^*] \\ &= \sigma_h^2 J_o(2\pi f_D \lambda) \end{aligned} \tag{2.17}$$

respectively. Note that the parameter λ in these equations is the delay variable and $J_o(\bullet)$ is the zero-order Bessel function.

It is easy to show that the delay-power profile $G(\tau_1)$ in Equ. (2.11) is

$$G(\tau_1) = \sigma_g^2 \delta(\tau_1) + \sigma_h^2 \delta(\tau_1 - \tau) \tag{2.18}$$

where σ_g^2 and σ_h^2 are variances of the two fading process g(t) and h(t).

We define the power split ratio α as

$$\alpha = \frac{\sigma_g^2}{\sigma_h^2}. \tag{2.19}$$

When the other channel parameters are fixed, the performance of the CDD, with the optimal sample timing, is the same for $\alpha_1 = a$ and $\alpha_2 = \frac{1}{a}$. However, the performance of the CDD with integer sample timing are different for $\alpha_1 = a$ and $\alpha_2 = \frac{1}{a}$. Specifically, if $a < 1$, the performance of the CDD with $\alpha_1 = a$ can be significantly worse than its $\alpha_2 = \frac{1}{a}$ counterpart. Due to the sequence estimation nature, the performance of the MSDD is believed to be insensitive to whether $\alpha_1 = a$ to $\alpha_2 = \frac{1}{a}$ in the actual channel. Consequently, we consider only the case of $\alpha \geq 1$.

The power split ratio α, together with the relative propagation delay τ in the two paths, play a key role in the performance of the differential detector. **In this thesis, we are going to study the performance of the differential detector within the realistic ranges of α and τ according to measurements of various environments. The power split ratio α, the power of the direct ray against that of the delay ray varies from 1 to ∞. The delay τ between the two paths is less than or equal to one symbol interval T, ie.** $0 < \tau < T$. We are

more interested in the normalized relative delay ρ which is defined as

$$\rho = \frac{\tau}{T} \tag{2.20}$$

Since τ is less than or equal to one symbol interval T, it is obvious that $\rho \in [0, 1]$. In [15], Cavers uses the first two moments of $G(\tau)$, τ_m and τ_{rms}, to characterize the time dispersion. As for this two-ray channel model, the relationships between α, ρ, τ_m and τ_{rms} are given below

$$\tau_m = T\frac{\rho}{1+\alpha} \tag{2.21}$$

$$\tau_{rms} = T\frac{\rho\sqrt{\alpha}}{1+\alpha} \tag{2.22}$$

The received symbol signal to noise ratio is defined as

$$\frac{E_s}{N_o} = \frac{A^2(\sigma_g^2 + \sigma_h^2)}{N_o} \tag{2.23}$$

while the bit signal to noise ratio for uncoded QPSK is simply

$$\frac{E_b}{N_o} = \frac{1}{2}\frac{E_s}{N_o} \tag{2.24}$$

2.2.3 Receiver

The received signal r(t), in (2.10) will pass through a matched filter with an impulse response of $\frac{p^*(-t)}{\sqrt{N_o}}$ and the output of the matched filter is

$$y(t) = \frac{1}{\sqrt{N_o}}\int_{-\infty}^{\infty} r(\lambda)p(\lambda - t)d\lambda + n(t)$$

$$= \frac{1}{\sqrt{N_o}} \int_{-\infty}^{\infty} \int_{-\infty}^{\infty} c(\tau_1; \lambda) x(\lambda - \tau_1) p(\lambda - t) d\tau_1 d\lambda + n(t)$$
$$= \frac{A}{\sqrt{N_o}} \sum_n x_n \int_{-\infty}^{\infty} \int_{-\infty}^{\infty} c(\tau_1; \lambda) p(\lambda - \tau_1 - nT) p(\lambda - t) d\tau_1 d\lambda + n(t) \quad (2.25)$$

and it is sampled once every T seconds. At the sampling instants $t = kT$ (the integer sample timing), the received sample can be written as

$$\begin{aligned} y_k = y(kT) &= \sum_n x_n u_{nk} + n_k \\ &= x_k u_{kk} + \sum_{n \neq k} x_n u_{nk} + n_k \end{aligned} \quad (2.26)$$

where

$$u_{nk} = \frac{A}{\sqrt{N_o}} \int_{-\infty}^{\infty} \int_{-\infty}^{\infty} c(\tau_1; \lambda) p(\lambda - \tau_1 - nT) p(\lambda - kT) d\tau_1 d\lambda \quad (2.27)$$

is the fading gain on the n^{th} transmitted PSK symbol at instants $t = kT$, and the $n_k's$ are a set of independent and identically distributed (iid) complex Gaussian variates, each assumed to have a zero mean and a unit variance. In the second expression of (2.26), the first term x_k is the desired transmitted PSK symbol and the rest in the second terms represent intersymbol interference (ISI). For a flat fading channel, the ISI terms are zero.

The structure of the decoder at the receiver is the emphasis of this thesis. We use the following separate section to describe the structures of two types of detectors: conventional differential detector (CDD) and multisymbol differential detector (MSDD).

2.3 The Differential Detector

The sequence of received samples

$$\cdots, y_{k-1}, y_k, y_{k+1} \cdots$$

is sent to a generic differential detector. This generic detector has an observation window of N samples, where $N \leq 2$. It processes all the N samples within the current window and makes a decision about the data symbol located at the middle of the observation window. Once a decision has been made, the window will be moved ahead by one sample. The CDD is of $N = 2$. Any detector with $N > 2$ is termed a multisymbol differential detector (MSDD). The structure of the two decoders are given in Figure 2.4, where part (a) represents a CDD while part (b) represents a MSDD of $N = 5$ with decision feedback (the branch AB). Note that it is straightforward to extend the methods described in this thesis to any other value of N ($N > 2$) samples.

The N received samples, y_{k-N_1+1} to y_{k-N_1+N}, can be written in vector form as

$$\mathbf{Y} = \begin{bmatrix} y_{k-N_1+1} \\ \vdots \\ y_{k-1} \\ y_k \\ \vdots \\ y_{k-N_1+N} \end{bmatrix} \tag{2.28}$$

where there are $N_1 - 1$ samples are ahead of y_k and $N - N_1$ samples after y_k ($N_1 < N$). Each element in (2.28) is defined by (2.26). For the sake of simplicity, y_k in (2.26)

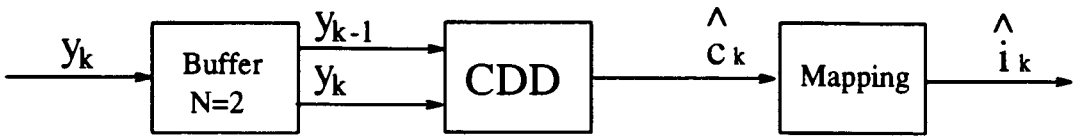

(a)

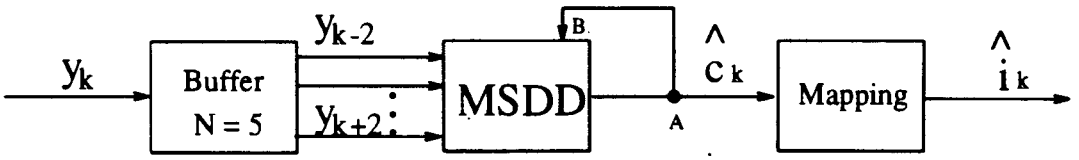

(b)

Figure 2.4: Decoding and demodulation

can be represented by finite number of terms as

$$y_k = \sum_{n=k-M_1}^{k+M_2} x_n u_{nk} + n_k \tag{2.29}$$

It is seen from (2.29) that the vector $\mathbf{Y}$ is a function of the fading gain vectors

$$\mathbf{U} = (U_{k-N_1+1}, \ldots, U_k, U_{k+1}, \ldots, U_{k-N_1+N})$$

where

$$U_k = (u_{k-M_1,k}, \ldots, u_{k-1,k}, u_{k,k}, u_{k+1,k}, \ldots, u_{k+M_2,k}) \tag{2.30}$$

as well as a function of the vector of transmitted symbols

$$\mathbf{X} = (x_{k-N_1+1-M_1}, \ldots, x_{k-2}, x_{k-1}, x_k, x_{k+1}, \ldots, x_{k-N_1+N+M_2}) \tag{2.31}$$

or equivalently a function of the vector of data symbols

$$\mathbf{C} = (c_{k-N_1+2-M_1}, \ldots, c_{k-1}, c_k, c_{k+1}, \ldots, c_{k-N_1+N+M_2}) \tag{2.32}$$

If we define

$$L = M_1 + M_2 + N \tag{2.33}$$

$$L_1 = M_1 + N_1 - 2 \tag{2.34}$$

then the length of $\mathbf{X}$ is L while the length of $\mathbf{C}$ is L-1 with L_1 symbols ahead of c_k. In the following subsections, first we consider the optimal generic decoder to determine the $(L_1 + 1)^{th}$ symbol c_k in the $\mathbf{C}$, then we will consider the specific examples of a CDD ($N = 2$), and a MSDD ($N = 5$).

2.3.1 The Optimal Generic Decoder

The random vector (2.28) is Gaussian and has a zero mean. Its probability density function (pdf) conditioned on c_k is denoted by $p_Y(\mathbf{Y}|c_k)$, while $p_Y(\mathbf{Y}|\mathbf{C})$ is the conditional pdf of $\mathbf{Y}$ given the vector $\mathbf{C}$. If all the data PSK symbols are used with equal probability, it is obvious that $p_Y(\mathbf{Y}|c_k)$ is the sum of the conditional pdfs of $\mathbf{Y}$ given the vector $\mathbf{C}$ containing c_k. Thus the optimal decoder is the one that computes for each possible value of c_k the metric

$$p_Y(\mathbf{Y}|c_k) = \sum_{\mathbf{C}:c_k \in \mathbf{C}} p_Y(\mathbf{Y}|\mathbf{C}). \tag{2.35}$$

Note that the above summation is over all the possible $\mathbf{C}$'s whose $(L_1+1)^{th}$ symbol is c_k. For any vector $\mathbf{C}$, the conditional density function $p_Y(\mathbf{Y}|\mathbf{C})$ is given by

$$p_Y(\mathbf{Y}|\mathbf{C}) = \frac{\mathbf{1}}{(\mathbf{2}\pi)^{\mathbf{N}}||\mathbf{\Phi_{yy}(C)}||}\mathbf{exp}\left\{-\frac{\mathbf{1}}{\mathbf{2}}\mathbf{Y}^{\dagger}\mathbf{\Phi}_{\mathbf{yy}}^{-\mathbf{1}}(\mathbf{C})\mathbf{Y}\right\} \tag{2.36}$$

where $\mathbf{\Phi_{yy}(C)}$ is the correlation matrix of $\mathbf{Y}$ given that $\mathbf{C}$ is the transmitted data vector, and $||\bullet||$ denotes the determinant of a matrix. The decoder selects the value of c_k that gives the largest metric. Note that the correlation matrix $\mathbf{\Phi_{yy}(C)}$ can be determined from the equations given in the next two subsections.

The optimal decoder in (2.35) requires the computation of exponential functions and their sums. A simpler decoder would be the one that uses the assumption that the sum in (2.35) is dominated by the largest term. In this case, the decoder simply selects the $\mathbf{C}$ vector whose metric

$$M(\mathbf{C}) = \mathbf{Y}^{\dagger}\mathbf{\Phi}_{\mathbf{yy}}^{-1}(\mathbf{C})\mathbf{Y} + \mathbf{2ln}\left(||\mathbf{\Phi}_{\mathbf{yy}}(\mathbf{C})||\right) \tag{2.37}$$

is the smallest. Subsequently, the value of the symbol c_k in $\mathbf{C}$ will be chosen as the decoded symbol.

2.3.2 Conventional Differential Detector

When using $N = 2$ received samples to decode, the metric used in the CDD is optimal for the **flat** fading channel. In this case, the diagonal elements of $\mathbf{\Phi}_{\mathbf{yy}}^{-1}(\mathbf{C})$, as well as the determinant $||\mathbf{\Phi}_{\mathbf{yy}}^{-1}(\mathbf{C})||$, are independent of the ISI symbols in the sequence $\mathbf{C}$. This implies the metric defined in (2.37) is reduced to

$$\begin{aligned} M(\hat{c_k}) &= \hat{c_k}^* y_k y_{k-1}^* + \hat{c_k} y_k^* y_{k-1} \\ &= 2Re[\hat{c_k}^* y_k y_{k-1}^*] \end{aligned} \tag{2.38}$$

where $Re[\bullet]$ means the real part of $[\bullet]$. The metric shown in (2.38) is simple and independent of the channel conditions. However, it is not optimal for a selective fading channel. In this thesis, we apply the CDD to the frequency-selective Rayleigh fading channel and investigate its performance. Detection is performed by calculating for each possible symbol $\hat{c_k}$ in the set $\{\exp[\frac{j2\pi n}{4}], n = 0, 1, 2, 3\}$ the likelihood of (2.38) and selecting the symbol $\hat{c_k}$ with the largest likelihood. The performance of the CDD will be shown in Chapter 3.

2.3.3 Multisymbol Differential Detector

Now let us consider the case $N > 2$ in (2.37), ie. MSDD. For demonstration purpose, we choose $N = 5$. The correlation matrix then becomes :

$$\mathbf{\Phi_{yy}(C)} = \begin{bmatrix} \sigma^2_{k-2,k-2} & \sigma^2_{k-2,k-1} & \sigma^2_{k-2,k} & \sigma^2_{k-2,k+1} & \sigma^2_{k-2,k+2} \\ \sigma^2_{k-1,k-2} & \sigma^2_{k-1,k-1} & \sigma^2_{k-1,k} & \sigma^2_{k-1,k+1} & \sigma^2_{k-1,k+2} \\ \sigma^2_{k,k-2} & \sigma^2_{k,k-1} & \sigma^2_{k,k} & \sigma^2_{k,k+1} & \sigma^2_{k,k+2} \\ \sigma^2_{k+1,k-2} & \sigma^2_{k+1,k-1} & \sigma^2_{k+1,k} & \sigma^2_{k+1,k+1} & \sigma^2_{k+1,k+2} \\ \sigma^2_{k+2,k-2} & \sigma^2_{k+2,k-1} & \sigma^2_{k+2,k} & \sigma^2_{k+2,k+1} & \sigma^2_{k+2,k+2} \end{bmatrix} \tag{2.39}$$

where

$$\begin{aligned} \sigma^2_{nm} &= \frac{1}{2}E[y_n y_m^*]; \qquad m,n \in \{k-2, k-1, k, k+1, k+2\}. \\ &= \sum_{i=m-M_1}^{m+M_2} \sum_{j=n-M_1}^{n+M_2} \phi_{mn}(i,j) x_i x_j^* \end{aligned} \tag{2.40}$$

and the term $\phi_{mn}(i,j)$ is defined in (A.2). From Appendix A, we know that $\phi_{mn}(i,j)$ depends on the shape of the combined impulse response q(t) and channel parameters.

Since we consider a MSDD with $N = 5$, we assume that the matrix (2.39) is mainly determined by L successively transmitted QPSK symbols of $\mathbf{X}$ in (2.31) or L-1 corresponding data QPSK symbols of $\mathbf{C}$ in (2.32). L is given in (2.33). At the receiver, a set of channel statistical parameters are predetermined including the maximum Doppler fade rate $f_D T$ in (2.12), the power split ratio α in (2.19), the relative delay ρ in (2.20), and the working bit signal to noise SNR in (2.24). There are 4^{L-1} different vector $\mathbf{C}$'s due to various combinations of $L-1$ data QPSK symbols. Thus

with the knowledge of channel statistical parameters we can calculate for each $\mathbf{C}$ the inverse and determinant of $\Phi_{yy}(\mathbf{C})$ and store them in the decoder codebook. The decision feedback (DF) feature in Figure 2.4 (b) is also very important and is explained in detail in Chapter 4. The MSDD feeds back L_1 previously decoded symbols to the decoder. When decoding with N successively received samples, the MSDD calculates the metric given by (2.37) for each $\mathbf{C}$ vector whose first L_1 symbols are the same as the L_1 previously decoded symbols, selects the $\mathbf{C}$ vector whose metric is the smallest, and chooses the $(L_1+1)^{th}$ symbol in the selected $\mathbf{C}$ as the decoded symbol.

One point worth discussing is that the decoder works under mismatching channel conditions. The use of the MSDD in (2.37) requires that the receiver can predetermine the correlation matrix associated with the channel. This translates into having knowledge about the Doppler frequency f_D, the relative delay ρ, the power split ratio α. Estimating all these parameters accurately can be a difficult task. Even if it is possible, the extra effort required may contradict the rationale of using partially coherent detection in the first place. Consequently, we focus our attention in mismatched decoders. As for a mismatched decoder, we are referring to the one that uses a fixed $\Phi_{yy}(\mathbf{C})$, regardless of the values of the actual channel parameters. As readers will find out in Chapter 4, it is more important to estimate accurately the relative delay ρ and the power split ratio α. The performance of the matched and mismatched MSDD will be presented in chapter 4.

The MSDD in this thesis is designed for the two-ray channel model. If the actual channel model is different from this two-ray channel model, definitely we can not

achieve the performance of the matched MSDD. The degradation of the performance of the MSDD can be large. For example, the actual channel model is a three-ray channel with equal split power on each ray. But we only design the decoding metrics for a two-ray channel, then the power on the third ray becomes the additive noise part in the received sample. Thus equivalently, the signal to noise ratio becomes very low and the degradation of the performance of the MSDD is large. But in this thesis we concentrate on the MSDD working under the actual two-ray channel model.

2.4 Channel Coding

Convolutional coding can be incorporated in both the CDD and the MSDD based systems. The system block diagram with convolutional coding is shown in Figure 2.5. The additional parts due to coding are shown in dash-line boxes. At the transmitter side, the information binary data $i'_k s$ is sent into a rate $\frac{1}{2}$ (53, 75) convolutional encoder, illustrated in Figure 2.6. (53, 75) is the octal notation representing the output branches from the encoder registers. The output of the encoder e_k's are mapped into data QPSK symbol c_k. These data QPSK symbols are interleaved by an ideal interleaver and then sent into the differential encoder.

At the receiver side, for the case of the CDD (see Figure 2.7(a)), the sequence of the metric $v'_k = y_k y^*_{k-1}$ obtained from the two successive received samples is deinterleaved. The output of the deinterleaver is sent into Viterbi Decoder (VD). With the branch output QPSK symbol c_b, the VD forms the branch metric $2Re[c^*_b y_k y^*_{k-1}]$. There are 32 nodes at each stage in the trellis diagram corresponding to the rate $\frac{1}{2}$

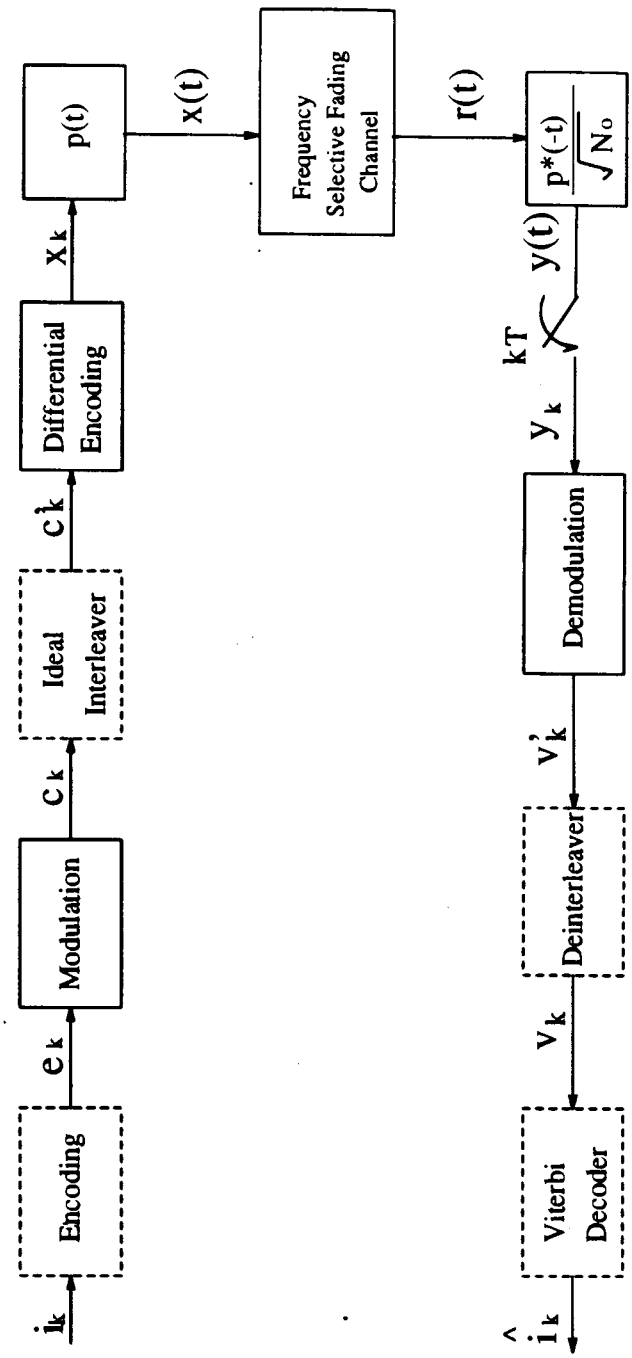

Figure 2.5: System block diagram with coding

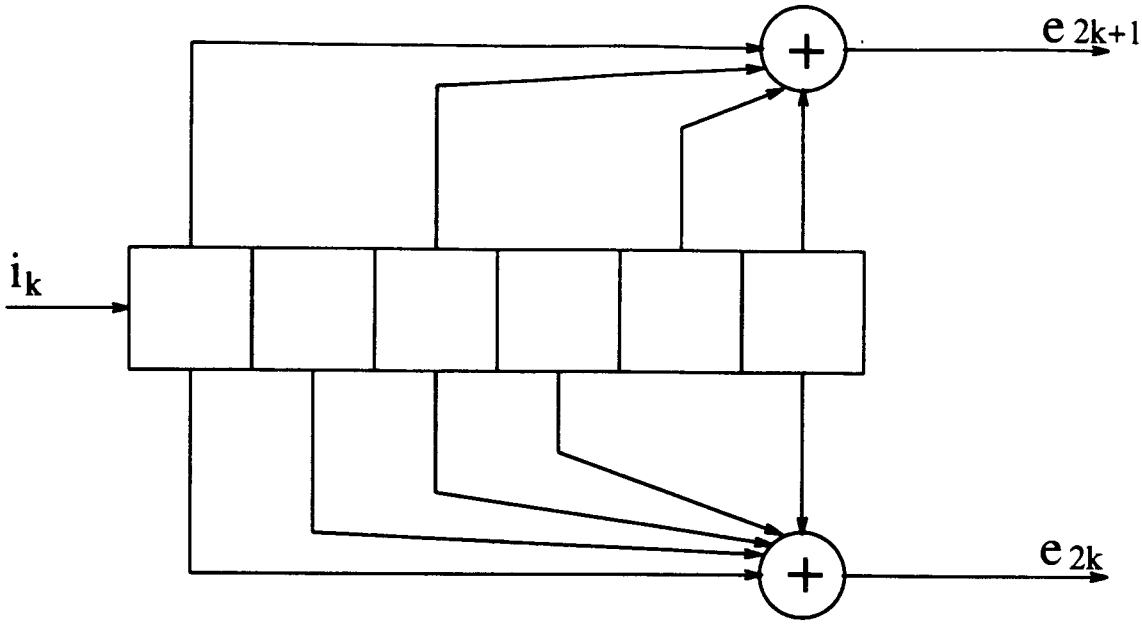

Figure 2.6: Structure of the rate $\frac{1}{2}$ (53, 75) convolutional encoder

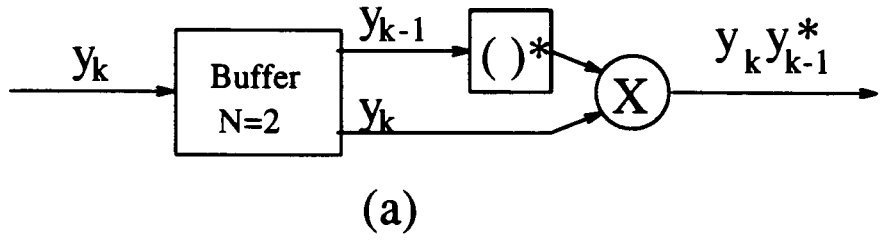

(a)

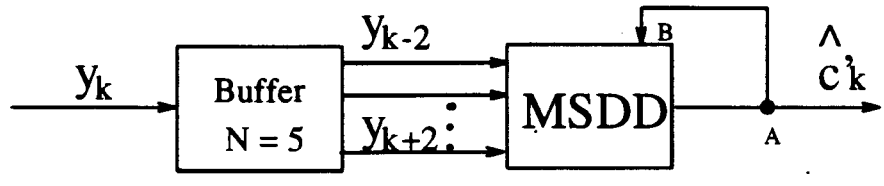

(b)

Figure 2.7: Demodulation

(53, 75) convolutional encoder while two paths are coming to and leaving each node respectively. Thus at each stage in the trellis diagram, VD computes 64 metrics corresponding to the 64 paths leading to nodes, discards half of them and saves the most probable half of transitions. The discarding and saving procedure is then repeated for each subsequently received sample. During decoding, the VD selects the path that has the largest metrics out of the 32 terminating nodes, traces back to the beginning node and finds out the corresponding input binary bits $\hat{i_k}$.

As for the MSDD (see Figure 2.5 and Figure 2.7(b)), v'_k is the estimate of the interleaved data PSK symbol $\hat{c'_k}$. The output of the deinterleaver, $v_k = \hat{c_k}$, is sent into the VD. Assuming that c_b is the output symbol on the transition branch in the trellis diagram, the branch metric is the Hamming distance between the binary representations of c_b and $\hat{c_k}$. Other procedures are similar to that in the CDD described above except that the VD selects the path that has the smallest metric among 32 terminating nodes.

Chapter 3

Performance of Conventional Differential Detection in A Frequency-selective Rayleigh Fading Channel

In this chapter, we investigate the performance of the conventional differential detector (CDD) in a frequency-selective Rayleigh fading channel. It is found that its performance depends on the transmitted pulses as well as the channel parameters.

In the first section, we will analyze the performance of the CDD to detect uncoded QPSK signals with an arbitrary transmitted pulse shape under any fading spectrum and delay power profile. In the second section, we restrict our attention to

a rectangular transmitted pulse shape with a duration of one symbol interval. The analytical results illustrate the dependence of the performance of the CDD on channel parameters while simulation results provide proof to show how good the analysis is. In the third section, we consider raised-cosine pulses and analyze the corresponding performance of the CDD. In the forth section, we will use the piece-wise-constant assumption to analyze the performance of CDD and show that it is a good assumption for analysis and simulation. And in the last section, we will consider the effect of optimal sampling on the error performance of the CDD.

3.1 General Performance of CDD

As shown in Chapter 2, two successive received samples are used to detect the transmitted information in the CDD. Rewriting the two received samples in (2.29) below:

$$y_k = \sum_{n=k-M_1}^{k+M_2} x_n u_{n,k} + n_k \tag{3.1}$$

$$y_{k-1} = \sum_{n=k-1-M_1}^{k-1+M_2} x_n u_{n,k-1} + n_{k-1} \tag{3.2}$$

where $u_{n,k}$'s and $u_{n,k-1}$'s are fading gains given by (2.27) and x_n's are the transmitted PSK symbols given by (2.1).

Given c_k is transmitted the CDD will make an erroneous decision if for some $\hat{c}_k$ not equal to c_k, the random variable D defined below is less than zero:

$$D = M(\hat{c}_k) - M(c_k) = y_k y_{k-1}^* d_k^* + y_k^* y_{k-1} d_k, \tag{3.3}$$

where $M(c_k)$ is the metric in (2.38) and d_k is given as

$$d_k = c_k - \hat{c}_k \tag{3.4}$$

For any pair of c_k and $\hat{c}_k$, the chance that D is less than zero is called the symbol pairwise error probability and is denoted by

$$P(c_k \rightarrow \hat{c}_k) = Prob(D < 0) \tag{3.5}$$

A union bound on the average bit error rate (BER) is simply

$$P_b \leq \frac{1}{m} \sum_{c_k \neq \hat{c}_k} \overline{a(c_k, \hat{c}_k) P(c_k \rightarrow \hat{c}_k)} \tag{3.6}$$

where $a(c_k, \hat{c}_k)$ is the information-bit error in making a wrong decision and m is the number of information bits per channel symbol. The overline over $P(c_k \rightarrow \hat{c}_k)$ means the average of the symbol pairwise error probability over all data PSK symbols and all possible interference symbol sequence.

Since we are interested in QPSK, c_k will take one of the four symbols from the set $\{1, j, -1, -j\}$. If c_k is assumed to be transmitted, there are three possible symbol

pairwise error probabilities $P(c_k \rightarrow \hat{c}_k)$ where $\hat{c}_k$ could be $jc_k, -c_k$, or $-jc_k$. According to the metric in (2.38), we find that

$$\begin{aligned} M(c_k) &= -M(-c_k) \\ M(jc_k) &= -M(-jc_k) \end{aligned} \tag{3.7}$$

Whenever

$$M(c_k) < M(-c_k) \tag{3.8}$$

$M(c_k)$ is negative, and since $Max[M(jc_k), M(-jc_k)]$ is always positive, thus

$$M(c_k) < Max[M(jc_k), M(-jc_k)] \tag{3.9}$$

which means that given c_k transmitted, the opportunity that the CDD chooses $-c_k$ is included in the opportunity that it chooses jc_k and $-jc_k$. Therefore, in our error analysis of the BER, we only consider the two nearest neighbor error events. It is assumed that gray mapping is used to map information bits into channel symbols. In other words, only one information bit error is made in a nearest neighbor error event. Consequently, (3.6) becomes

$$P_b = \frac{1}{2}\overline{P(c_k \rightarrow jc_k)} + \overline{P(c_k \rightarrow -jc_k)} \tag{3.10}$$

where the overline represents a statistical average with respect to the all possible values of c_k and the interference symbols.

From the above equation, it is clear that the key to the error analysis is to determine a general expression for the pairwise error probability. To determine this probability, we make use of the fact that the random variable D in (3.3) is a quadratic form of complex Gaussian variates conditioned on the data QPSK sequence. Using the characteristic function technique described in [1] and [2], it can be shown that the pairwise error probability is given by

$$P(c_k \rightarrow \hat{c}_k) = \frac{1}{2}(1 - \sqrt{\frac{1}{1+z}}) \tag{3.11}$$

where

$$z = \frac{4|d_k|^2(\sigma_k^2\sigma_{k-1}^2 - |\sigma_{k,k-1}^2|^2)}{(d_k^*\sigma_{k,k-1}^2 + d_k\sigma_{k,k-1}^{2\,*})^2} \tag{3.12}$$

and σ_{k-1}^2 and σ_k^2 are the variances of the samples y_{k-1} and y_k, and $\sigma_{k,k-1}^2$ is the corresponding covariance. Note that notation $|\bullet|$ is used to denote the magnitude of a complex number.

3.2 The Rectangular Pulse Shape

The method to analyze the performance of the CDD given in Section 3.1 is general. Any kind of transmitted pulse shape can be applied. In this section, we consider a rectangular pulse with pulse duration T. This means q(t) is a triangle pulse given in (2.6).

3.2.1 The Error Performance

Since q(t) is of duration 2T, it is obvious that there is only one interference symbol in the received sample y_k and y_{k-1} respectively. Thus $M_1 = 1$ and $M_2 = 0$. Equ. (3.1) and (3.2) become

$$y_k = u_{k,k}c_k c_{k-1}x_{k-2} + u_{k-1,k}c_{k-1}x_{k-2} + n_k \tag{3.13}$$

$$y_{k-1} = u_{k-1,k-1}c_{k-1}x_{k-2} + u_{k-2,k-1}x_{k-2} + n_{k-1} \tag{3.14}$$

Let σ_k^2 and σ_{k-1}^2 be the variances of the samples y_k and y_{k-1} and $\sigma_{k,k-1}^2$ be their corresponding covariance, then

$$\sigma_k^2 = 1 + \phi_{k,k}(k,k) + \phi_{k,k}(k-1,k-1) + \phi_{k,k}(k,k-1)c_k + \phi_{k,k}(k-1,k)c_k^*; \tag{3.15}$$

$$\begin{aligned}\sigma_{k-1}^2 = {} & 1 + \phi_{k-1,k-1}(k-1,k-1) + \phi_{k-1,k-1}(k-2,k-2) \\ & + \phi_{k-1,k-1}(k-1,k-2)c_{k-1} + \phi_{k-1,k-1}(k-2,k-1)c_{k-1}^*;\end{aligned} \tag{3.16}$$

$$\begin{aligned}\sigma_{k,k-1}^2 = {} & \phi_{k,k-1}(k,k-1)c_k + \phi_{k,k-1}(k-1,k-1) \\ & + \phi_{k,k-1}(k,k-2)c_k c_{k-1} + \phi_{k,k-1}(k-1,k-2)c_{k-1};\end{aligned} \tag{3.17}$$

where $\phi_{k,k}(\bullet,\bullet)$, $\phi_{k-1,k-1}(\bullet,\bullet)$, and $\phi_{k,k-1}(\bullet,\bullet)$ are defined by (A.2) and determined by (A.11) in Appendix A. c_k is the desired data PSK symbol while c_{k-1} is the interference symbol. Applying (3.15), (3.16), and (3.17) to (3.10) - (3.12), we can obtain

the performance of CDD in a frequency-selective Rayleigh fading channel.

The pairwise error probability given by (3.11) and (3.12) can be applied to any M-ary PSK modulation in a straightforward fashion. In the following, we will first apply it to BPSK and get a rough idea of the performance of the CDD in the frequency-selective Rayleigh fading channel. Then the performance of the CDD of QPSK signals in the frequency-selective Rayleigh fading channel will also be shown. Once again, the received signal is assumed to be sampled at integer sample timing.

3.2.2 Example One: BPSK

Let us first consider the special case of BPSK with **static fading** ($f_D = 0.0$) and a normalized relative delay of $\rho = 1$. Since BPSK symbols are real, this implies the error probability in (3.11) becomes

$$P(c_k \rightarrow \hat{c}_k) = \frac{1}{2}(1 - \frac{\sigma^2_{k,k-1}}{\sqrt{\sigma^2_k \sigma^2_{k-1}}}) \tag{3.18}$$

and σ^2_k, σ^2_{k-1} and $\sigma^2_{k,k-1}$ are

$$\sigma^2_k = \sigma^2_{k-1} = \Gamma + 1 \tag{3.19}$$

$$\sigma^2_{k,k-1} = \frac{\alpha}{\alpha+1}\Gamma + \frac{1}{\alpha+1}\Gamma c_{k-1} \tag{3.20}$$

Where Γ is symbol signal-to-noise ratio $\frac{E_s}{N_o}$ defined in (2.23). Consequently, the BER, after taking average over the two possible values of the interfering symbol c_{k-1}, is

$$P_b = \frac{1 + \Gamma + \alpha}{2(1 + \Gamma)(1 + \alpha)} \tag{3.21}$$

At large symbol signal-to-noise ratio Γ, the above reduces to $\frac{0.5}{1+\alpha}$. In other words, even in the case of static fading, there exists an irreducible error floor. In the worst case of equal power split, this error floor is as large as $\frac{1}{4}$. Once again, it should be pointed out that the above results is for the special case of a relative delay equal to 1 symbol interval. For smaller relative delays, the average bit error rate will be better than the above.

As for the performance of BPSK at the optimal sampling time, see Section 3.5.

3.2.3 Example Two: QPSK

We have studied in detail the error performance of uncoded QPSK in the 2-ray frequency-selective Rayleigh fading channel.

The BER versus bit signal-to-noise ratio (SNR) curve for QPSK at a Doppler frequency of $f_D T = 0.004$ and a normalized delay of $\rho = 1$ is shown in Fig. 3.1 with the power split ratio α, in dB, as a parameter. The case of $\alpha = 10000$ approaches the channel conditions of a flat fading channel while $\alpha = 0$ dB corresponds to equal power split among the two arrival rays. The results in this figure suggest that the error floor is dominated by the power split ratio α as long as the relative delay is relatively big. From (2.22), τ_{rms}, the root-mean-square of the delay τ, is related to both α and

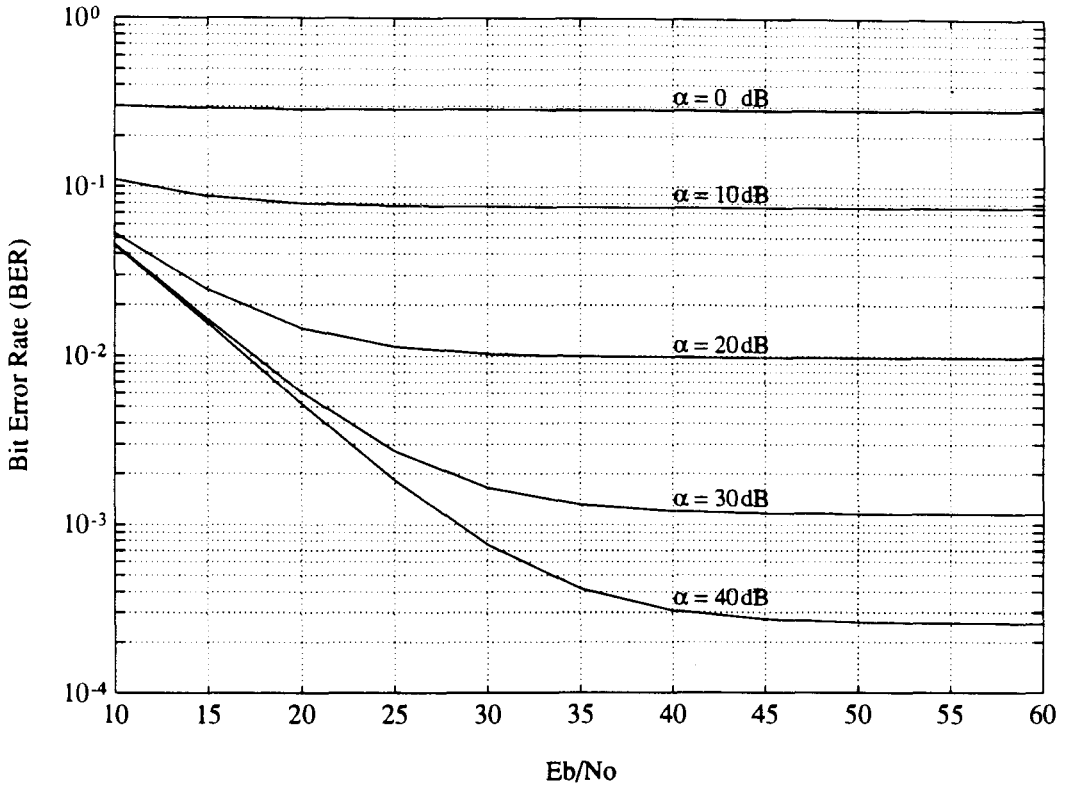

Figure 3.1: The BER vs $\frac{E_b}{N_o}$ curves of QPSK using a rectangular pulse and with $f_D T = 0.004$ and $\rho = 1.0$. The different curves are $(1)\alpha = 0dB$, $(2)\alpha = 10dB$, $(3)\alpha = 20dB$ $(4)\alpha = 30dB$ and $(5)\alpha = 40dB$ respectively

ρ. Thus it is obvious that the error floors also depend on the combined parameter τ_{rms}.

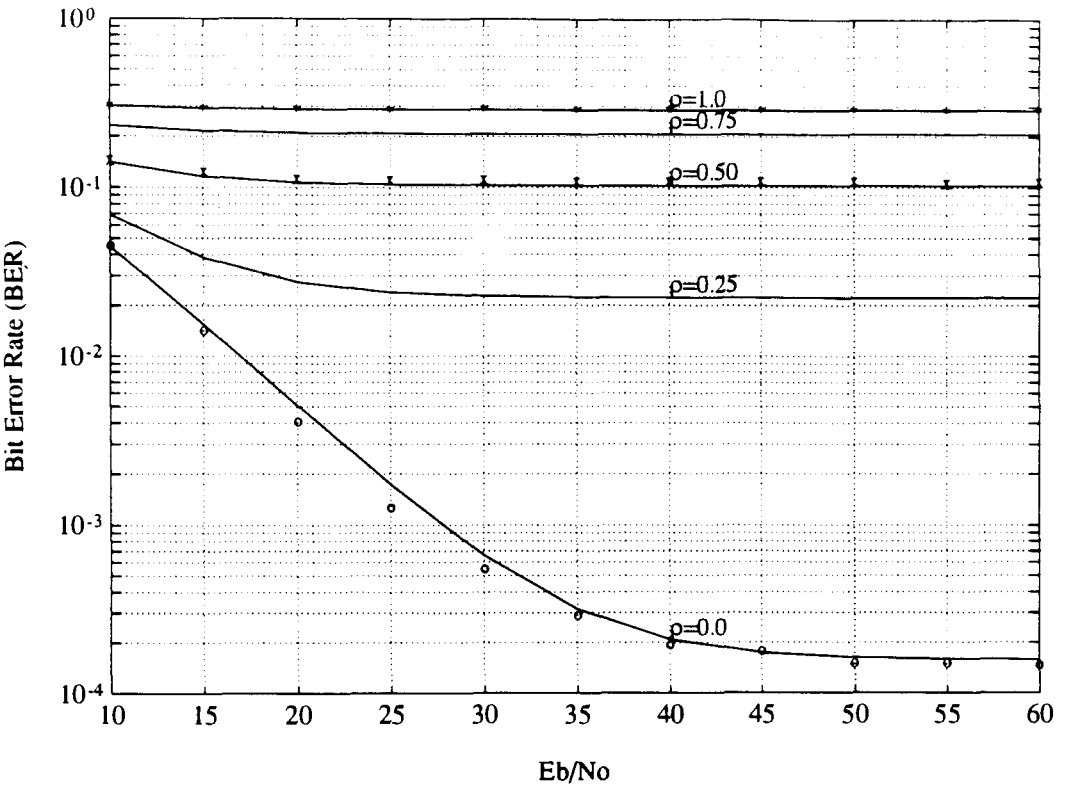

Figure 3.2: The BER vs $\frac{E_b}{N_o}$ curves of QPSK using a rectangular pulse and with $f_DT = 0.004$ and $\alpha = 0dB$. The various curves are $(1)\rho = 1.0$, $(2)\rho = 0.75$, $(3)\rho = 0.5$ $(4)\rho = 0.25$, and $(5)\rho = 0$. Signs "$*$", "x", and "o" are simulation results for the cases of $(1)\rho = 1.0$, $(3)\rho = 0.5$ and $(5)\rho = 0$ respectively

The effect of the relative propagation delay on the error performance is shown in Fig. 3.2. The Doppler frequency is $f_DT = 0.004$ and the power split ratio α is 0 dB. The case of a zero relative delay corresponds to flat fading. It is observed that with the given channel parameters, a small delay of $\rho = 0.25$ already causes two orders of magnitude change in the error probability from the flat fading case. For larger values of α though, the change in the error probability becomes less dramatic as ρ changes,

see Fig. 3.3.

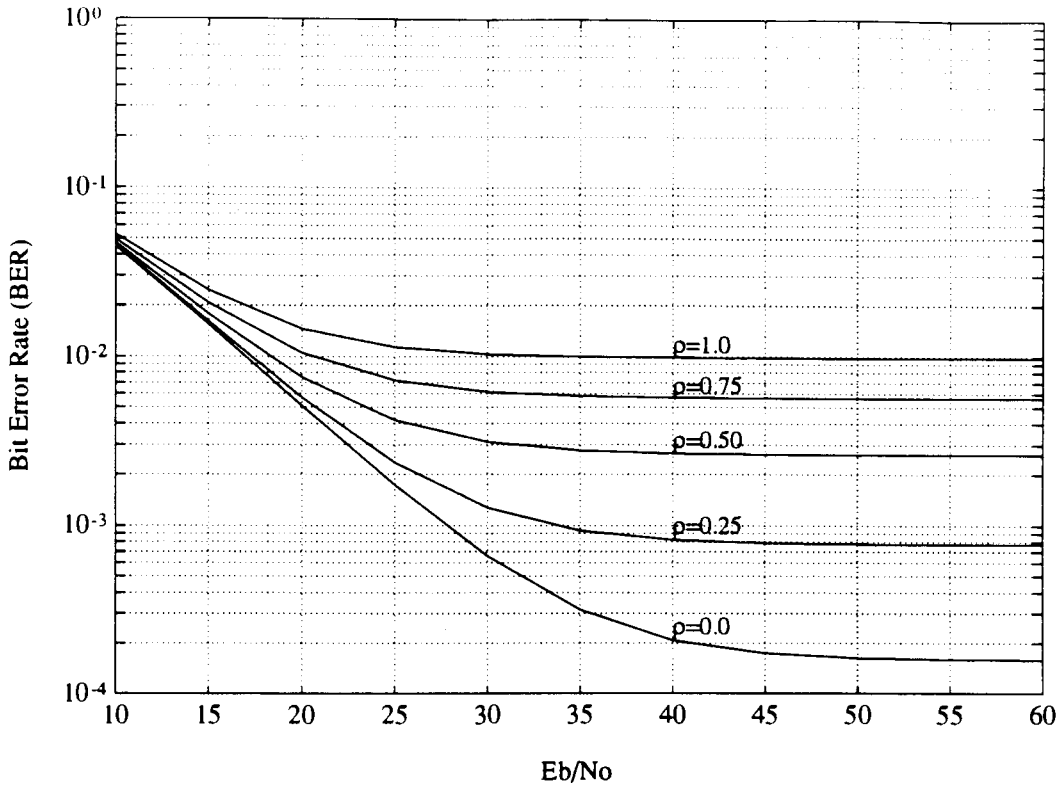

Figure 3.3: The BER vs $\frac{E_b}{N_o}$ curves of QPSK using a rectangular pulse and with $f_D T = 0.004$ and $\alpha = 20dB$. The various curves are $(1)\rho = 1.0$, $(2)\rho = 0.75$, $(3)\rho = 0.5$ $(4)\rho = 0.25$, and $(5)\rho = 0$.

The simulation results are also given in Figure 3.2. The signs "o" are for the case $\rho = 0.0$; The signs "x" are for the case $\rho = 0.5$; and the signs "$*$" are for the case $\rho = 1.0$. It is observed that the simulation results agree very well with the analytical results. Thus we can see that the analytical results given by (3.10) are accurate.

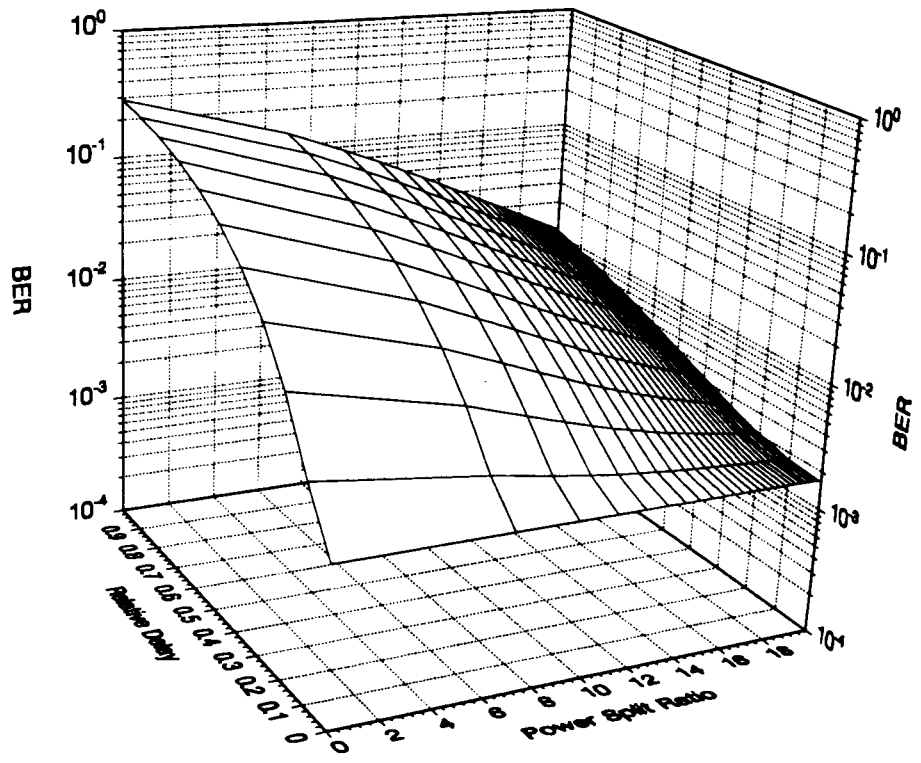

Figure 3.4: A three dimensional BER plot of QPSK at a SNR of 25dB using a rectangular pulse. The normalized Doppler frequency is $f_dT = 0.004$.

The dependence of the BER on both the power split ratio α and the normalized relative delay ρ is illustrated in the three dimensional error plot in Fig. 3.4. The total received bit signal-to-noise ratio is equal to 25 dB and the normalized Doppler Frequency is once again $f_D T = 0.004$. The roles played by α and ρ are quite evident from this figure.

3.3 The Raised-Cosine Pulse Shape

In the previous section, we illustrate the performance of the CDD for QPSK with a rectangular pulse operating in the frequency-selective Rayleigh fading channel. There is only one interference symbol in the received sample. In this section, we will analyze the performance of the CDD for a raised-cosine pulse although the method is also suitable to other kind of pulses. In this case, the received sample will contain a few interfering symbols.

Recall once again that the received samples y_k and y_{k-1} are shown in (3.1) and (3.2). Given c_k being transmitted, the CDD will make an erroneous decision if for some $\hat{c}_k$ not equal to c_k, the random variable D defined in (3.3) is less than zero. It is obvious that the way to find out the BER is the same as before, ie (3.5) - (3.12) still hold. However, the raised-cosine pulse has finite frequency duration and therefore infinite time duration. Thus there are a number of significant ISI terms in the received sample, instead of one ISI term as in the case of the rectangular pulse. Even for a pulse with a small roll-off factor in a frequency-selective fading channel with

small delay spread, the significant ISI terms can easily span more than 5 symbols, corresponding to more than 1024 patterns of interference symbol sequence when using QPSK. This significantly hinders the average BER calculation in (3.10).

In [15], Cavers suggests a way to average the variances and covariances over the interference symbol sequences first and then calculate the BER. He finds that the method works well without restriction of the length of ISI and the result on the BER is an extremely tight approximation. This method is adopted in the thesis.

3.3.1 Approximation to the Pairwise Error Probability

Since the two received sample are given by (3.1) and (3.2), σ_k^2 and σ_{k-1}^2, the variances of the samples y_k and y_{k-1}, and $\sigma_{k,k-1}^2$, the corresponding covariance are

$$\sigma_k^2 = \sum_{i=k-M_1}^{k+M_2} \sum_{j=k-M_1}^{k+M_2} \phi_{k,k}(i,j) x_i x_j^* + 1 \tag{3.22}$$

$$\sigma_{k-1}^2 = \sum_{i=k-1-M_1}^{k-1+M_2} \sum_{j=k-1-M_1}^{k-1+M_2} \phi_{k-1,k-1}(i,j) x_i x_j^* + 1 \tag{3.23}$$

$$\sigma_{k,k-1}^2 = \sum_{i=k-M_1}^{k+M_2} \sum_{j=k-1-M_1}^{k-1+M_2} \phi_{k,k-1}(i,j) x_i x_j^* \tag{3.24}$$

where $\phi_{k,k}(\bullet,\bullet)$, $\phi_{k-1,k-1}(\bullet,\bullet)$, and $\phi_{k,k-1}(\bullet,\bullet)$ are defined by (A.3) in Appendix A, and x_i and x_j are the transmitted PSK symbols. Using Cavers' tight approximation shown in Appendix B, (3.22), (3.23), and (3.24) become

$$\overline{\sigma_k^2} = \sum_{i=k-M_1}^{k-1+M_2} \phi_{k,k}(i,i) + 2Re[c_k \phi_{k,k}(k,k-1)] + 1 \quad (3.25)$$

$$\overline{\sigma_{k-1}^2} = \sum_{i=k-1-M_1}^{k-1+M_2} \phi_{k-1,k-1}(i,i) + 2Re[c_k \phi_{k-1,k-1}(k,k-1)] + 1 \quad (3.26)$$

$$\overline{\sigma_{k,k-1}^2} = \sum_{i=k-M_1}^{k-1+M_2} \phi_{k,k-1}(i,i) + c_k \phi_{k,k-1}(k,k-1) \quad (3.27)$$

where c_k is the data PSK symbol. Note that $\overline{\sigma_k^2}$, $\overline{\sigma_{k-1}^2}$, and $\overline{\sigma_{k,k-1}^2}$ given above only depend on the data PSK symbol c_k. Substituting $\overline{\sigma_k^2}$, $\overline{\sigma_{k-1}^2}$, and $\overline{\sigma_{k,k-1}^2}$ for σ_k^2, σ_{k-1}^2 and $\sigma_{k,k-1}^2$ in (3.11), we obtain approximation to $\overline{P(c_k \rightarrow jc_k)}$ and $\overline{P(c_k \rightarrow -jc_k)}$ respectively and finally obtain the BER in equation (3.10).

3.3.2 The Error Performance

The previous subsection provides a method to calculate the BER for a given M_1 and M_2. In the following, we set $M_1 = 8$ and $M_2 = 7$. Then there are sixteen terms in the received sample. In the case of the raised-cosine pulse with a roll-off factor of 0.35, the maximum variance of the fading gains in the ISI terms which are thrown away is less than 10^{-6} of the maximum variance of the fading gains on the data PSK symbol. The rest of fading gains decay in the order of t^{-3}. So keeping 16 terms in the received sample is accurate enough to represent the actual received sample and thus (3.25), (3.26), and (3.27) become

$$\overline{\sigma_k^2} = \sum_{i=k-8}^{k+7} \phi_{k,k}(i,i) + 2Re[c_k \phi_{k,k}(k,k-1)] + 1 \tag{3.28}$$

$$\overline{\sigma_{k-1}^2} = \sum_{i=k-9}^{k+6} \phi_{k-1,k-1}(i,i) + 2Re[c_k \phi_{k-1,k-1}(k,k-1)] + 1 \tag{3.29}$$

$$\overline{\sigma_{k,k-1}^2} = \sum_{i=k-8}^{k+6} \phi_{k,k-1}(i,i) + c_k \phi_{k,k-1}(k,k-1) \tag{3.30}$$

where $\phi_{k,k}(\bullet,\bullet)$, $\phi_{k-1,k-1}(\bullet,\bullet)$, and $\phi_{k,k-1}(\bullet,\bullet)$ are given in (A.11). We substitute (3.28), (3.29) and (3.30) into (3.11) and (3.12) to calculate the BERs.

The numerical results presented in this subsection are valid for both the conventional and the $\frac{\pi}{4}$-shift version of QPSK. The BER versus bit SNR curves for QPSK with a raised-cosine pulse at a Doppler frequency of $f_D T = 0.004$ and power split ratio of $\alpha = 1$ is shown in Figure 3.5. Figure 3.5 is generally similar to Figure 3.2 but its error floors are a little bit higher. This is due to more ISI terms in the received sample so that the performance of the CDD becomes worse. Simulation results are also shown for the cases $\rho = 0$ (by signs "o"), $\rho = 0.5$ (by signs "x") and $\rho = 1.0$ (by signs "$*$"). It is obvious the analytical results are in accordance to the simulations.

Figure 3.6 illustrates the effects of truncating the interference symbols. The conditions are Doppler frequency $f_D T = 0.004$, a normalized delay of $\rho = 0.25$ and power split ratio $\alpha = 1$. It is discovered that the results of the performance of the CDD are accurate enough if we keep more than six ISI terms in the received sample.

Before ending the section, we will show in Figure 3.7 the effect of the roll-off factor β on the performance of the CDD. The conditions are the same as the previous figure, a fade rate of $f_D T = 0.004$, a normalized delay of $\rho = 0.25$ and a power split ratio

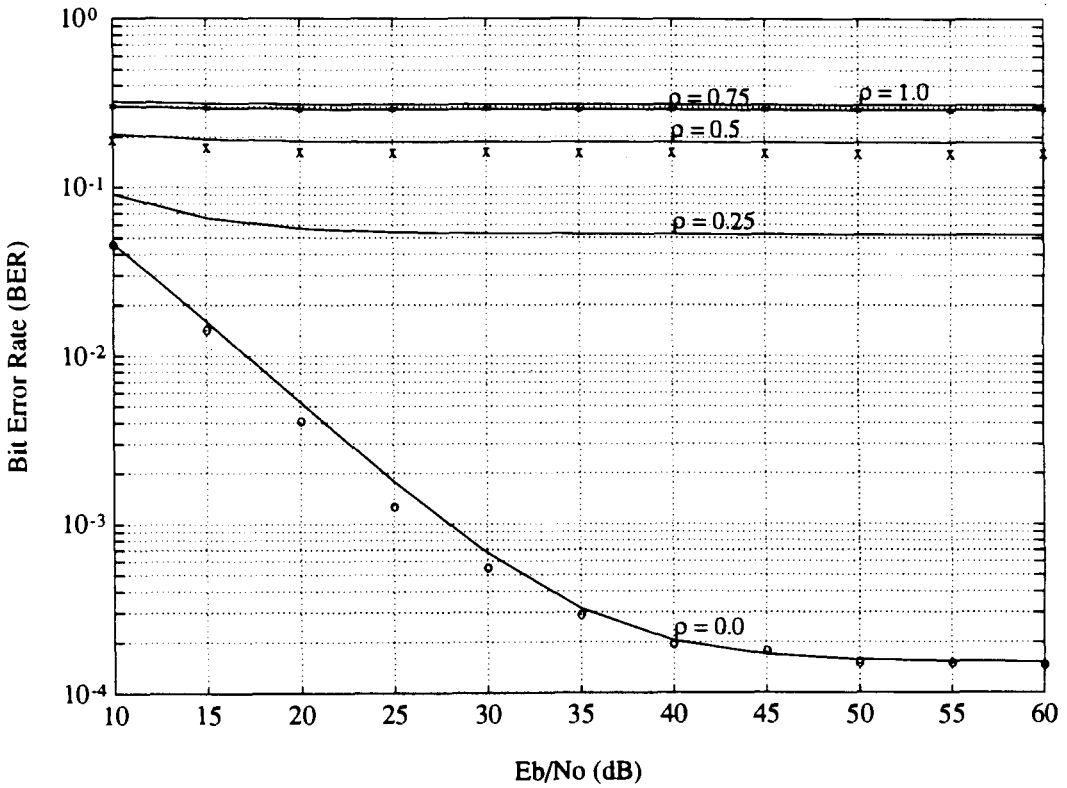

Figure 3.5: The BER vs $\frac{E_b}{N_o}$ curves of QPSK using a raised-cosine pulse with $\beta = 0.35$ at $f_D T = 0.004$ and $\alpha = 0dB$. The various curves are $(1)\rho = 1.0$, $(2)\rho = 0.75$, $(3)\rho = 0.5$ $(4)\rho = 0.25$, and $(5)\rho = 0$.

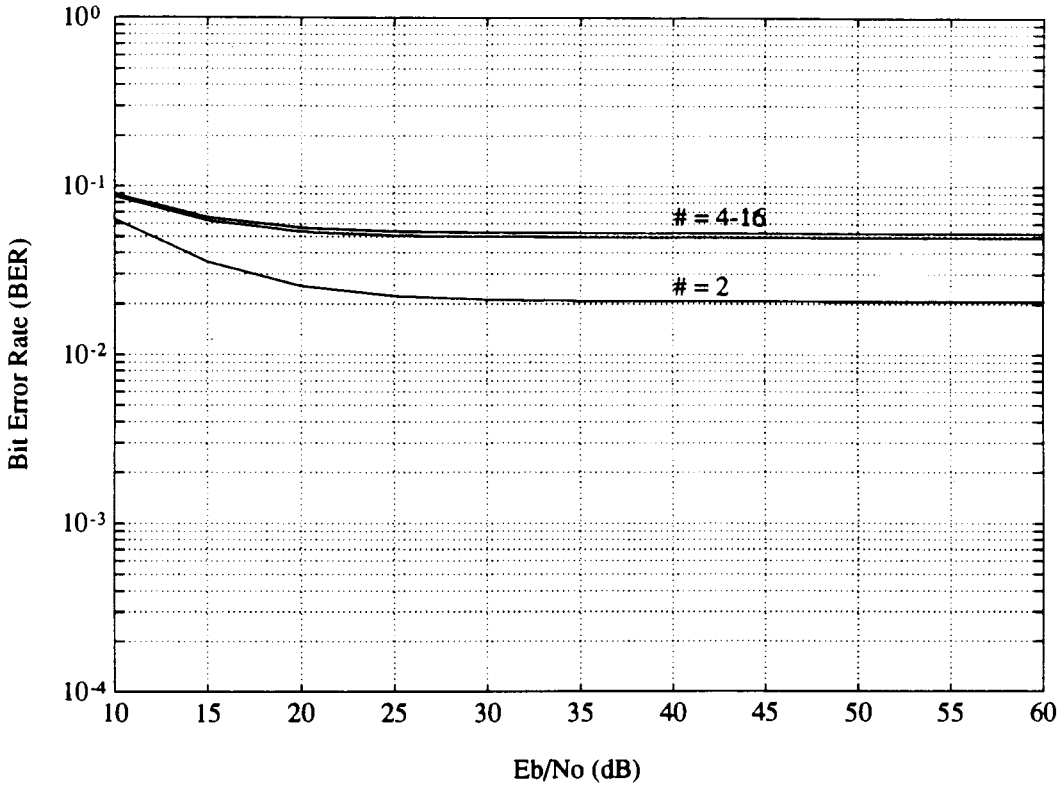

Figure 3.6: The BER vs $\frac{E_b}{N_o}$ curves of QPSK using raised-cosine pulses with $\beta = 0.35$ at $f_D T = 0.004$, $\rho = 0.25$ and $\alpha = 0dB$. The various curves show different BERs when different number of interference terms are kept in the received sample.

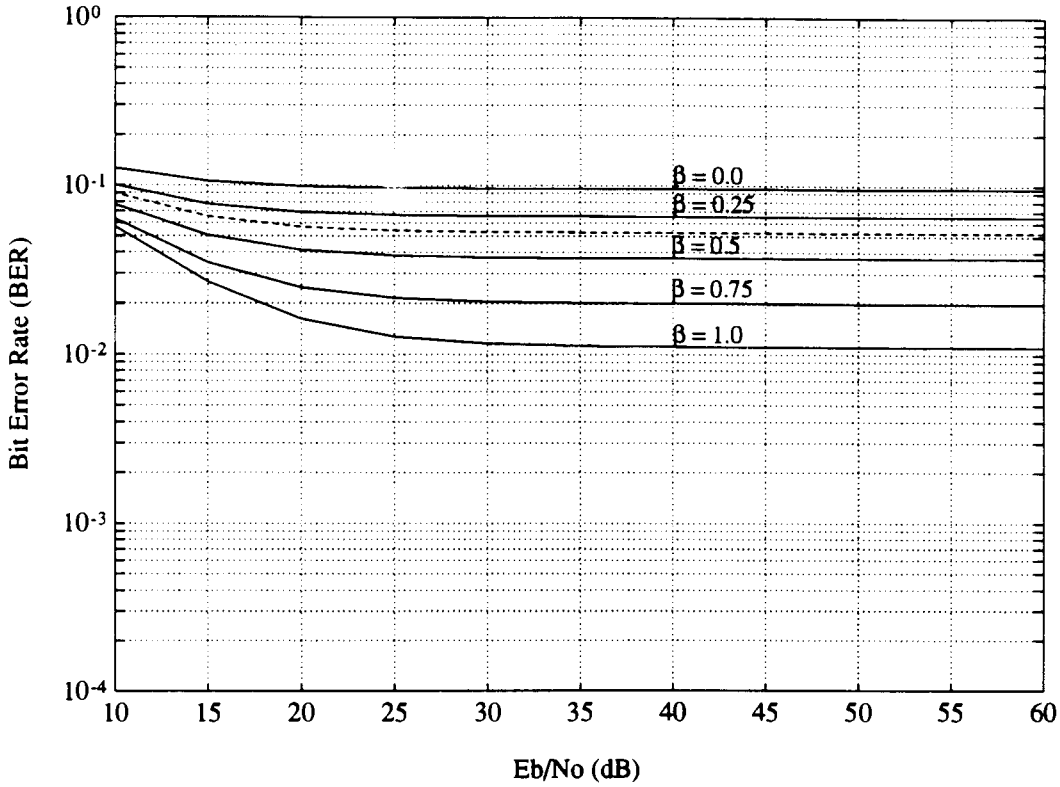

Figure 3.7: The BER vs $\frac{E_b}{N_o}$ curves of QPSK using different raised-cosine pulses at $f_D T = 0.004$, $\rho = 0.25$ and $\alpha = 0dB$. The various curves show different BERs when raised-cosine pulses with different β are used to transmit.

$\alpha = 1$. Sixteen terms are kept in the received sample. It is obvious that the best pulse used for transmission is $\beta = 1.0$ and the worse is $\beta = 0.0$. It shows the trade-off between bandwidth and performance. Larger bandwidth provides better performance in the CDD. Another thing worth pointing out is that the performance of the CDD for QPSK with a raised-cosine pulse of $\beta = 1.0$ is better than that of the rectangular pulse. When the roll-off factor of $\beta = 1.0$, side lobes of the raised-cosine pulse are very small compared with the main lobe. And more importantly, the slopes of the main lobe of the raised-cosine pulse q(t) decay faster than the slopes of triangle pulse. That is the reason why the CDD works better with a raised-cosine pulse of $\beta = 1.0$.

3.4 Validity of the Piece-Wise-Constant assumption

In the analysis and simulation of fading channels, the piece-wise-constant assumption is often used because of its convenience. In other words, the fading process in the channel is assumed to change so slowly that the complex fading gain is roughly constant within one or a few successive symbol intervals. Cavers shows, in [21], the validity of this assumption for the **flat** slow and moderate fading channel. In this section, we are going to show the effectiveness of this piece-wise-constant assumption in the **frequency-selective** slow fading channel.

Assuming the received signal r(t) is given by (2.15). It can be rewritten as

$$r(t) = g(t)x(t) + h(t)x(t-\tau) + n_w(t)$$

$$= A\sum_k x_k[g(t)p(t-kT) + h(t)p(t-\tau-kT)] + n_w(t) \qquad (3.31)$$

If we adopt the piece-wise-constant assumption, ie. the fading process g(t) and h(t) change so slowly that they keep roughly constant within one symbol interval, then r(t) can be written as

$$r(t) = A\sum_k x_k[g_k p(t-kT) + h_k p(t-\tau-kT)] + n_w(t) \qquad (3.32)$$

where g_k and h_k are the values of g(t) and h(t) at the $t = kT$ instants. The received waveform r(t) passes through the matched filter and the output y(t) is

$$y(t) = \frac{A}{\sqrt{N_o}}\sum_k x_k[g_k q(t-kT) + h_k q(t-\tau-kT)] + n(t) \qquad (3.33)$$

where q(•) is given by (2.4).

3.4.1 The Rectangular Pulse Shape

If p(t) is a rectangular pulse and then q(t) is a triangle pulse given in (2.6), according to [20], the k^{th} and $(k-1)^t h$ samples are

$$y_k = a_k x_{k-2} c_{k-1} c_k + b_k x_{k-2} c_{k-1} + n_k \qquad (3.34)$$

$$y_{k-1} = a_{k-1} x_{k-2} c_{k-1} + b_{k-1} x_{k-2} + n_{k-1} \qquad (3.35)$$

In the above equations, the $n_k's$ are a set of iid complex Gaussian variates, each having

a zero mean and a unit variance. On the other hand, the $a_k's$ and the $b_k's$ are samples of the two fading processes g(t) and h(t) in (2.15). Specifically,

$$a_k = \frac{A}{\sqrt{N_o}} g_k + \frac{A}{\sqrt{N_o}} h_k(1-\rho) \tag{3.36}$$

$$b_k = \frac{A}{\sqrt{N_o}} h_{k-1}\rho \tag{3.37}$$

Since we are going to use (3.10) - (3.12) in the performance evaluation, we have to first determine σ_k^2 and σ_{k-1}^2, the variances of the samples y_k and y_{k-1}, and $\sigma_{k,k-1}^2$, their corresponding covariance. According to [20], The received symbol SNR for each propagation path, in the absence of the other path, is given by:

$$\Gamma_g = \sigma_g^2 \frac{A^2}{N_o} \tag{3.38}$$

$$\Gamma_h = \sigma_h^2 \frac{A^2}{N_o} \tag{3.39}$$

$$\sigma_k^2 = \sigma_a^2 + \sigma_b^2 + \sigma_n^2 + 2Re[\sigma_{ab}^2 c_k] \tag{3.40}$$

$$\sigma_{k-1}^2 = \sigma_a^2 + \sigma_b^2 + \sigma_n^2 + 2Re[\sigma_{ab}^2 c_{k-1}] \tag{3.41}$$

and

$$\sigma_{k,k-1}^2 = \sigma_a^2 J_1 c_k + \Gamma_h \rho(1-\rho) + [\sigma_b^2 J_1 + \Gamma_h \rho(1-\rho) J_2 c_k] c_{k-1} \tag{3.42}$$

where $Re[\bullet]$ is used to denote the real part of a complex number,

$$\sigma_a^2 = \Gamma_g + (1-\rho)^2 \Gamma_h \tag{3.43}$$

is the variance of a_k in (3.36),

$$\sigma_b^2 = \rho^2 \Gamma_h \tag{3.44}$$

is the variance of b_k in (3.37),

$$\sigma_{ab}^2 = \Gamma_h (1 - \rho) \rho J_1 \tag{3.45}$$

is the covariance of a_k and b_k,

$$\sigma_n^2 = 1 \tag{3.46}$$

is the filtered noise power, and

$$J_k = J_0(2\pi k f_D T) \tag{3.47}$$

is the value of the zero-order Bessel function evaluated at k times the fade rate $f_D T$. Equations (3.38)-(3.47) can then substituted into (3.12) for calculating the pairwise error probability. Since the value of the pairwise error probability depends on the data symbol c_k and the interfering symbol c_{k-1}, the average pairwise error probability, obtained over all values of c_k and c_{k-1}, should be used in the union bound in (3.10). If the channel conditions are: a fade rate $f_D T = 0.004$ and a power split ratio $\alpha = 0$dB, the dependence of the performance of the CDD on the relative delay ρ is shown in Figure 3.8. It is obvious that Figure 3.8 is almost the same as Figure 3.2. We tried other channel conditions, the results are the same. So it can be concluded that the piecewise-constant assumption is valid at least for the rectangular pulse. Now let us see the case when the transmitted pulse is a raised-cosine pulse.

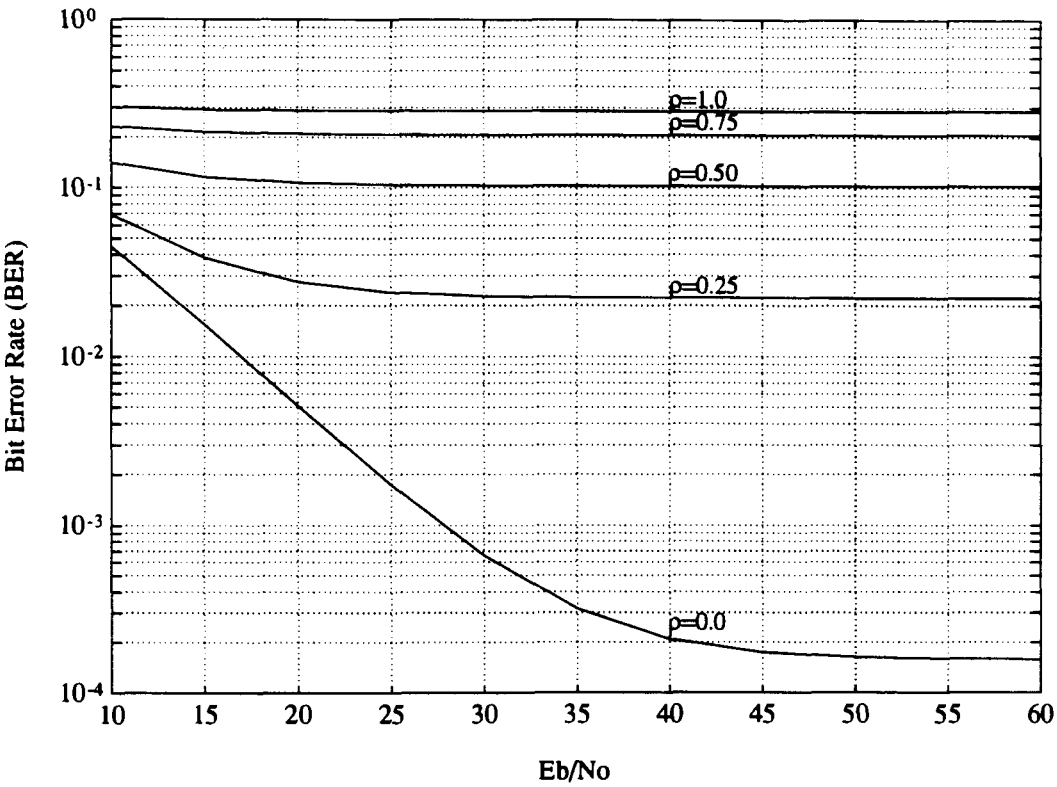

Figure 3.8: The BER vs $\frac{E_b}{N_o}$ curves of QPSK using a rectangular pulse at $f_D T = 0.004$ and $\alpha = 0dB$ with piece-wise-constant assumption. The various curves are $(1)\rho = 1.0$, $(2)\rho = 0.75$, $(3)\rho = 0.5$ $(4)\rho = 0.25$, and $(5)\rho = 0$.

3.4.2 The Raised-Cosine Pulse Shape

If q(t) is the raised-cosine pulse given by (2.8), the k^{th} and $(k-1)^th$ samples are

$$y_k = \frac{A}{\sqrt{N_o}}[g_k + h_k q(-\tau)]x_k + \frac{A}{\sqrt{N_o}} \sum_{n \neq k} x_n h_n q((k-n)T - \tau) + n_k \tag{3.48}$$

$$y_{k-1} = \frac{A}{\sqrt{N_o}}[g_{k-1} + h_{k-1} q(-\tau)]x_{k-1} + \frac{A}{\sqrt{N_o}} \sum_{n \neq k-1} x_n h_n q((k-1-n)T - \tau) + n_{k-1} \tag{3.49}$$

Using Caver's tight approximation shown in Appendix B and considering 16 most significant terms in (3.48) and (3.49), we can approximate σ_k^2 and σ_{k-1}^2, and $\sigma_{k,k-1}^2$ as

$$\overline{\sigma_k^2} = \sigma_a^2 + \Gamma_h \sum_{n=k-8}^{k+7} q^2((k-n)T - \tau) + 1 + 2Re[c_k \Gamma_h q(-\tau) q(T-\tau) J_1] \tag{3.50}$$

$$\overline{\sigma_{k-1}^2} = \sigma_a^2 + \Gamma_h \sum_{n=k-9}^{k+6} q^2((k-n)T - \tau) + 1 + 2Re[c_{k-1} \Gamma_h q(-\tau) q(T-\tau) J_1] \tag{3.51}$$

$$\overline{\sigma_{k,k-1}^2} = \sum_{n=k-8}^{k+6} \Gamma_h q((k-n)T - \tau) q((k-1-n)T - \tau) + c_k \sigma_a^2 J_1 \tag{3.52}$$

where σ_a^2 is

$$\sigma_a^2 = \Gamma_g + q(-\tau)^2 \Gamma_h \tag{3.53}$$

and Γ_g, Γ_h, and J_1 are all given by (3.38), (3.39), and (3.47). Substituting $\overline{\sigma_k^2}$, $\overline{\sigma_{k-1}^2}$, and $\overline{\sigma_{k,k-1}^2}$ for σ_k^2, σ_{k-1}^2 and $\sigma_{k,k-1}^2$ in (3.11), we obtain approximation to $\overline{P(c_k \rightarrow jc_k)}$

and $\overline{P(c_k \rightarrow -jc_k)}$ respectively and finally obtain the BER in equation (3.10). If the channel conditions are a fade rate $f_D T = 0.004$ and a power split ratio $\alpha = 0$dB, the dependence of the performance of the CDD on the relative delay ρ is shown in Figure 3.9, which is obviously almost the same as Figure 3.5. We tried other channel

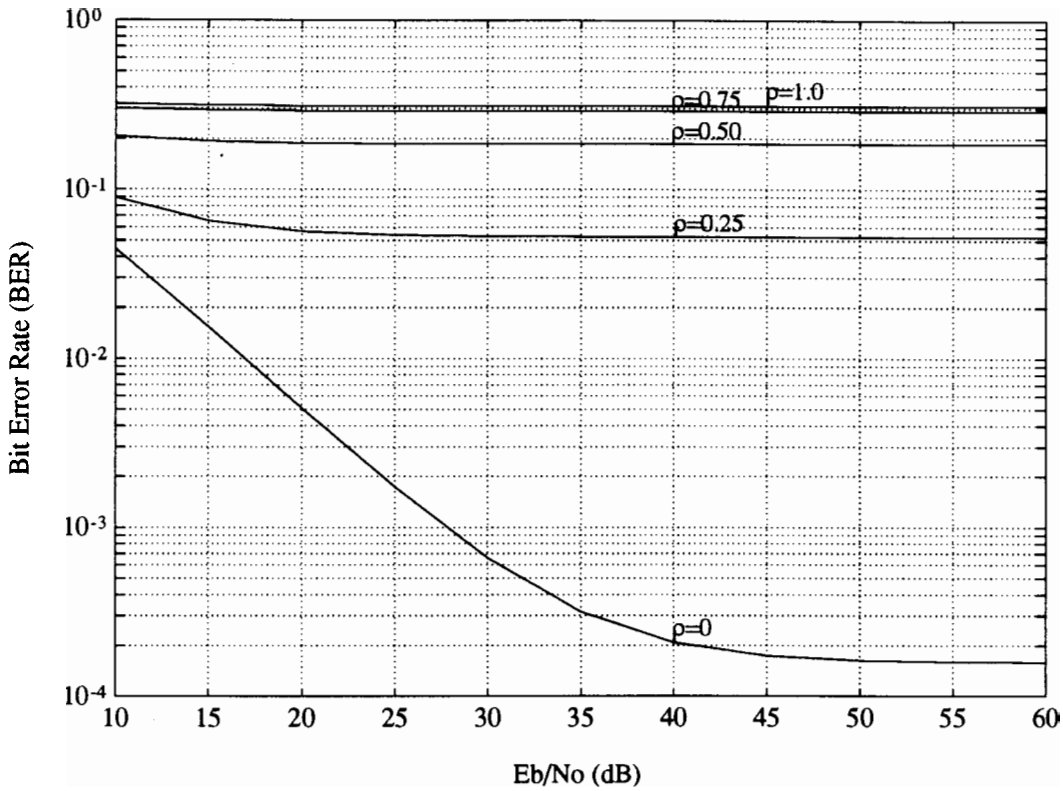

Figure 3.9: The BER vs $\frac{E_b}{N_o}$ curves of QPSK using a raised-cosine pulse with $\beta = 0.35$ at $f_D T = 0.004$ and $\alpha = 0dB$ with piece-wise-constant assumption. The various curves are $(1)\rho = 1.0$, $(2)\rho = 0.75$, $(3)\rho = 0.5$ $(4)\rho = 0.25$, and $(5)\rho = 0$.

conditions, the results are the same.

3.4.3 Explanations of the Assumption

The above two subsections, using numerical results, show that piece-wise-constant is an accurate and convenient assumption in the analysis of the CDD in the frequency-selective Rayleigh fading channel. In the following, we try to explain, through the derivation, why we have the coincidence.

First assuming the piece-wise-constant assumption, we calculate the correlation of the fading gains on two symbols as follows. Considering Equ. (3.33), also (2.16) and (2.17) and assuming that q(t) is an even function , the correlation of fading gains on any two symbols are

$$\begin{aligned}
\phi'_{k,l}(n,m) &= \frac{A^2}{N_o} E\ \{\ [g_n q((k-n)T) + h_n q((k-n)T-\tau)][g_m q((l-m)T) + h_m q((l-m)T-\tau \\
&= \frac{A^2}{N_o}[\sigma_g^2 q((k-n)T)q((l-m)T) + \sigma_h^2 q((k-n)T-\tau)q((l-m)T-\tau)] \\
&\quad \times J_o(2\pi f_D T(k-l)) \\
&= \frac{A^2}{N_o}\int_{\tau_1} G(\tau_1)q(\delta_1)q(\delta_2)J_o(2\pi f_D T(k-l))d\tau_1 \qquad (:
\end{aligned}$$

where δ_1 and δ_2 are given in (A.10) and $G(\tau_1)$ is the power-delay profile given in (2.13).

Then without the piece-wise-constant assumption, let us derive a reasonable approximation to the correlation of (A.11). Since we only deal with slow fading, the maximum Doppler frequency f_D is very small compared with the sampling rate $\frac{1}{T}$. Numerically, the fade rate $f_D T < 0.004$, much smaller than 1. Thus within the range of frequency $[-f_D, f_D]$, $P(f-\xi)$ can be simplified as

$$\begin{aligned} P(f-\xi) &= P(\xi-f) \\ &\approx P(\xi) - fP'(\xi) \end{aligned} \tag{3.55}$$

where $P(\bullet)$ is the frequency spectrum of the impulse response p(t) of the pulse shaping filter. The derivative of $P(\xi)$ is given by

$$P'(\xi) = \frac{dP(\xi)}{d\xi} \tag{3.56}$$

and therefore $A(f,\delta)$ in (A.11) can be approximated as

$$A(f,\delta) \approx \int_{-f_D}^{f_D} P^2(\xi) e^{j2\pi\xi\delta} d\xi - f \int_{-f_D}^{f_D} P(\xi)P'(\xi) e^{j2\pi\xi\delta} d\xi \tag{3.57}$$

The combined-transmitter-and-receiver filter q(t), defined in (2.4), has a frequency response of

$$Q(\xi) = P^2(\xi) = F[q(t)] \tag{3.58}$$

and its derivative is

$$Q'(\xi) = 2P(\xi)P'(\xi) = F[-j2\pi t q(t)] \tag{3.59}$$

where $F[\bullet]$ represents the Fourier transform. This means $A(f,\delta)$ in the range $-f_D \leq f \leq f_D$ can be written as

$$A(f,\delta) \approx q(\delta)(1 + j\pi f\delta) \tag{3.60}$$

The approximation shown in (3.60) coincides with Figure A.1 and Figure A.2. If q(t) is a raised-cosine pulse, fixing $f = 0$, $A(0,\delta)$ gives the raised-cosine pulse shape, which is in accordance with Figure A.1. On the other hand, fixing $\delta = \frac{3}{2}T$ and being in the range of $-0.004 \leq f \leq 0.004$, the real part of $A(0,\frac{3}{2}T)$ is nearly constant and the imaginary part is a line segment, which is in accordance with Figure A.2.

With the approximation in (3.60) and the condition that

$$\pi f_D T J_o'[2\pi f_D(k-l)] \;<<\; J_o[2\pi f_D T(k-l)] \tag{3.61}$$

$$(\pi f_D T)^2 J_o''[2\pi f_D(k-l)] \;<<\; J_o[2\pi f_D T(k-l)] \tag{3.62}$$

due to very small $f_D T$, the correlation in (A.3) is simply:

$$\begin{aligned}
\phi_{k,l}(n,m) &\approx \frac{A^2}{N_o}\int_{\tau_1} G(\tau_1)q(\delta_1)q(\delta_2)[J_o(2\pi f_D T(k-l)) \\
&\quad +(n-k-m+l)(\pi f_D T)J_o'(2\pi f_D T(k-l)) \\
&\quad -(n-k)(m-l)(\pi f_D T)^2 J_o''(2\pi f_D T(k-l))]d\tau_1 \\
&\approx \frac{A^2}{N_o}\int_{\tau_1} G(\tau_1)q(\delta_1)q(\delta_2)J_o(2\pi f_D T(k-l))d\tau_1
\end{aligned} \tag{3.63}$$

It is obvious that the approximated correlation given above is in accordance with the correlation given by (3.54) derived from the piece-wise-constant assumption.

Summarizing the derivation above, when the maximum Doppler frequency f_D is very small compared with the sampling rate $\frac{1}{T}$, ie. when **the fade rate** $f_D T << 1$, we can simplify P(f) as shown in (3.55) and subsequently obtain the simplification of $A(f, \delta)$ as shown in (3.60). Again due to $f_D T << 1$, two conditions are obtained in (3.61) and (3.62), then we come to the same correlation equation as the one derived from the piece-wise-constant assumption. Therefore we can conclude that **when the fading process is slow enough, the piece-wise-constant is a reasonable and good assumption.**

3.5 Optimal Sampling Time Instants

In [15], Cavers points out that using a raised-cosine pulse, the optimal sample timing for the CDD is at $t = kT + t_o$, where t_o can be obtained from equation below (Equ. (A.3) in [15])

$$\int_0^{\tau} G(\tau_1) sin(\frac{2\pi(t_o - \tau_1)}{T}) d\tau_1 = 0 \tag{3.64}$$

where $G(\tau_1)$ is the power delay profile. For the flat fading channel, $t_o = 0.0$, ie. integer sample timing is optimal. For the two-ray frequency-selective fading channel, when equal power split, ie. $\alpha = 1$, t_o is one half of the delay between the two rays, ie. $t_o = \frac{\rho}{2} T$; when $\alpha > 1$, t_o is less than one half of the delay spread. In general the k^{th}

received sample y_k in (2.26) can be written as

$$y_k = y(kT + t_o) \tag{3.65}$$

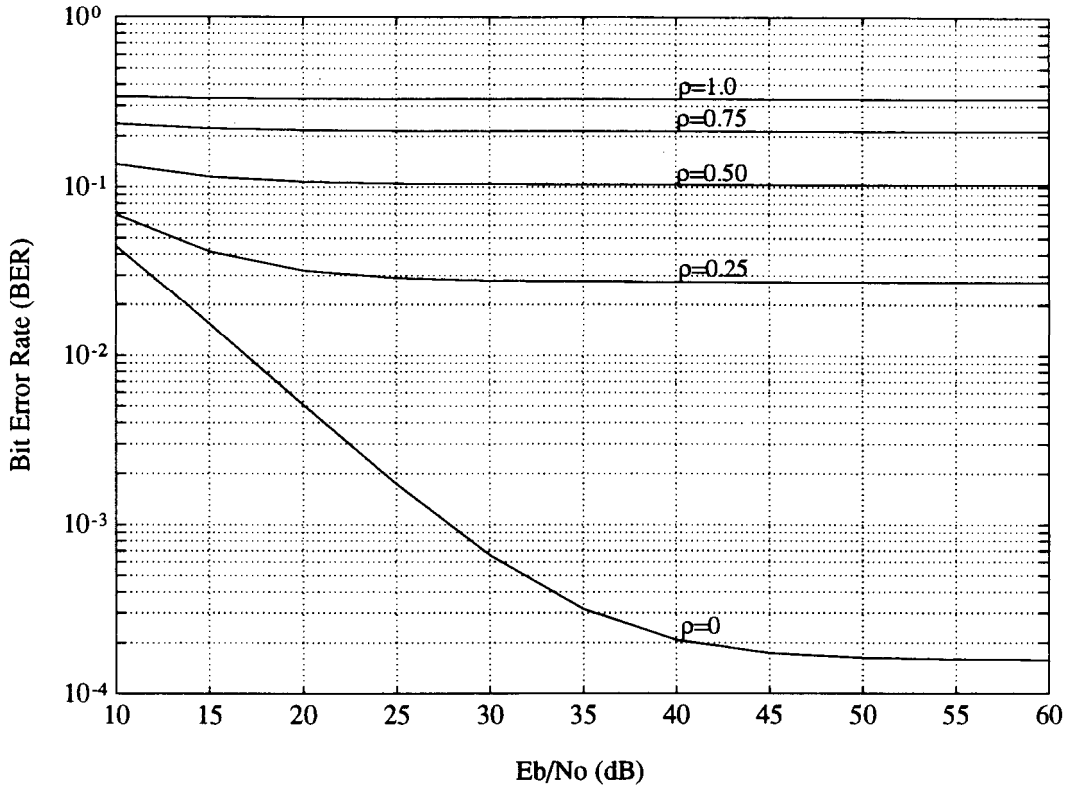

Figure 3.10: The BER vs $\frac{E_b}{N_o}$ curves of QPSK using a raised-cosine pulse with $\beta = 0.35$ at $f_D T = 0.004$ and $\alpha = 0dB$. The received samples are obtained at the optimal sampling instants. The various curves are $(1)\rho = 1.0$, $(2)\rho = 0.75$, $(3)\rho = 0.5$ $(4)\rho = 0.25$, and $(5)\rho = 0$.

Figure 3.10 illustrates the performance of the CDD using a raised-cosine pulse when the received samples are obtained at the optimal sampling instants. Compared with Figure 3.5 where the same channel conditions and the same transmitted pulse are used, we found that the BER can be reduced by as much as $\frac{1}{2}$ if optimal sample timing, rather than integer sample timing, is used. The reason why the performance

of the CDD can be improved by using optimal sampling is that the desired QPSK symbol has a larger influence on the variance of the corresponding received sample.

Although the numerical results of the CDD using optimal sample timing are better than those using integer sample timing, the methods to analyze the performance of the CDD and major conclusions shown in this chapter do not depend on the sampling instants. For simplicity, we only consider integer sample timing for MSDD in the next chapter.

Chapter 4

Performance of Multi-Symbol Differential Detection in a Frequency-Selective Rayleigh Fading Channel

As indicated in chapter 3, under some channel conditions, the performance of the conventional differential detector (CDD) is not acceptable at the receiver because the BER is above 10^{-1}. This chapter discusses using a multi-symbol differential detector (MSDD) for the decoder to improve the performance of the receiver. It is illustrated that the MSDD works much better than the CDD under most of the channel conditions and that MSDD is a robust detector using a rectangular pulse or a square-root raised-cosine pulse with $\beta = 1$ as the transmitted pulse p(t).

The first section describes in detail how the MSDD works, with $N = 5$ as an example. However, we do not restrict our attention to any specific transmitted pulse. The second section focuses on the rectangular transmitted pulse, and the third section considers the square-root raised-cosine transmitted pulse.

4.1 General Description of the MSDD

As shown in chapter 2, the MSDD uses more than two received samples to make each decision. The MSDD performs better than the CDD because more received samples provide more accurate channel information to the decoder so that the decoder can make decisions more correctly. Figure 2.4 (b) shows the structure of the MSDD decoder.

In this chapter, we use $N = 5$ received samples to demonstrate how the MSDD works although the method is also available for any other values of N. For the case of $N = 5$ and $N_1 = 3$, , the received five-sample vector is

$$\mathbf{Y} = \begin{bmatrix} y_{k-2} \\ y_{k-1} \\ y_k \\ y_{k+1} \\ y_{k+2} \end{bmatrix} \tag{4.1}$$

where y_{k-2}, y_{k-1}, y_k, y_{k+1}, and y_{k+2} are the received signal in (2.25) sampled at t =(k-2)T, (k-1)T, kT, (k+1)T, and (k+2)T respectively and can be easily determined by (2.26).

If we know the statistical channel information such as $G(\tau_1)$, f_DT and $\frac{E_b}{N_o}$ defined in (2.13), (2.12), and (2.24) respectively, the correlation matrix $\mathbf{\Phi_{yy}(C)}$ in (2.37) can then be determined. As mentioned in chapter 3, the piece-wise-constant assumption is a very useful and reliable assumption to model the fading channel as long as f_DT is much smaller than 1. Consequently this is the assumption we use in this chapter to determine the correlation matrix $\mathbf{\Phi_{yy}(C)}$ in (2.37).

When making a decision, the MSDD calculates metrics $M(\mathbf{C})$'s for each possible $\mathbf{C}$ vector whose first L_1 symbols are the same as the L_1 previous fed back symbols, and selects the $\mathbf{C}$ whose $M(\mathbf{C})$ is the smallest. Subsequently, the $(L_1+1)^{th}$ symbol of the corresponding $\mathbf{C}$ is chosen as the decoded symbol.

4.1.1 Decision Feedback

The reasons why DF is important in the MSDD is following: First, the DF gets rid of those Cś whose corresponding $\Phi_{yy}(\mathbf{C})$ results in the same metrics due to symmetrical reasons under some channel conditions. Thus the performance of the decoder is improved greatly. For example, considering the following set of channel conditions:

$$\alpha = 1.0 \qquad \rho = 1.0$$
$$\frac{E_b}{N_o} = 10dB \quad f_DT = 0.004$$

the transmitted pulse p(t) is rectangular, equivalently q(t) is a triangle pulse given by (2.6). There are two terms in each element in $\mathbf{Y}$, which means $M_1 = 1$ and $M_2 = 0$ in (2.32). The lengths of $\mathbf{X}$ and $\mathbf{C}$ are L=6 and L-1=5 respectively. There are $L_1 = 2$ fed back symbols. The vector $\mathbf{C}$ contains five successive data symbols: c_{k-2}, c_{k-1}, c_k, c_{k+1}, and c_{k+2}. We found that $\mathbf{C}_1$ = (1, j, 1, j, 1) and $\mathbf{C}_2$ = (j, 1, j, 1, j) generate the same matrix, ie. $\mathbf{\Phi_{yy}}(\mathbf{C}_1) = \mathbf{\Phi_{yy}}(\mathbf{C}_2)$. But the MSDD can work only if each $\mathbf{C}$ vector generates its unique $\mathbf{\Phi_{yy}}(\mathbf{C})$.

In order to resolve this ambiguity, decision feedback (DF) is suggested in the MSDD. The MSDD keeps the two previous decoded symbols in the buffer. During decoding of the current symbol, the MSDD only calculates and compares the metrics M($\mathbf{C}$)'s for those $\mathbf{C}$ vectors whose first two symbols are identical to the two previous decoded symbols. Then the metric related to $\mathbf{C}_1$ = (1, j, 1, j, 1) and $\mathbf{C}_2$ = (j, 1, j, 1, j) will obviously not be used at the same time. Consequently, the ambiguity is resolved.

Another advantage of DF is that it greatly reduces the computational complexity of the MSDD. In the above example, the MSDD without DF has to calculate **1024** metrics. But the MSDD with DF needs only to calculate **64** metrics and also has better performance. From this illustrative example, we can see the importance of DF in the MSDD.

For given number of DF symbols, the location of the decoded symbol in the $\mathbf{C}$

vector influences the performance of MSDD. From simulation tests, we find that making a decision on the middle symbol is better than on the end symbol in the selected C.

4.1.2 Assumptions and Notations

It is very difficult to determine the performance of the MSDD with DF just by analysis. In this chapter, the received signal is sampled at the integer sample timing. We adopt the piece-wise-constant assumption and use simulation to determine the performance of the MSDD. In Section 3.5, we discuss the optimal sampling time for the CDD. As for the case of the MSDD, we are not sure where the optimal sampling instants should be. However, we can easily predict that the results of MSDD using the received samples obtained at the optimal sample timing are equal to or better than those numerical results shown below. Since we are more interested in how the techniques of the MSDD improves the performance of communication systems in this chapter, we just sample the received signal at integer sample timing. The techniques of MSDD shown in this chapter does not depend on the sampling instants. On the other hand, one of the advantages of using the integer sample timing is that the received sample has fewer ISI terms and hence the simulation process can be simpler.

Once again, we adopt the two-ray channel model to represent the frequency-selective Rayleigh fading channel. In the following sections, the normalized 95% confidence interval $[0.8, 1.2]$ is used in the simulations to make sure that the simulation results are accurate enough. In the simulation, we generate a long sequence of random binary bits at the transmitter, modulate them using QPSK, transmit the

QPSK signal over the frequency-selective fading channel, decode the received signal using a MSDD, compare the decoded binary sequence with the transmitted one, and finally count the number of error bits calculating the corresponding BER. According to [16], the definition of the 95% confidence interval is given below:

$$\bar{X} = \frac{\sum X_i}{N} \tag{4.2}$$

$$c.i. = \bar{X} * (1 \pm \frac{y}{\bar{X}}) \tag{4.3}$$

$$y = 1.96 * \frac{s}{\sqrt{N-1}} \tag{4.4}$$

$$s = \sqrt{\frac{\sum (X_i - \bar{X})^2}{N}} \tag{4.5}$$

where $\bar{X}$ is the estimated BER; when the i^th decoded bit is the same as the i^{th} transmitted bit, $X_i = 0$, otherwise $X_i = 1$; N is the number of the total transmitted bits; c.i. is the 95 % confidence interval; $1 - \frac{y}{\bar{X}}$ and $1 + \frac{y}{\bar{X}}$ are the lower and upper limits of the normalized confidence interval respectively; s is the standard derivation.

Before we discuss the performance of the MSDD, some terminology used in the following must be introduced.

The MSDD needs some statistical channel parameters to set up the decoding metrics. The statistical channel parameters used in the MSDD are called the **chosen channel conditions** while those statistical channel parameters in the real channel are referred to as the **actual channel conditions.** When the chosen channel conditions are the same as the actual channel conditions, we refer to the MSDD as **matched.** As

mentioned before, the actual channel conditions are often very difficult to estimate. When the chosen channel conditions are different from the actual channel conditions, we refer to the MSDD as **mismatched**.

4.2 The Rectangular Pulse Shape

In this section, we will consider a rectangular pulse with a pulse duration T as the transmitted pulse p(t). This means the corresponding q(t) is the triangle pulse given in (2.6). In chapter 3, it is shown that the CDD breaks down under certain channel condition, see Figure 3.2. In this section, we see that the performance improvement brought along by the MSDD.

Here we consider a MSDD with $N = 5$. The k^{th} received sample y_k is shown in (3.13). Expressions for the other four samples y_{k-2}, y_{k-1}, y_{k+1}, and y_{k+2} are similar. Each of the five samples contains one interference symbol. Equivalently, we set $N = 5$, $N_1 = 3$, $M_1 = 1$ and $M_2 = 0$ in (2.32). Their variances and covariances, shown below, depend on only $L-1 = 5$ data QPSK symbols (c_{k-2}, c_{k-1}, c_k, c_{k+1}, c_{k+2})

$$\begin{aligned}\sigma_m^2 &= E[|y_m|^2] \\ &= 1 + \phi_{m,m}(m,m) + \phi_{m,m}(m-1,m-1) + \phi_{m,m}(m,m-1)c_m + \phi_{m,m}(m-1,m)c_m^*;\end{aligned} \tag{4.6}$$

$$\sigma_{m,n}^2 = E[y_m * y_n]$$

$$
\begin{aligned}
&= \phi_{m,n}(m,n)z_{mn} + \phi_{m,n}(m,n-1)z_{m,n-1} \\
&\quad + \phi_{m,n}(m-1,n)z_{m-1,n} + \phi_{m,n}(m-1,n-1)z_{m-1,n-1}; \qquad (4.7) \\
&\quad \text{where } m,n \in \{k-2,k-1,k,k+1,k+2\}
\end{aligned}
$$

where $\phi_{m,n}(\bullet,\bullet)$ can be evaluated by (3.63) and $z_{m,n}$ is

$$
\begin{aligned}
z_{m,n} &= x_m \cdot x_n^* \\
&= \begin{cases} c_m \cdot c_{m-1} \cdots c_{n+1} & \text{when } m > n \\ 1 & \text{when m=n} \\ c_n^* \cdot c_{n-1}^* \cdots c_{m+1}^* & \text{when } m < n \end{cases} \qquad (4.8) \\
&\quad \text{where } m,n \in \{k-2,k-1,k,k+1,k+2\}
\end{aligned}
$$

$\mathbf{\Phi_{yy}(C)}$'s composed of σ_m^2 and $\sigma_{m,n}^2$ given above are exact ones, and thus the decoding metrics M(C)'s are the optimal decoding metrics. With (4.6) and (4.7), the MSDD calculates the inverses and the determinants of 1024 $\mathbf{\Phi_{yy}(C)}$'s and sets up the code book at the receiver. We show next the performance of the matched MSDD, followed by that of the mismatched MSDD.

4.2.1 The Matched MSDD

Consider a channel with $f_D T = 0.004$, $\alpha = 1$, and $0 \leq \rho \leq 1$. If we have information about these statistics, then as shown in Figure 4.1, the performance of the MSDD is very good. Compared with the performance of the CDD under the same channel conditions, see Figure 3.2, the matched MSDD performs much better, especially

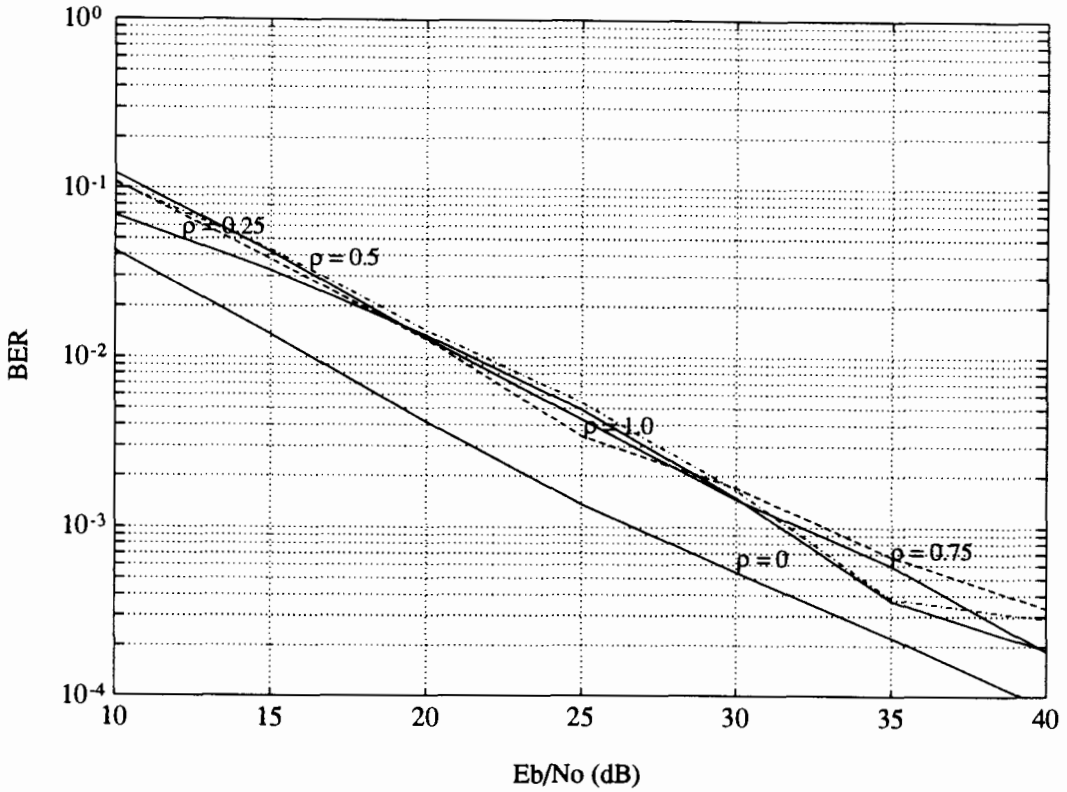

Figure 4.1: The BER of the matched MSDD vs $\frac{E_b}{N_o}$ curves of QPSK using a rectangular pulse. The channel conditions are: $f_D T = 0.004$, $\alpha = 0dB$, and $(1)\rho = 1.0$, $(2)\rho = 0.75$, $(3)\rho = 0.5$ $(4)\rho = 0.25$, and $(5)\rho = 0$ corresponding to various curves respectively.

under those channel conditions with a large relative delay ρ. There is no noticeable irreducible error floor within the range of bit SNR of interests. We also find that the performance of the matched MSDD changes little when the relative delay ρ is nonzero while the performance is about 5 dB better in the **flat fading channel** ($\rho = 0$) than that in the **selective fading channel**. We tried other channel conditions and the results are similar. So we conclude that the performance of the matched MSDD is almost independent of the channel conditions in the selective fading channel when the transmitted pulse is rectangular.

4.2.2 The Mismatched MSDD

Now, let us consider the case of a mismatched MSDD. This corresponds to the case in which the channel conditions assumed in the MSDD are different from those in the actual channel. When we can not estimate the statistical information of the channel, a mismatched MSDD is more practical. Recall once again, the **actual channel conditions** are the channel conditions in the real channel while the **chosen channel conditions** refers to the channel conditions assumed in the MSDD decoder.

A Mismatch in ρ

We at first study the effect of a mismatch in relative delay ρ, see Figure 4.2. The decoder assumes a frequency-selective fading channel with $\rho = 0.5$ while the actual delay differences are ρ =1.0, 0.75, 0.5, 0.25, and 0 respectively. The mismatched decoder still provides acceptable performance. It is observed that the performance

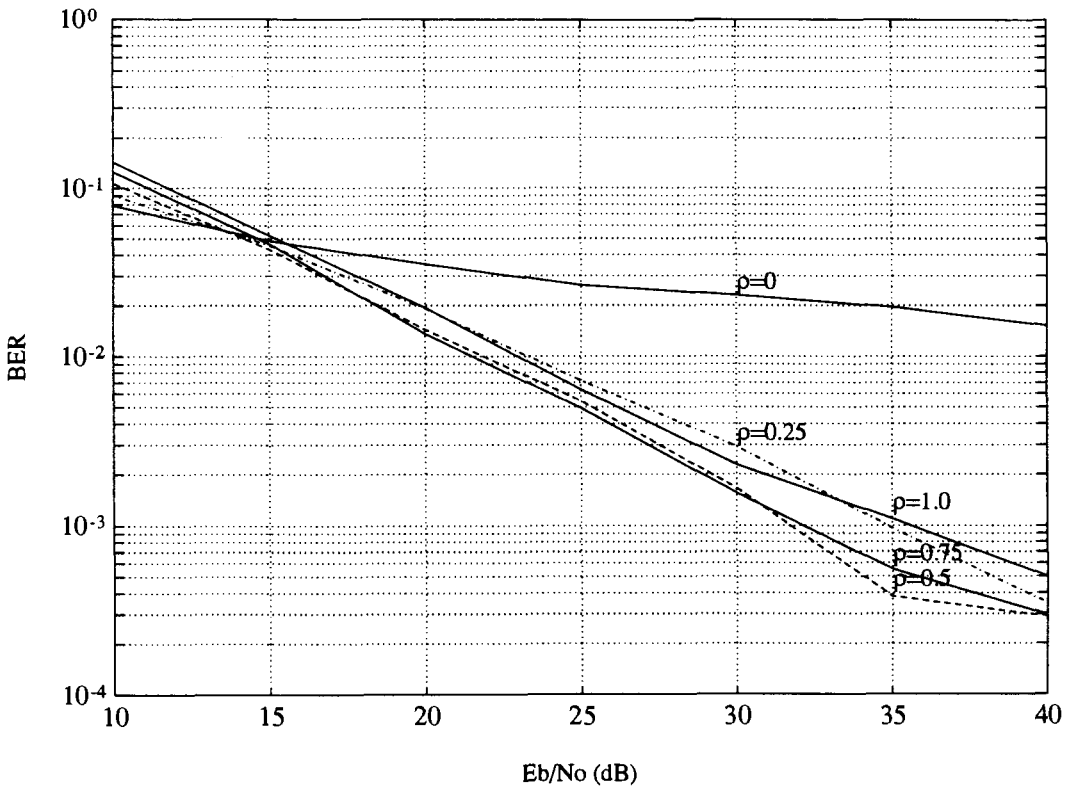

Figure 4.2: The BER of the mismatched MSDD vs $\frac{E_b}{N_o}$ curves of QPSK using a rectangular pulse. The chosen channel conditions in the MSDD are: $f_DT = 0.004$, $\alpha = 1.0$ and $\rho = 0.5$ while the actual channel conditions are $f_DT = 0.004$, $\alpha = 1.0$, and the relative delay: $(1)\rho = 1.0$, $(2)\rho = 0.75$, $(3)\rho = 0.5$ $(4)\rho = 0.25$, and $(5)\rho = 0$ corresponding to various curves respectively.

is pretty good as long as there is ISI in the received samples while the performance is barely acceptable when the chosen channel conditions are mismatched to the flat fading channel. Also it is obvious that the smaller the mismatch to the actual relative delay ρ is, the more closely the performance approaches that of the matched MSDD. The reason why we choose the relative delay $\rho = 0.5$ as the chosen condition is that it is the midpoint in the range $[0, 1]$ of the relative delay ρ.

A Mismatch in α

Figure 4.3 illustrates the effect of a mismatch in the power split ratio α. The MSDD assumes equal power split, ie. $\alpha = 1.0$, while the actual power split ratios are α =10000, 1000, 100,10, and 1 respectively. All the other statistical channel parameters (the Doppler frequency $f_D T = 0.004$, the relative delay $\rho = 0.5$) are matched to the actual channel conditions. As we can see, the performance of the mismatched MSDD is acceptable: the error floors are around 10^{-2} or lower. It is also seen that the bigger the mismatch, the worse the performance. The channel is close to the flat fading channel when $\alpha = 10000$, thus the performance is very close to the case of mismatch to the flat fading shown in Figure 4.2. The error floors of all curves in Figure 4.3 are all below 2×10^{-2}. The reason why this is important is that, as shown in Chapter 5, the performance of communication systems can be improved further through channel coding if the raw BER is below 10^{-1}.

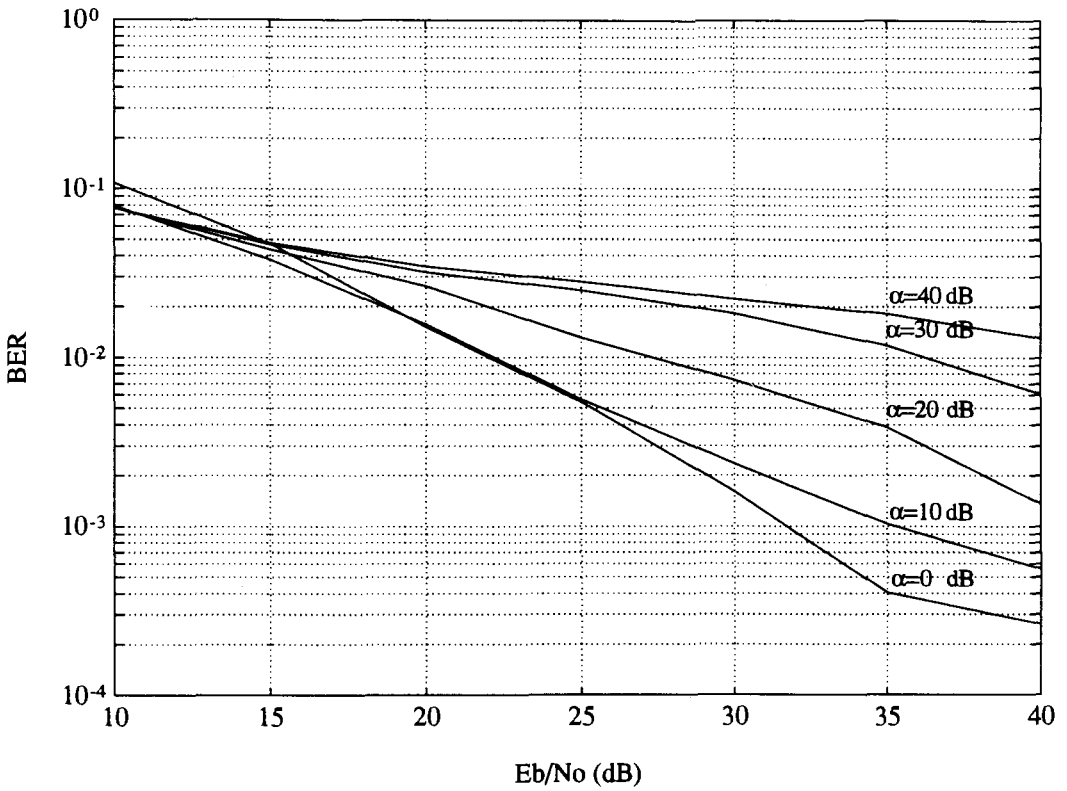

Figure 4.3: The BER of the mismatched MSDD vs $\frac{E_b}{N_o}$ curves of QPSK using a rectangular pulse. The chosen channel conditions in the MSDD are: $f_DT = 0.004$, $\alpha = 1.0$ and $\rho = 0.5$ while the actual channel conditions are $f_DT = 0.004$, $\rho = 1.0$, and the power split ratio: $(1)\alpha = 10000$, $(2)\alpha = 1000$, $(3)\alpha = 100$ $(4)\alpha = 10$, and $(5)\alpha = 1$ corresponding to various curves respectively.

A Mismatch in f_DT

Now let us examine a mismatch in the fade rate f_DT. In Figure 4.4, the chosen power

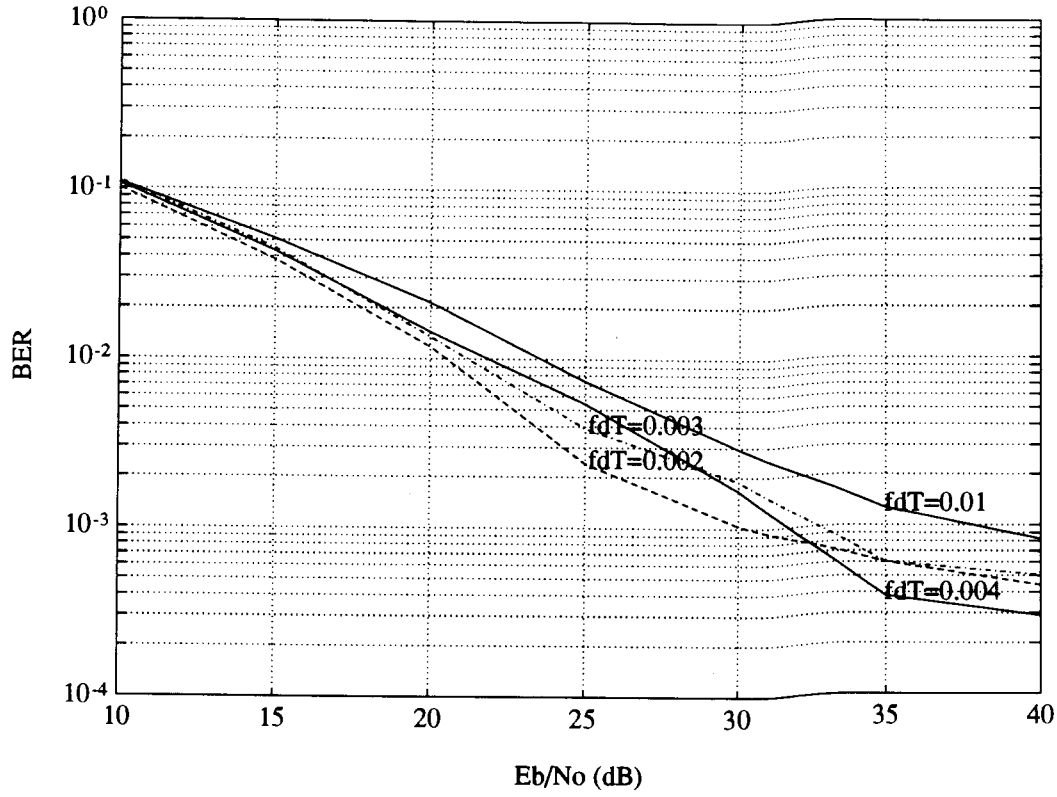

Figure 4.4: The BER of the mismatched MSDD vs $\frac{E_b}{N_o}$ curves of QPSK using a rectangular pulse. The chosen channel conditions in the MSDD are: $f_DT = 0.004$, $\alpha = 1.0$ and $\rho = 0.5$ while the actual channel conditions are $\alpha = 1.0$, $\rho = 0.5$, and the fade rates are: $(1)f_DT = 0.002$ $(2)f_DT = 0.003$, $(3)f_DT = 0.004$, and $(4)f_DT = 0.01$ corresponding to various curves respectively.

split ratio of $\alpha = 1$ and the chosen relative delay of $\rho = 0.5$ are matched to those in the actual channel. The chosen fade rate is $f_DT = 0.004$ while the actual fade rate is $f_DT = 0.002$, 0.003, 0.004, and 0.01 respectively. It is observed that if the actual fade rates are slower than the chosen one, the performance of MSDD is almost the same

as the matched case. On the other hand, if the actual fade rates is higher than the chosen one, performance degradation is a result. According to the carrier frequency and the symbol rate given in chapter 2, $fdT = 0.01$ corresponds to the case when the speed of the vehicle is) km/h, which is well beyond the normal speed of all vehicles.

A Mismatch in $\frac{E_b}{N_o}$

Finally let us examine a mismatch in the $\frac{E_b}{N_o}$. In Figure (4.5), only the $\frac{E_b}{N_o}$ is mismatched. It is observed that for any given actual channel $\frac{E_b}{N_o}$, the matched MSDD works better than the mismatched MSDD. The larger the mismatch in $\frac{E_b}{N_o}$ is, the worse the performance of MSDD is. The mismatch between the chosen and actual $\frac{E_b}{N_o}$ results in the irreducible error floor. But if the target BER is 10^{-2}, the performance of the mismatch MSDD in the SNR is still acceptable.

Several Mismatched channel Parameters

In the above four examples, we study the performance of the MSDD when only one channel parameter is mismatched between the chosen and the actual channel parameters.

Furthermore, Figure 4.6 shows the performance of the MSDD under the assumption that three chosen channel parameters, α, ρ, $f_D T$, are mismatched to the actual channel conditions. As we can see, the performance of the MSDD is still acceptable, around 10^{-2} or less.

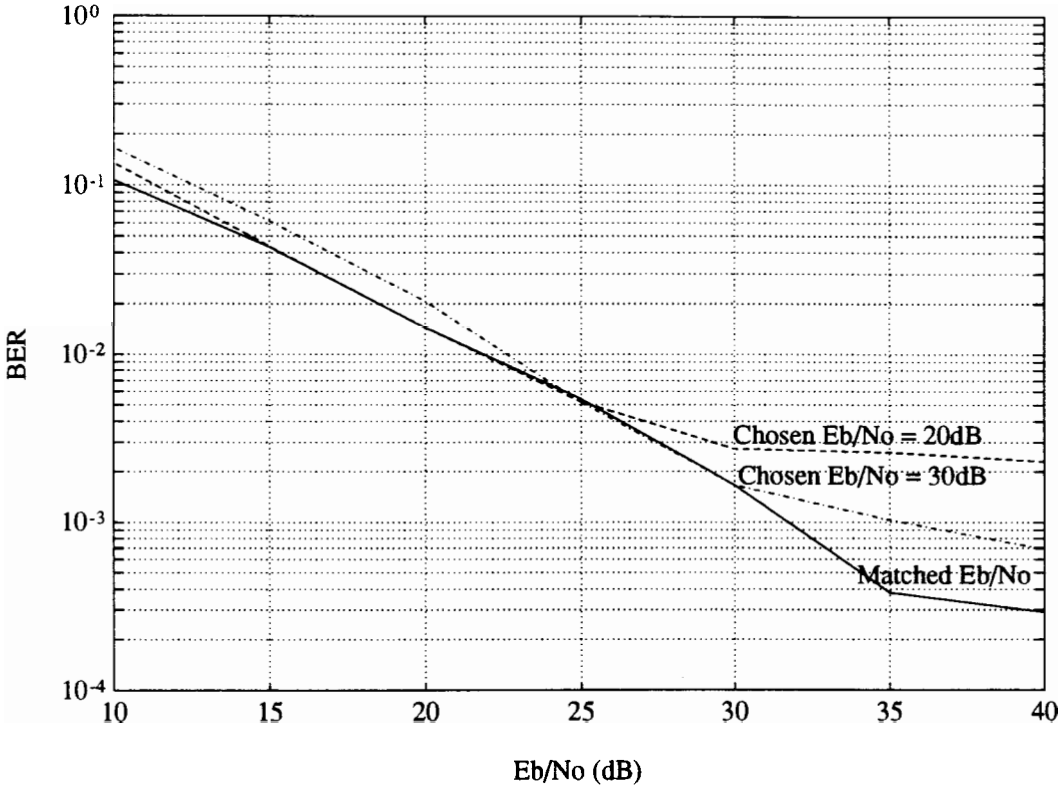

Figure 4.5: The BER of the mismatched MSDD vs $\frac{E_b}{N_o}$ curves of QPSK using a rectangular pulse. The chosen channel conditions in the MSDD are: $f_D T = 0.004$, $\alpha = 1.0$ and $\rho = 0.5$, which are the same as those in the actual channel. But the chosen $\frac{E_b}{N_o}$'s are set to: (1) $\frac{E_b}{N_o} = 20dB$, (2) $\frac{E_b}{N_o} = 20dB$, (3) matching to the actual $\frac{E_b}{N_o}$.

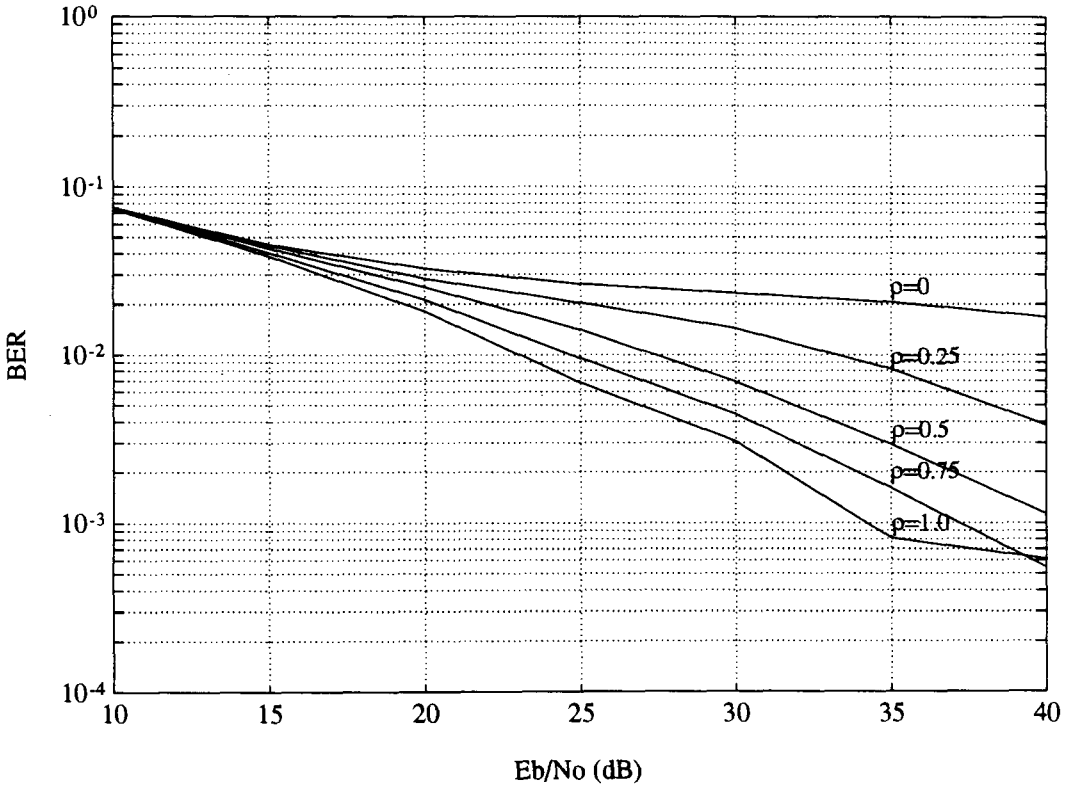

Figure 4.6: The BER of the mismatched MSDD vs $\frac{E_b}{N_o}$ curves of QPSK using a rectangular pulse. The chosen channel conditions in the MSDD are: $f_DT = 0.004$, $\alpha = 1.0$ and $\rho = 0.5$ while the actual channel conditions are $f_DT = 0.002$, $\alpha = 100.0$, and the relative delay: $(1)\rho = 0$, $(2)\rho = 0.25$, $(3)\rho = 0.5$ $(4)\rho = 0.75$, and $(5)\rho = 1.0$ corresponding to various curves respectively.

Thus it can be concluded that under the condition of a rectangular transmitted pulses, the MSDD is a robust detector for communications over frequency-selective fading channels. The irreducible error floors are at most around 10^{-2}. No error propagation is found with decision feedback.

4.3 The Square-Root Raised-Cosine Pulse Shape

While a rectangular pulse requires a big bandwidth, a raised-cosine pulse has finite bandwidth and thus it is more useful in practice. In this section, we consider a square-root raised-cosine pulse as the transmitted pulse p(t). The equivalent q(t) is the raised-cosine pulse given in (2.8). The roll-off parameter considered is $\beta = 1.0$ or $\beta = 0.35$. It will be shown that, compared with the CDD in chapter 3, there is a big improvement to the error performance by using MSDD as long as a suitable transmitted pulse (ie. β) is chosen.

Although we still use five received samples y_{k-2}, y_{k-1}, y_k, y_{k+1}, and y_{k+2} in the MSDD, each of the five samples contains **one** desired QPSK symbol and **many** interference symbols. We use 16 terms to respresent each received sample in (2.29) and set $N = 5$, $N_1 = 3$, $M_1 = 8$ and $M_2 = 7$. Then the length of $\mathbf{C}$ is $L - 1 = 19$ and there are 4^{19} possible $\mathbf{C}$ vectors. Thus it is impractical to implement directly the MSDD introduced in Chapter 2 when using a square-root raised-cosine pulse.

When using a square-root raised-cosine pulse, one way to make the MSDD work is to reduce the effective length of $\mathbf{C}$. From Appendix B, we know that among the

symbols in $\mathbf{C}=(c_{k-10}, \ldots, c_{k-2}, c_{k-1}, c_k, c_{k+1}, c_{k+2}, \ldots, c_{k+9})$, the five symbols in $\mathbf{C}'$ given by (B.3) are the dominant symbols which determine the variances and covariances in the correlation matrix $\mathbf{\Phi_{yy}(C)}$, see (B.13) and other symbols in $\mathbf{C}$ have just minor effects on $\mathbf{\Phi_{yy}(C)}$.

Using (B.5), (B.8), (B.9) and (B.12), the variance and covariance are shown below:

$$\begin{aligned}\sigma_m^2 &= E[|y_m|^2] \\ &\approx 1 + \sum_{p=k-3}^{k+2}\sum_{q=k-3}^{k+2} \phi_{m,m}(p,q) z_{p,q} + \sum_{p=m-8 \& p \notin [k-3,k+2]}^{m+7} \phi_{m,m}(p,p) \qquad (4.9)\end{aligned}$$

$$\begin{aligned}\sigma_{m,n}^2 &= E[y_m * y_n^*] \\ &\approx \sum_{p=k-3}^{k+2}\sum_{q=k-3}^{k+2} \phi_{m,n}(p,q) z_{p,q} + \sum_{p=max[m-8,n-8] \& p \notin [k-3,k+2]}^{min[m+7,n+7]} \phi_{m,n}(p,p) \qquad (4.10)\end{aligned}$$

where $\quad m, n \in \{k-2, k-1, k, k+1, k+2\}$

where $\phi_{m,n}(\bullet,\bullet)$ can be evaluated by (3.63) and $z_{p,q}$ is given by (4.8). Substituting (4.9) and (4.10) for σ_m^2 and $\sigma_{m,n}^2$ in (2.39), we obtain $\mathbf{\Phi_{yy}(C')}$. The rest detection procedure is similar to that using a rectangular pulse. Since the length of $\mathbf{C}'$ is five, inverses and determinants of 1024 correlation matrix are calculated and stored in the codebook. When decoding, two decoded symbols $\hat{c}_{k-2}$ and $\hat{c}_{k-1}$ are fed back. We calculate the decoding metric in (2.37) and decode the desired QPSK symbol c_k in the k^{th} received sample y_k.

One thing worth mentioning is that $\mathbf{\Phi_{yy}(C')}$ obtained from (4.9) and (4.10) is the approximation and just represents the correlation matrix determined by $\mathbf{C}$ roughly,

therefore the $\mathbf{M}(\mathbf{C}')$ using raised-cosine transmitted pulses is not the optimal decoding metric. However, the $\mathbf{M}(\mathbf{C}')$'s obtained are good approximation to the optimal ones, see Appendix B. Thus the performance of the matched MSDD is still very good and the acceptable performance of the mismatched MSDD depends on the transmitted pulse shape.

4.3.1 The Matched MSDD

Just like in Section 4.2, we first consider the matched MSDD. If the statistical channel information is known at the receiver, the performance of the MSDD using a raised-cosine pulse with a roll-off parameter $\beta = 1.0$ is shown in Figure 4.7. The channel conditions are: $f_D T = 0.004$, $\alpha = 1$, and $\rho = 0$, 0.25, 0.5, 0.75, 1.0 respectively. It is observed in Figure 4.7 that the matched MSDD using the raised-cosine pulse with $\beta = 1.0$ works almost as well as the matched MSDD using the rectangular pulse. If the transmitted pulse is changed to the raised-cosine pulse with $\beta = 0.35$, see Figure 4.8, the performance is similarly good. Thus summerizing the performance of the matched MSDD shown above, we can say that as long as the statistical channel information is known at the decoder, the MSDD works well no matter what the transmitted pulses and the channel conditions are.

4.3.2 The Mismatched MSDD

As indicated in chapter 3, when $\beta = 1.0$, the slopes of the main lobe of the raised-cosine pulse q(t) decays very fast while the side lobes are very small, thus the corresponding performance of the CDD is similar to and even better than that using a

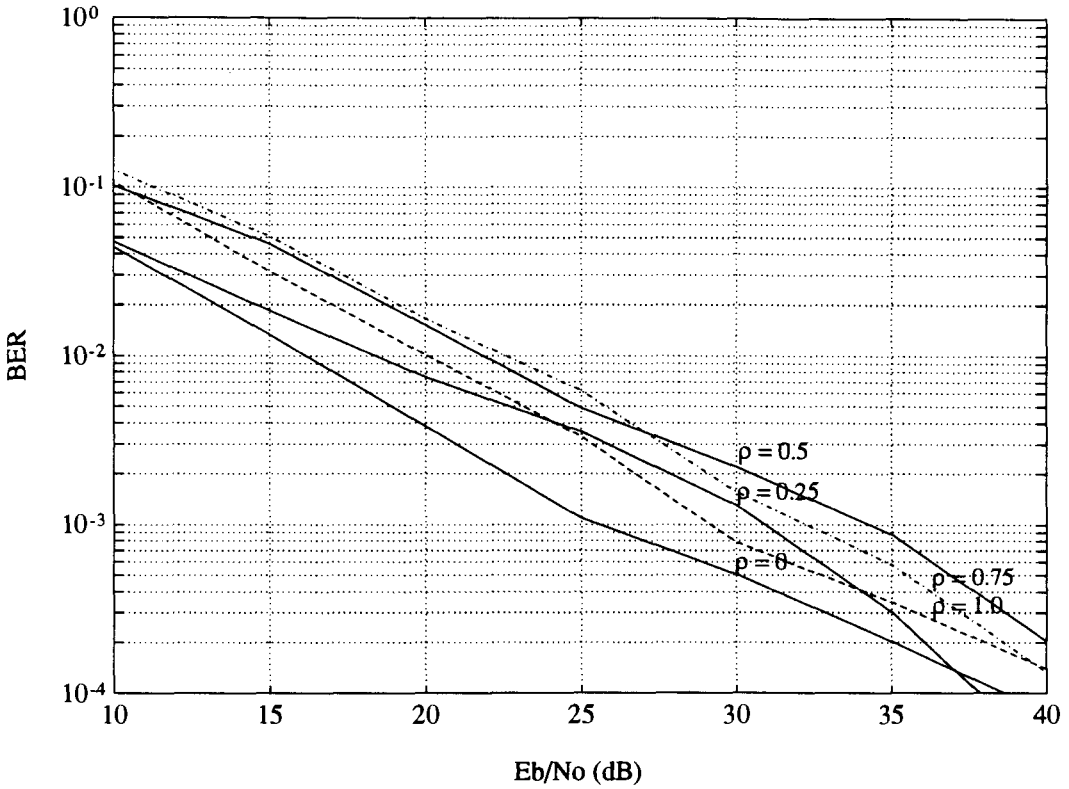

Figure 4.7: The BER of the matched MSDD vs $\frac{E_b}{N_o}$ curves of QPSK using a raised-cosine pulse with $\beta = 1.0$. The chosen channel conditions in the MSDD are: $f_D T = 0.004$, $\alpha = 1.0$ and $\rho = 0.5$ while the actual channel conditions are $f_D T = 0.004$, $\alpha = 1.0$, and the relative delay: $(1)\rho = 1.0$, $(2)\rho = 0.75$, $(3)\rho = 0.5$ $(4)\rho = 0.25$, and $(5)\rho = 0$ corresponding to various curves respectively.

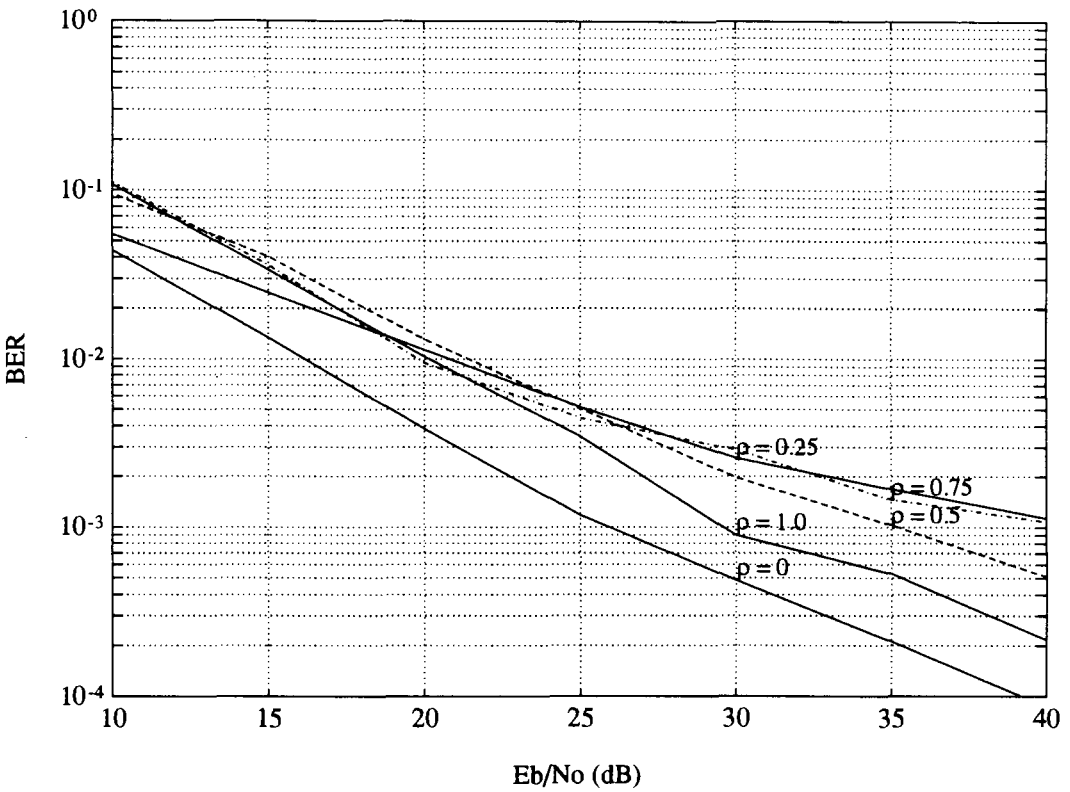

Figure 4.8: The BER of the matched MSDD vs $\frac{E_b}{N_o}$ curves of QPSK using a raised-cosine pulse with $\beta = 0.35$. The chosen channel conditions in the MSDD are: $f_D T = 0.004$, $\alpha = 1.0$ and $\rho = 0.5$ while the channel conditions: $f_D T = 0.004$, $\alpha = 1.0$, and the relative delay: $(1)\rho = 1.0$, $(2)\rho = 0.75$, $(3)\rho = 0.5$ $(4)\rho = 0.25$, and $(5)\rho = 0$ corresponding to various curves respectively.

rectangular pulse. For the same reasons, the mismatched MSDD using a raised-cosine pulse with $\beta = 1.0$ works well. If there is only one mismatched channel parameter, ie. one of α, ρ, and $f_D T$, the performance of the mismatched MSDD using a raised-cosine pulse with $\beta = 1.0$ is very similar to those using a rectangular pulse; see Figure 4.2, 4.3, and Figure 4.4. Under the conditions that all the chosen channel parameters are mismatched to the actual channel parameters, the mismatched MSDD using a raised-cosine pulse with $\beta = 1.0$ also works well, and even better than that using a rectangular pulse; compare Figure 4.9 with Figure 4.3.

Unfortunately, we find experimentally that the mismatched MSDD breaks down under some channel conditions and when certain raised-cosine pulses are used. As an example, when the actual $f_D T = 0.004$, $\alpha = 1.0$, and a raised cosine pulse with $\beta = 0.35$, the performance of a MSDD mismatch in ρ is not acceptable; see Figure 4.10. The matched MSDD works better than those mismatched MSDD. As the difference between the chosen ρ and the actual ρ increases, the performance generally becomes worse and worse, except for the flat fading channel.

The reason why the performance of the mismatched MSDD degrades is the following. When calculating the variances and covariances of the received samples, we do not consider the influence of the eleven ISI terms. When the roll-off parameter β becomes smaller, the side lobes in a raised-cosine pulse are getting larger and thus the effect of those ISI terms in the received sample is getting stronger; see (B.7) and (B.11). Consequently, the decoding metric is no longer a good approximation to the optimal one and hence the performance shown above degraded faster as the mismatch

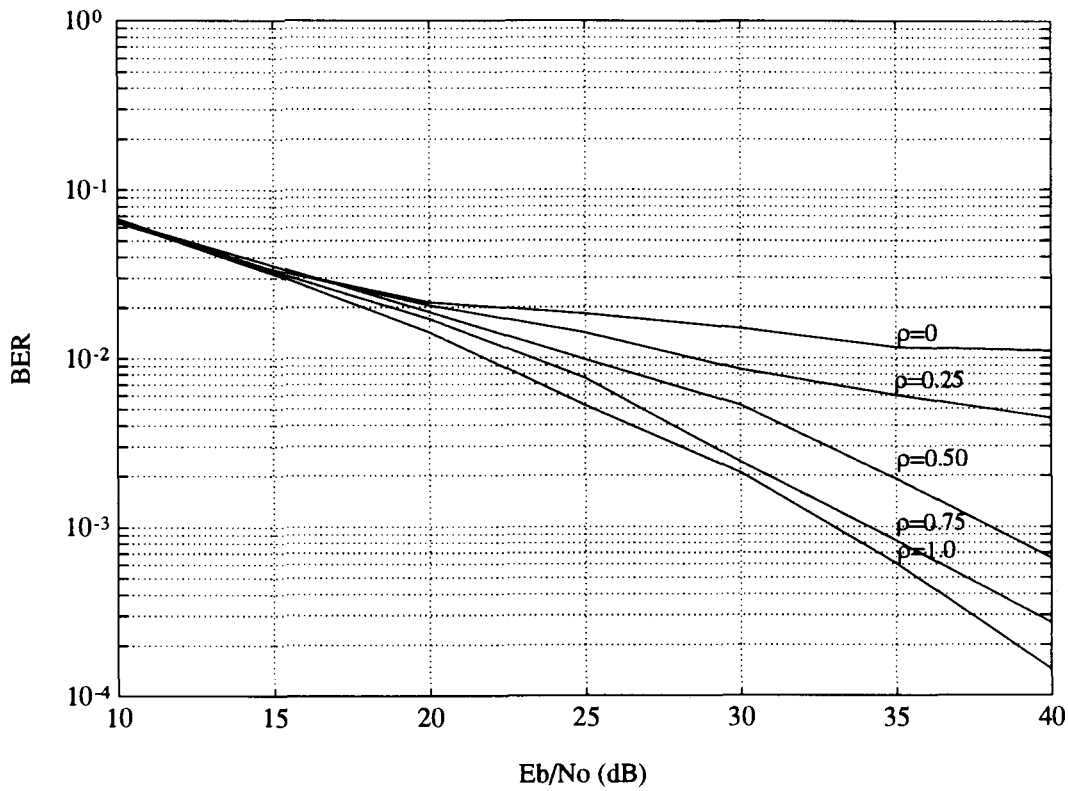

Figure 4.9: The BER of the mismatched MSDD vs $\frac{E_b}{N_o}$ curves of QPSK using a raised-cosine pulse with $\beta = 1.0$. The chosen channel conditions in the MSDD are: $f_D T = 0.004$, $\alpha = 1.0$ and $\rho = 0.5$ while the actual channel conditions are: $f_D T = 0.002$, $\alpha = 100$, and the relative delay: $(1)\rho = 1.0$, $(2)\rho = 0.75$, $(3)\rho = 0.5$ $(4)\rho = 0.25$, and $(5)\rho = 0$ corresponding to various curves respectively.

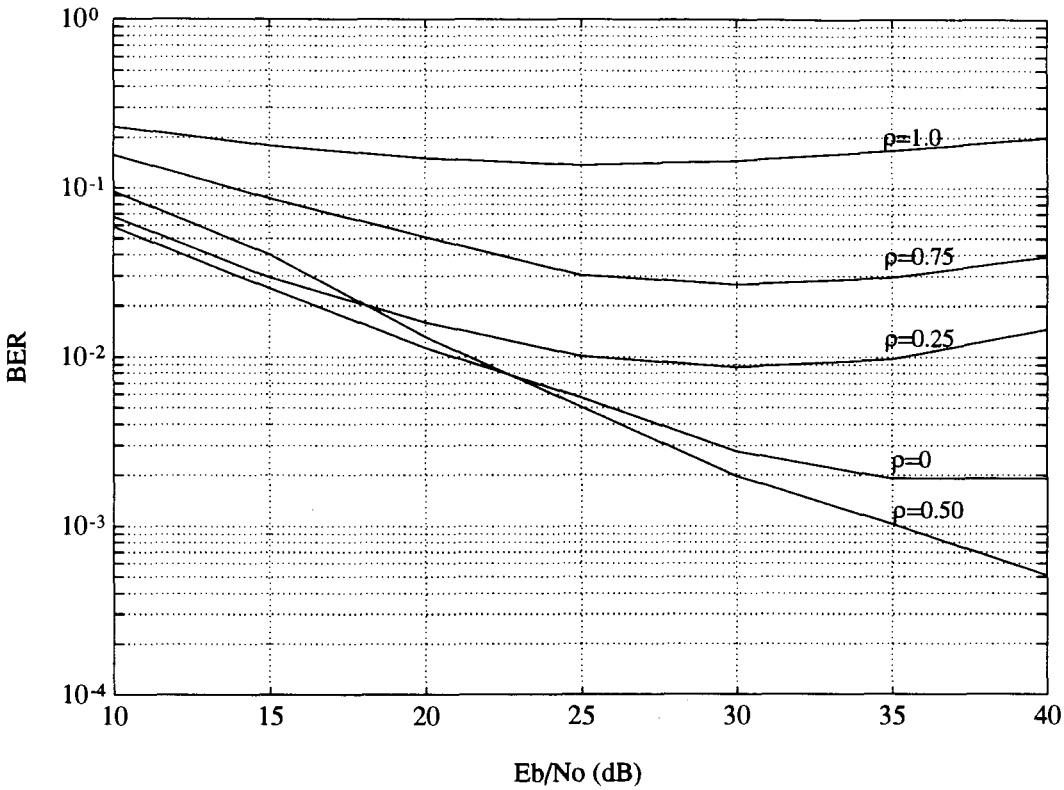

Figure 4.10: The BER of the mismatched MSDD vs $\frac{E_b}{N_o}$ curves of QPSK using a raised-cosine pulse with $\beta = 0.35$. The chosen channel conditions in the MSDD are: $f_D T = 0.004$, $\alpha = 1.0$ and $\rho = 0.5$ while the actual channel conditions are $f_D T = 0.004$, $\alpha = 1$, and the relative delay: $(1)\rho = 1.0$, $(2)\rho = 0.75$, $(3)\rho = 0.5$ $(4)\rho = 0.25$, and $(5)\rho = 0$ corresponding to various curves respectively.

becomes larger. We also see part of the tails of the error curves in Figure 4.10 are bending up. One of the possible reasons is the nonlinear approximation of variances and covariances to the decoding metrics.

Chapter 5

Performance of (Multisymbol) Differential Detection of QPSK with Convolutional Coding in the Frequency-Selective Rayleigh Fading Channel

In this chapter, we combine the rate $\frac{1}{2}$ optimum 32-state convolution code and our MSDD decoder, and examine their performance in the frequency-selective fading channel. We find that the performance of a coded system depends largely on the corresponding uncoded system. Coding helps only when the bit error rate (BER) of the uncoded communication system is not high, say at least less than 10^{-1}. The numerical results shown below indicate that a communication system can be enhanced greatly

with convolutional coding if the BER of the corresponding uncoded system is lower than 10^{-2}.

The organization of this chapter is following: Section 5.1 introduces the general information about the system and defines the notations and assumptions in the analysis and simulation. The performance of coding and conventional differential detector (the coded CDD) is examined in Section 5.2. The performance of the coding and multisymbol differential detector (the coded MSDD) is examined in 5.3.

5.1 General Description of the Coding System

Chapter 2 describes the structure of the coded system. Its system block diagram is shown in Figure 2.5. We adopt the rate $\frac{1}{2}$ optimum convolutional code with memory of 32 states. This code is recommended in IS 54 for the emerging North American narrow-band digital cellular systems. The octal notation of this encoder is (53, 75) [1] and the encoder structure is shown in Figure 2.6.

To obtain the performance of the coded system, at the transmitter, we encode a long sequence of random binary bits generated at the transmitter, modulate them using QPSK, interleave and differentially encode these QPSK symbols, transmit the QPSK signal over the frequency-selective fading channel. At the receiver, we demodulate and deinterleave the received signal, then decode using a Viterbi Decoder, compare the decoded sequence with the original transmitted random sequence, count the total number of erroneous bits in the decoded sequence and then calculate the

BER. This chapter also adopts the piece-wise-constant assumption. This chapter implements coding on those uncoded systems introduced in Chapter 3 and Chapter 4.

Once again, the normalized 95% confidence interval of $[0.8, 1.2]$ is used in all the simulations to make sure that the simulation results are accurate enough. Summarizing the simulation results, we find that the performance of improvement due to channel coding depends on the performance of the uncoded system. If the BER of the uncoded system is 10^{-2} or lower, the BER of the corresponding coded system is usually improved two orders or more. On the other hand, coding can not help to improve the performance of the uncoded system when the BER of the corresponding uncoded system is larger than 10^{-1}. This is one of the reasons why people often consider $10^{-1} \sim 10^{-2}$ as the raw target BER for the uncoded system. The following two sections show how the rate $\frac{1}{2}$ (53, 75) convolutional code helps to improve the performance of the communication system.

5.2 CDD with Convolutional Coding

The description of the structure of the coded CDD was given Section 5.1. Now let us examine the performance of the coded CDD.

First, we use a rectangular pulse as the transmitted pulse p(t). Figure 5.1 illustrates the BER versus bit signal-to noise (SNR) curves for the coded CDD, where the channel conditions are: a fade rate of $f_D T = 0.004$, a power split ratio of $\alpha = 1.0$, and a relative delay of $\rho = 0.0$, 0.25, 0.5, 0.75, and 1.0. It is observed that for the

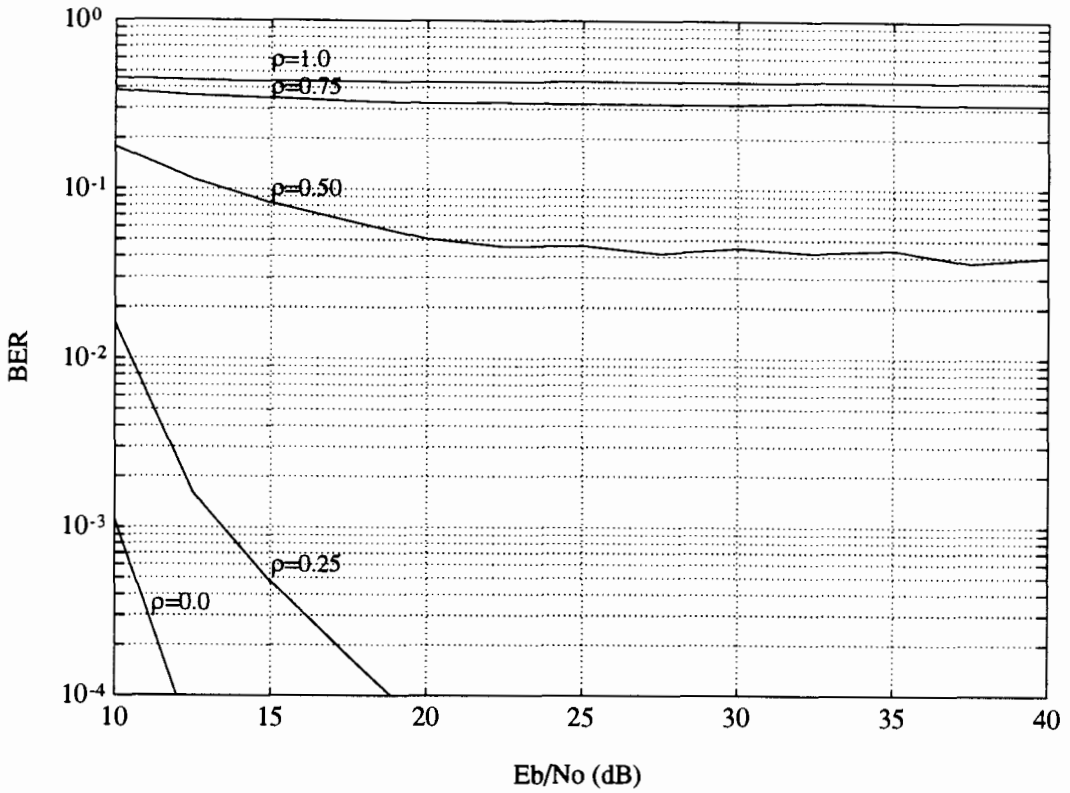

Figure 5.1: The BER vs $\frac{E_b}{N_o}$ curves for the performance of the coded CDD using a rectangular pulse and with $f_D T = 0.004$, $\alpha = 1.0$, and $(1)\rho = 1.0$, $(2)\rho = 0.75$, $(3)\rho = 0.5$ $(4)\rho = 0.25$, and $(5)\rho = 0$ corresponding to different curves.

relative delay less than 0.25, coding helps to improve the performance of the CDD significantly. Compared with Figure 3.2, the error floor is much smaller than that in the uncoded CDD. However, the same is not true for a relative delay larger than 0.5. When $\rho = 1.0$, the error floor is even higher.

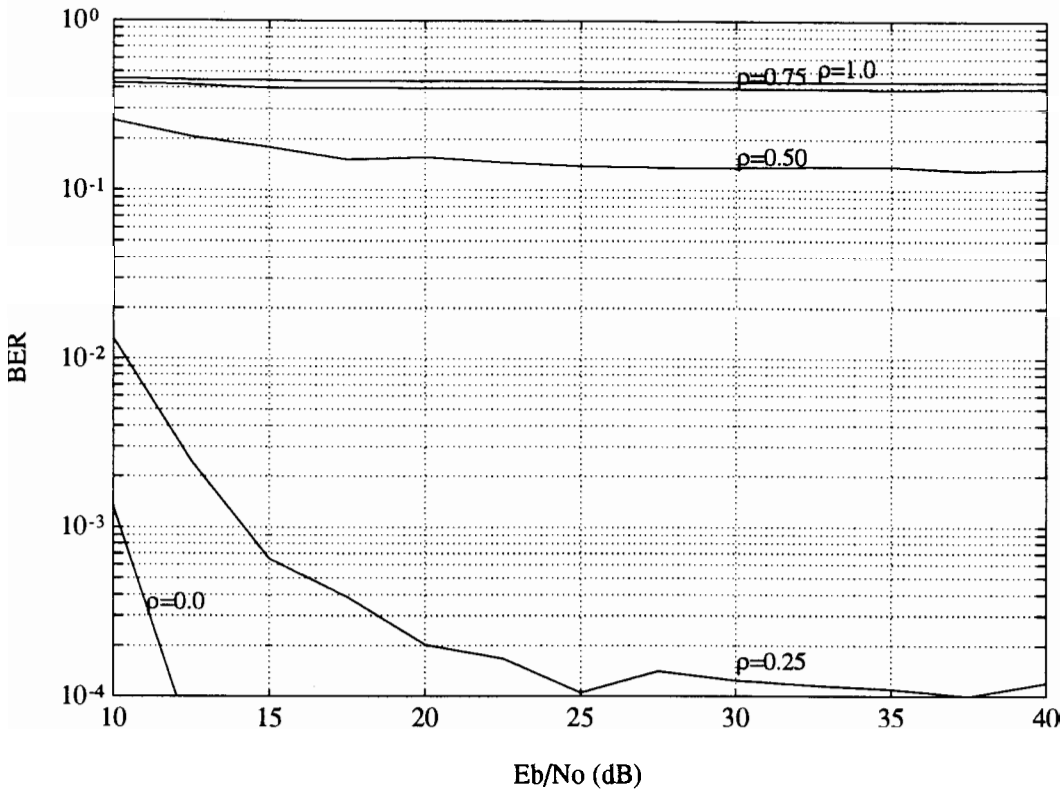

Figure 5.2: The BER vs $\frac{E_b}{N_o}$ curves for the performance of the coded CDD using a raised-cosine pulse with $\beta = 0.35$ and under channel conditions: $f_D T = 0.004$, $\alpha = 1.0$. and $(1)\rho = 1.0$, $(2)\rho = 0.75$, $(3)\rho = 0.5$ $(4)\rho = 0.25$, and $(5)\rho = 0$ corresponding to the various curves respectively.

When using a raise-cosine pulse as the transmitted pulse, we can see a similar phenomenon. Figure 5.2 shows the performance of the coded CDD using a raised-cosine

pulse with $\beta = 0.35$ under the same channel conditions as above.

Summarizing the simulation results, we can conclude that coding helps the CDD only when the delay difference is small. The reason why the coded CDD under channel conditions of large relative delay does not work is that the performance of the corresponding uncoded CDD is too poor. As mentioned in Chapter 4, the uncoded MSDD can make the BER lie around 10^{-2} or lower under any channel conditions as long as the proper transmitted pulse is chosen. The next section shows how coding can improve the performance of the MSDD significantly.

5.3 MSDD with Convolutional Coding

This section indicates that coding can reduce the irreducible error floor of the MSDD within the range SNR of interests as long as proper transmitted pulse is chosen. In the following, we first discuss the matched MSDD and then consider the mismatched MSDD.

5.3.1 The Matched MSDD

Chapter 4 indicates that the performance of the uncoded matched MSDD works well no matter what the channel conditions or the transmitted pulses are. This implies the performance of the coded matched MSDD can be enhanced greatly. Here we use a raise-cosine pulse with $\beta = 0.35$ as an example to illustrate the performance of the

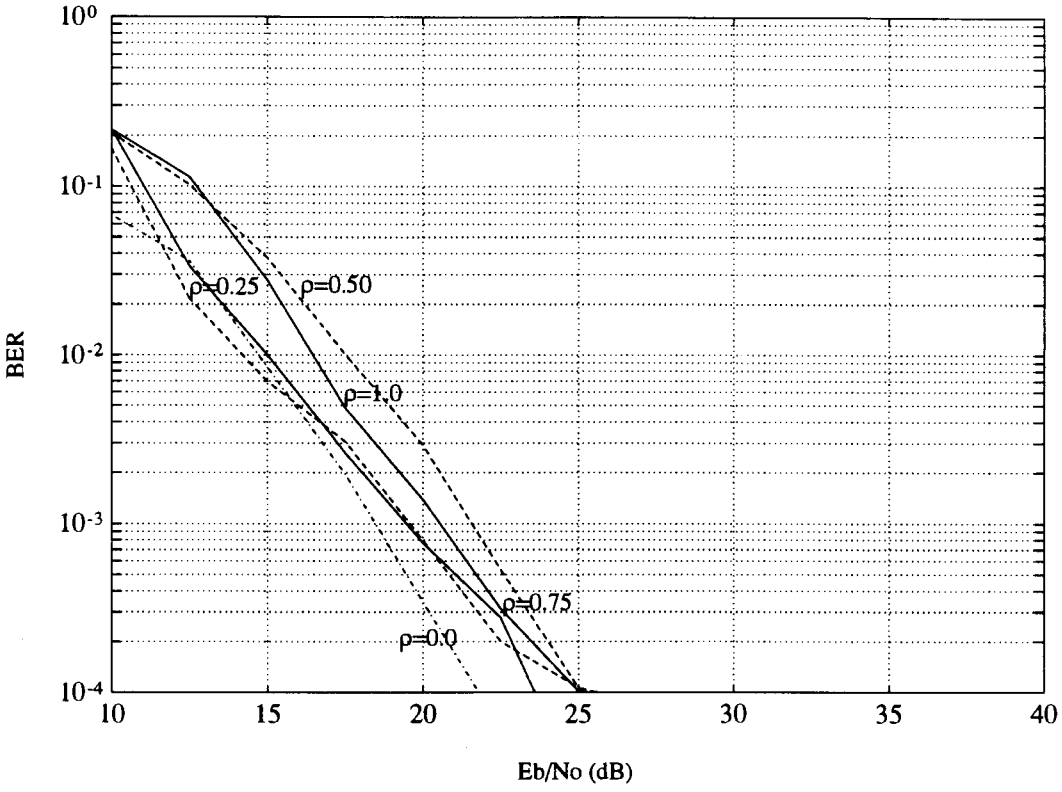

Figure 5.3: The BER of the coded matched MSDD vs $\frac{E_b}{N_o}$ curves of QPSK using a raised-cosine pulse with roll-off parameter $\beta = 0.35$. The channel conditions are: $f_D T = 0.004$, $\alpha = 1.0$ and the relative delay: $(1)\rho = 1.0$, $(2)\rho = 0.75$, $(3)\rho = 0.5$ $(4)\rho = 0.25$, and $(5)\rho = 0$ corresponding to various curves respectively.

coded matched MSDD. Figure 5.3 shows the simulation results under the following channel conditions: $f_DT = 0.004$, $\alpha = 1.0$, and $\rho = 0.0, 0.25, 0.5, 0.75, 1.0$. From Figure 5.3, we discover that coding makes the curves decay much faster, compared with Figure 4.8. No noticeable error floors appear within the range of bit SNR of interest.

5.3.2 The Mismatched MSDD

As for the mismatched MSDD, the performance of the coded MSDD depends on different transmitted pulse shapes and/or the statistical channel parameters. When the transmitted pulse p(t) is either a rectangular pulse or a square-root raised-cosine pulse with $\beta = 1.0$, the coded mismatched MSDD works well under any mismatched channel conditions. For example, when the chosen channel parameters in the MSDD are: $f_DT = 0.004$, $\alpha = 1.0$, and $\rho = 0.5$ while the actual channel parameters are: $f_DT = 0.002$, $\alpha = 100.0$, and ρ varies from 0.0 to 1.0, we have the results in Figure 5.4 and Figure 5.5. Figure 5.4 is for a rectangular pulse and Figure 5.5 is for a square-root raised-cosine pulse with $\beta = 1.0$. Comparing the two figures, we find that the performance of the mismatched MSDD using a raised-cosine pulse with $\beta = 1.0$ is better than using a rectangular. Recall that the corresponding uncoded MSDD using a raised-cosine pulse with $\beta = 1.0$ performs only a little bit better than that using a rectangular pulse, see Figure 4.6 and Figure 4.9. This indicates that the system is perhaps improved greatly after coding even though there is only a slight improvement in the corresponding uncoded system.

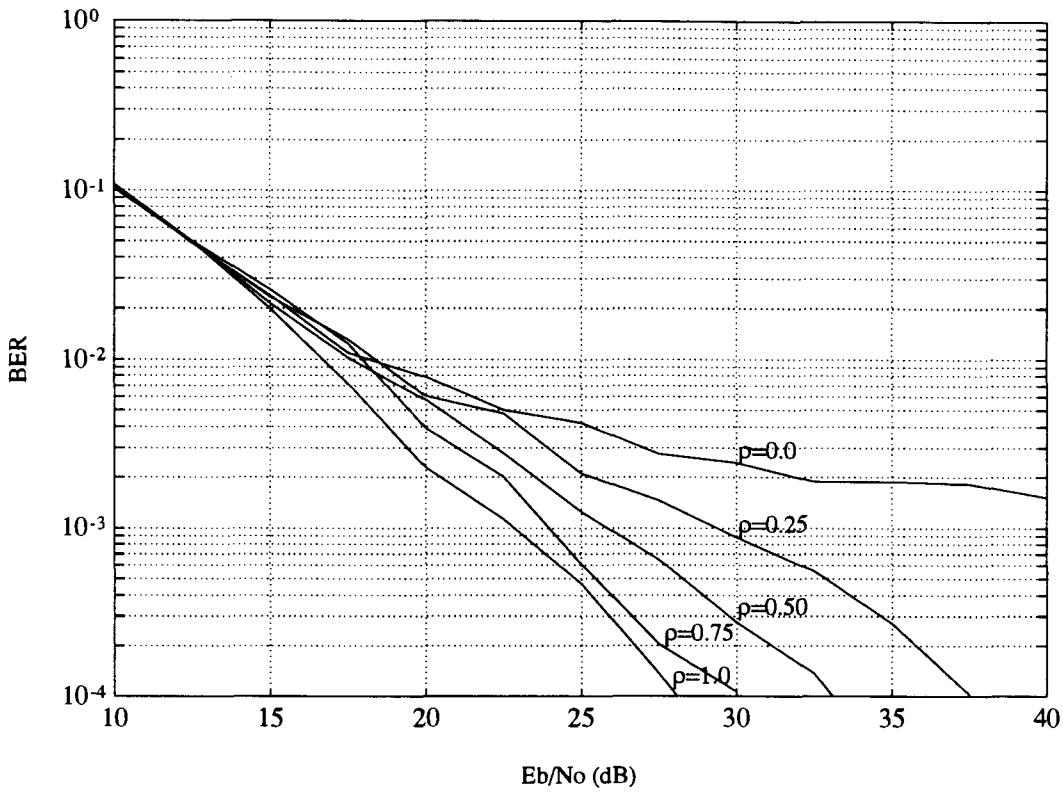

Figure 5.4: The BER of the coded mismatched MSDD vs $\frac{E_b}{N_o}$ curves of QPSK using a rectangular pulse. The chosen channel conditions are: $f_D T = 0.004$, $\alpha = 1.0$, and $\rho = 0.5$. The actual channel conditions are: $f_D T = 0.002$, $\alpha = 100.0$, and $(1)\rho = 1.0$, $(2)\rho = 0.75$, $(3)\rho = 0.5$ $(4)\rho = 0.25$, and $(5)\rho = 0$ corresponding to various curves respectively.

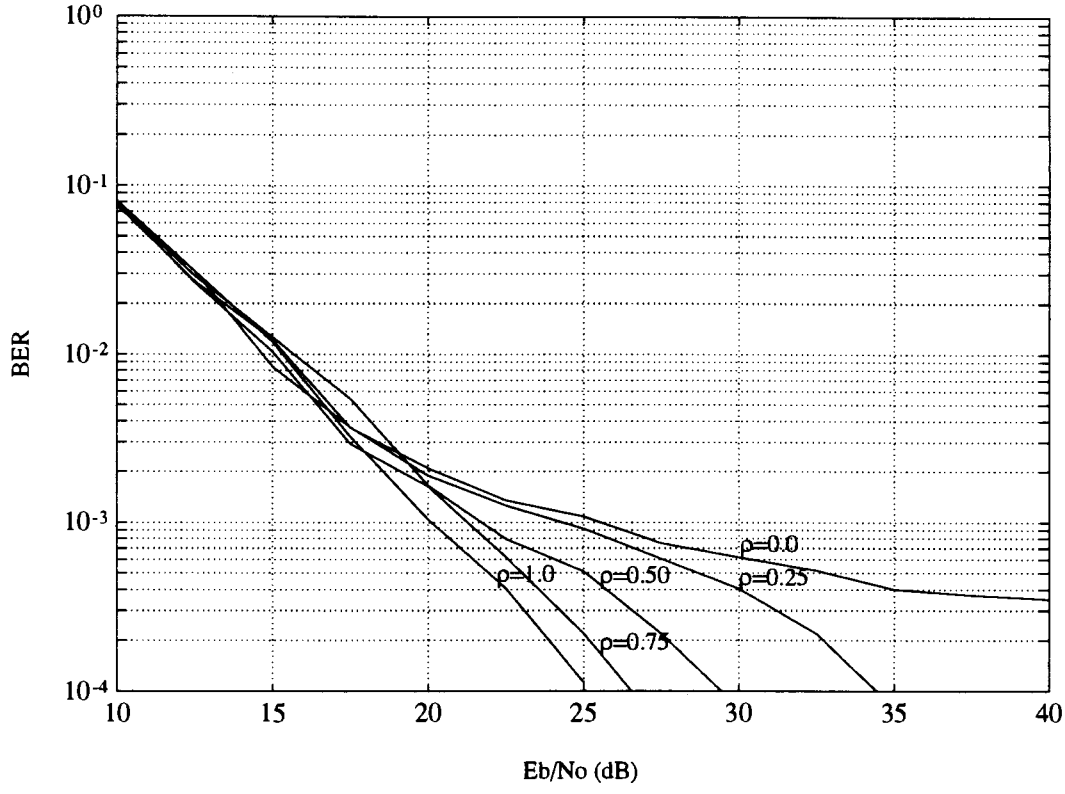

Figure 5.5: The BER of the coded mismatched MSDD vs $\frac{E_b}{N_o}$ curves of QPSK using a raised-cosine pulse with $\beta = 1.0$. The chosen channel conditions are: $f_D T = 0.004$, $\alpha = 1.0$, and $\rho = 0.5$. The actual channel conditions are: $f_D T = 0.002$, $\alpha = 100.0$, and $(1)\rho = 1.0$, $(2)\rho = 0.75$, $(3)\rho = 0.5$ $(4)\rho = 0.25$, and $(5)\rho = 0$ corresponding to various curves respectively.

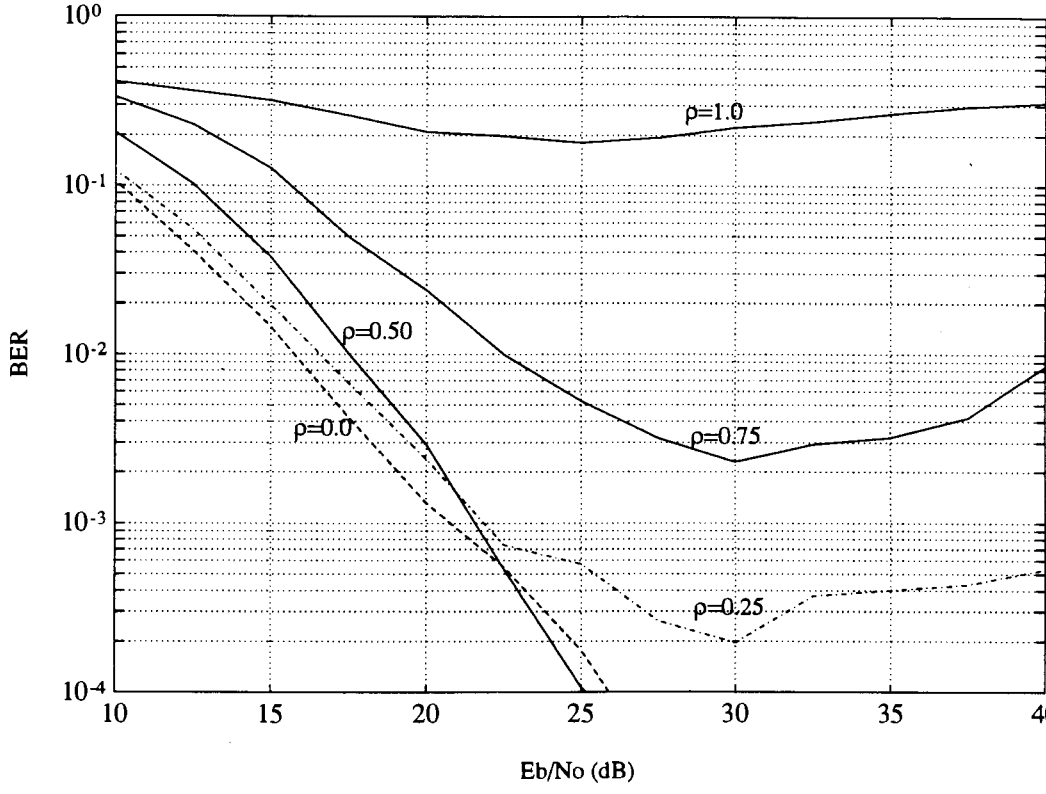

Figure 5.6: The BER of the coded mismatched MSDD vs $\frac{E_b}{N_o}$ curves of QPSK using a raised-cosine pulse with $\beta = 0.35$. The chosen channel conditions are: $f_D T = 0.004$, $\alpha = 1.0$, and $\rho = 0.5$. The actual channel conditions are: $f_D T = 0.004$, $\alpha = 1.0$, and $(1)\rho = 1.0$, $(2)\rho = 0.75$, $(3)\rho = 0.5$ $(4)\rho = 0.25$, and $(5)\rho = 0$ corresponding to various curves respectively.

As mentioned earlier, coding can only improve the uncoded system whose performance is reasonably good, say around 10^{-2}. Using an improper pulse shape, the uncoded mismatched MSDD does not work under some channel conditions, for example in a raised-cosine pulse with $\beta = 0.35$. Thus even coding can not enhance its performance. Figure 5.6 shows the performance of the mismatched MSDD using a raised-cosine pulse with $\beta = 0.35$. The chosen channel conditions are: $f_D T = 0.004$, $\alpha = 1.0$, and $\rho = 0.5$ while the actual channel parameters are: $f_D T = 0.004$, $\alpha = 1.0$, and ρ varies from 0.0 to 1.0. The trade-off between bandwidth and performance is shown clearly in Figure 5.5 and 5.6.

Chapter 6

Conclusions

6.1 Conclusions

In this thesis, we study the performance of differential detection of QPSK signals in a frequency-selective Rayleigh fading channel. A two-ray channel model is adopted to represent frequency-selective fading. We investigate the performance of the conventional differential detector (CDD) and the multisymbol differential detector (MSDD), and also their performance incorporating the rate $\frac{1}{2}$ 32-state optimum convolutional code. The validity of the piece-wise-constant assumption in differential detection is shown from both numerical results and analytical derivation under practical channel conditions.

The CDD is discussed first. Based on the numerical results obtained, it can be concluded that the performance of the CDD depends mainly on the statistical channel

parameters and also slightly on the transmitted pulses. It is observed that the performance of the conventional differential detector in the frequency-selective Rayleigh fading channel is acceptable as long as the power split ratio α is relatively large and/or the differential propagation delay ρ is relatively small. Also the pulse shape has influence on the performance of the CDD: the raised-cosine pulse with roll-off parameter $\beta = 1.0$ provides better performance than the rectangular pulse and those raised-cosine pulses with $\beta < 1$. To maintain a target bit error rate of 10^{-2} at bit signal-to-noise ratio $\frac{E_b}{N_o}$ around 25 dB with the normalized fade rate $f_D T = 0.004$ using the rectangular pulse, α must be larger than 20 dB if $\rho = 1$. On the other hand, when $\frac{E_b}{N_o} = 25dB$, $\rho = 0.25$, $\alpha = 1$, and $f_D T = 0.004$, the performance of the CDD using the raised-cosine pulse with $\beta = 1.0$ is almost 10 times better than that using the raised-cosine pulse with $\beta = 0.0$. This shows the tradeoff between the performance and the bandwidth. The CDD works well under some channel conditions while it breaks down under other conditions.

In order to improve the performance of differential detection in the frequency-selective fading channel, the MSDD is suggested in order to make full use of the information from N ($N > 2$) received samples rather than just two in the CDD. It is found that when using the rectangular pulse, the MSDD can work well under all practical channel conditions while it provides best performance if the statistical channel information is known at the receiver. As for using a raised-cosine pulse, the performance of the MSDD depends on the roll-off parameters β. The performance of the matched and mismatched MSDD using a raised-cosine pulse with $\beta = 1.0$ is better than that using rectangular pulse. When using a raised-cosine pulse with $\beta = 0.35$, the matched MSDD works well, but the mismatched MSDD breaks down. This is

mainly due to the larger effects of ISI terms in the received samples and the use of of a non-optimal metric. It is true that the more received samples the MSDD uses, the better the performance is. But in reality though increasing N is subject to the exponential growth of the decoding complexity.

We have used the optimal rate $\frac{1}{2}$ 32-state convolutional code in conjunction with the CDD and the MSDD. It is found that coding helps greatly when the performance for uncoded cases is around 10^{-2} or lower. If the BER is between 10^{-1} and 10^{-2}, coding makes the error floors of the performance lower and the performance is usually tens of times better. But Coding can not help when the performance of the corresponding uncoded system is larger than 10^{-1}.

We also prove the validity of the piece-wise-constant assumptions in the Rayleigh fading channel by analysis and simulation. We found that if the carrier frequency is around 900 MHz and the symbol rate is 24 KHz, the piece-wise-constant assumption holds very well in the analysis of Rayleigh fading channel. It is safe to use the piece-wise-constant in analysis and simulation in the practical Rayleigh fading environment.

6.2 Suggestions for Further Research

Some suggestions for further work are given below:

- The analysis of pairwise error probability could be extended to M-ary DPSK Modulation and can be used to study the performance of DPSK in any other channel model.

- As for the MSDD, how much gain can be achieved when N is increased each time and what the limit of the improved performance of the MSDD is.

- The study of the performance of the MSDD will also be very interesting under different channel models for the frequency-selective fading.

Appendix A

Correlation Between Two Fading Gains In Received Samples In Frequency-selective Rayleigh Fading Channel

In this appendix, we will show the correlation between the fading gains on two symbols in the same received sample or two different received samples.

The received sample is defined by (2.10) and is sampled every T seconds. The k^{th} sample in (2.26) and its n^{th} fading gain $u_{n,k}$ in (2.27) are rewritten below:

$$y_k = y(kT) = \sum_n x_n u_{n,k} + n_k$$

$$= x_k u_{k,k} + \sum_{n \neq k} x_n u_{n,k} + n_k$$

where

$$u_{n,k} = \frac{A}{\sqrt{N_o}} \int_{-\infty}^{\infty} \int_{-\infty}^{\infty} c(\tau_1; \lambda) p(\lambda - \tau_1 - nT) p(\lambda - kT - lT_1) d\tau_1 d\lambda \qquad \text{(A.1)}$$

We want to examine the correlation between fading gains $u_{n,k}$ and u_{ml} in k^{th} and l^{th} samples respectively. When $k = l$, $u_{n,k}$ and u_{ml} are the fading gains on two PSK symbols in the same received sample. The correlation coefficient is defined as

$$\begin{aligned} \phi_{k,l}(n,m) &= \frac{1}{2} E[u_{n,k}^* u_{ml}] \\ &= \frac{1}{2} \frac{A^2}{N_o} \int_{\lambda_1} \int_{\lambda_2} \int_{\tau_1} \int_{\tau_2} \overline{c^*(\tau_1; \lambda_1) c(\tau_2; \lambda_2)} p(\lambda_1 - kT) p(\lambda_2 - lT) \\ &\quad \times p(\lambda_1 - \tau_1 - nT) p(\lambda_2 - \tau_2 - mT) d\lambda_1 d\lambda_2 d\tau_1 d\tau_2 \qquad \text{(A.2)} \end{aligned}$$

Using (2.11), (A.2) can be rewritten as

$$\begin{aligned} \phi_{k,l}(n,m) &= \frac{A^2}{N_o} \int_{\lambda_1} \int_{\lambda_2} \int_{\tau_1} \int_{\tau_2} J_o(2\pi f_D(\lambda_1 - \lambda_2)) G(\tau_1) \delta(\tau_1 - \tau_2) p(\lambda_1 - kT) p(\lambda_2 - lT) \\ &\quad \times p(\lambda_1 - \tau_1 - nT) p(\lambda_2 - \tau_2 - mT) d\lambda_1 d\lambda_2 d\tau_1 d\tau_2 \\ &= \frac{A^2}{N_o} \int_{\lambda_1} \int_{\lambda_2} \int_{\tau_1} J_o(2\pi f_D(\lambda_1 - \lambda_2)) G(\tau_1) p(\lambda_1 - kT) p(\lambda_2 - lT) \\ &\quad \times p(\lambda_1 - \tau_1 - nT) p(\lambda_2 - \tau_2 - mT) d\lambda_1 d\lambda_2 d\tau_1 \qquad \text{(A.3)} \end{aligned}$$

where power-delay profile $G(\tau_1)$ given in (2.13) represents statistical characteristic of the two-ray channel model. $J_o(2\pi f_D(\lambda_1 - \lambda_2))$ is zero-order Bessel function and its Fourier transform is

$$S(f) = \int_{-f_D}^{f_D} J_o(2\pi f_D(\lambda_1 - \lambda_2)) e^{j2\pi f(\lambda_1 - \lambda_2)} d(\lambda_1 - \lambda_2) \qquad \text{(A.4)}$$

We define the Fourier transforms of the transmitted pulse p(t) as $P(\xi)$ and also define $A(f,\delta)$.

$$P(\xi) = \int_{-\infty}^{\infty} p(t)e^{-j2\pi\xi t}dt \tag{A.5}$$

$$A(f,\delta) = \int_{-\infty}^{\infty} P(\xi)P(f-\xi)e^{j2\pi\xi\delta}d\xi \tag{A.6}$$

Using properties of Fourier transforms, the following two integrations can be simply written as :

$$\int_{-\infty}^{\infty} p(\lambda_1 - kT)p(\lambda_1 - \tau_1 - nT)e^{-j2\pi f\lambda_1}d\lambda_1 = e^{-j2\pi fkT}A(f,-\delta_1) \tag{A.7}$$

and

$$\int_{-\infty}^{\infty} p(\lambda_2 - lT)p(\lambda_2 - \tau_1 - mT)e^{-j2\pi f\lambda_2}d\lambda_2 = e^{-j2\pi flT}A(-f,-\delta_2) \tag{A.8}$$

where

$$\delta_1 = \tau_1 + nT - kT \tag{A.9}$$

$$\delta_2 = \tau_1 + mT - lT \tag{A.10}$$

Applying (A.4)-(A.10) to (A.3) and changing the order of integration, we get

$$\phi_{k,l}(n,m) = \frac{A^2}{N_o}\int_{\tau_1} G(\tau_1)\int_{-f_D}^{f_D} A(f,-\delta_1)A(-f,-\delta_2)S(f)e^{j2\pi f(k-l)T}df\,d\tau_1 \tag{A.11}$$

where $A(\bullet,\bullet)$ is given in (A.6).

Before the end of this appendix, let us examine the shape of $A(f,\delta)$. Since $A(f,\delta)$ is a function of both f and δ, we examine how $A(f,\delta)$ changes with one of the two variables while fixing the other. First we set $f = 0$, then Figure A.1 shows the shape of the real part of $A(0,\delta)$ as a raised-cosine pulse (dash line). The x axis is normalized

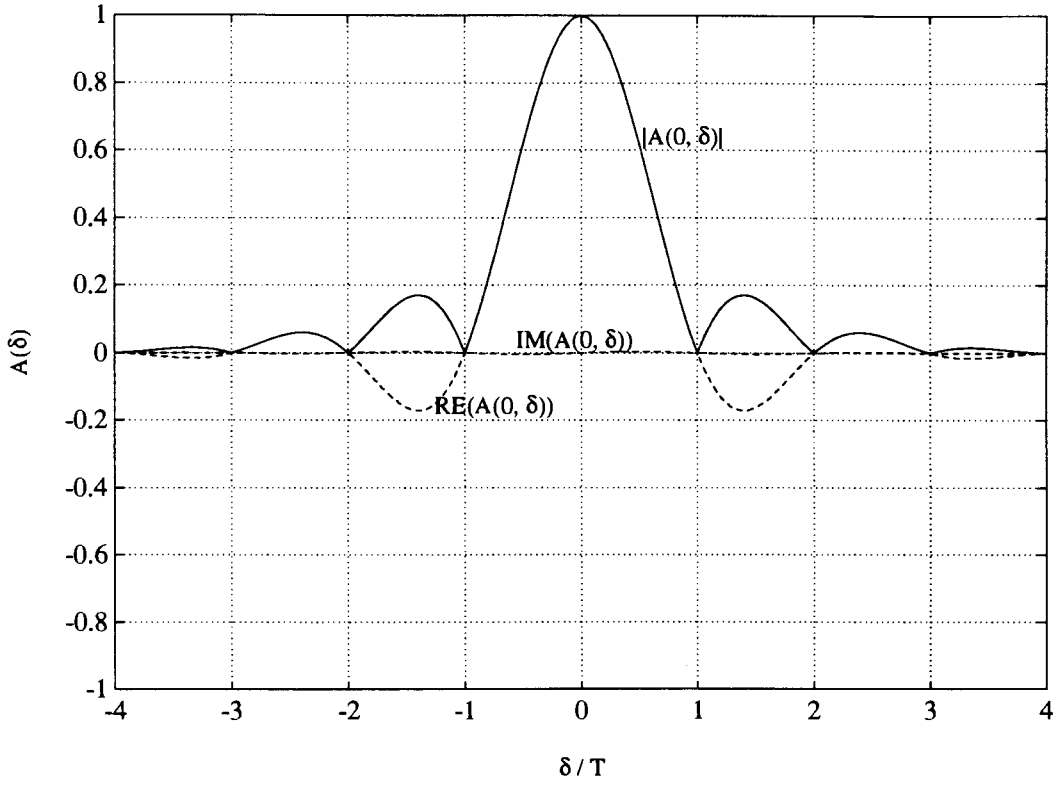

Figure A.1: A(0, δ) using a raised-cosine pulse ($\beta = 0.35$). $|A(0,\delta)|$, RE$(A(0,\delta))$, and IM$(A(0,\delta))$ are the amplitude, real part and imaginary part of $A(0,\delta)$ respectively.

δ, ie. δ/T, where T is the symbol interval. Due to (A.11), we are only interested in the range $-f_D \leq f \leq f_D$, where $f_D \in [0.0, 0.004]$. Since the f_D is very small, for other fixed f, the shape of $A(f,\delta)$ is very similar to $A(0,\delta)$.

Now let us fix $\delta = \frac{3}{2}T$. The shape of $A(f, \frac{3}{2}T)$ is shown in Figure A.2. The x axis is normalized frequency, ie. the frequency f divided by the symbol rate $\frac{1}{T}$. We also

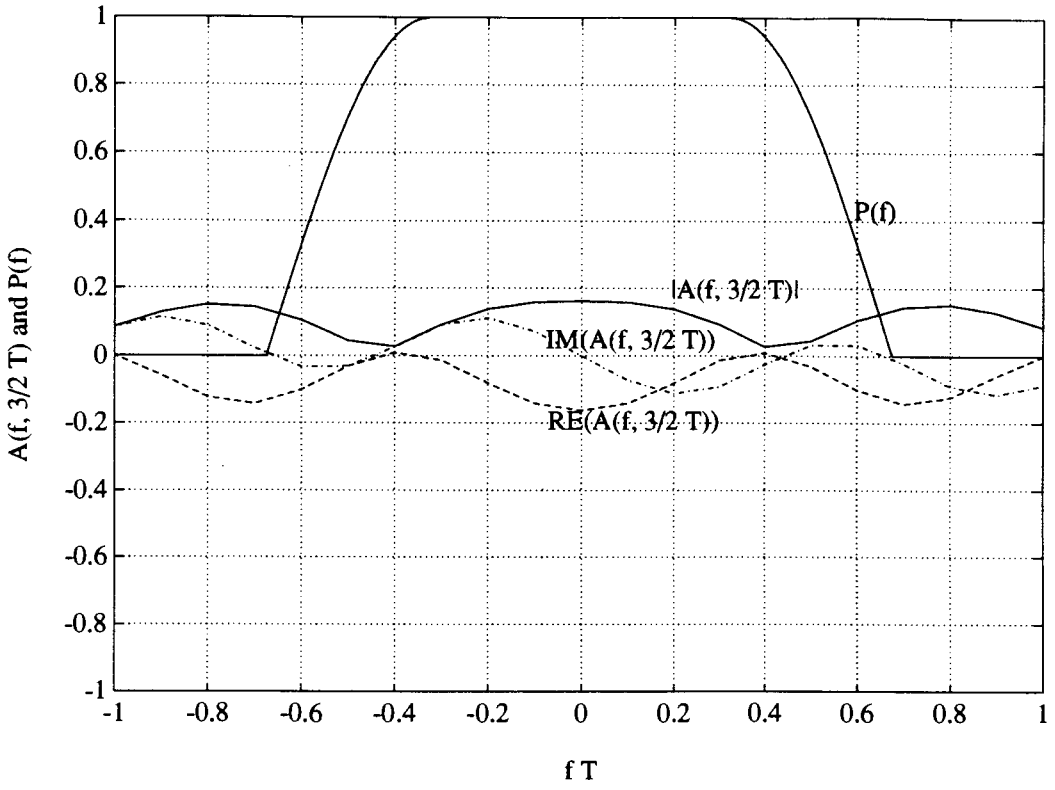

Figure A.2: A(f, 3/2T) using a square-root raised-cosine pulse ($\beta = 0.35$). $|A(f, 3/2T)|$, RE$(A(f, 3/2T))$, and IM$(A(f, 3/2T))$ are the amplitude, real part and imaginary part of $A(f, 3/2T)$ respectively.

put P(f) in Figure A.2, the spectrum of square-root raised-cos pulse, as a reference. Noting that within the region around $fT = 0$, the real part of $A(f, \frac{3}{2}T)$ is nearly constant and the imaginary part of $A(f, \frac{3}{2}T)$ is close to a straight line. These two figures give us a brief idea what $A(f, \delta)$ in (A.6) looks like. In Section 3.4, we can see the simplied $A(f, \delta)$, which finally results in simplying $\phi_{k,l}(n, m)$ in (A.11).

Appendix B

Approximation to the variances and the covariances of the received samples

In this appendix, we show how to approximate the variances and the covariances of the received samples containing many ISI terms.

If the raised-cosine pulse is adopted, there are infinite number of terms in the received sample. In this thesis, we use 16 terms to represent each received sample y_k in (2.29) where $M_1 = 8$ and $M_2 = 7$ are set. If only one data QPSK symbol c_k in y_k is of interest, the tight approximation to the variances and covariances of the received samples is shown by Dr. Cavers in [15]. They can be rewritten as

$$\begin{aligned}
\overline{\sigma_k^2} &= \frac{1}{2}E[y_k y_k^*] \\
&= \sum_{i=k-8}^{k+7} \phi_{k,k}(i,i) + 2Re[c_k \phi_{k,k}(k,k-1)] + 1 \qquad \text{(B.1)} \\
\overline{\sigma_{k,k-1}^2} &= \frac{1}{2}E[y_k y_{k-1}^*] \\
&= \sum_{i=k-8}^{k+6} \phi_{k,k-1}(i,i) + c_k \phi_{k,k-1}(k,k-1) \qquad \text{(B.2)}
\end{aligned}$$

In Chapter 4, we consider MSDD using five received samples y_{k-2}, y_{k-1}, y_k, y_{k+1}, and y_{k+2}. The desired data QPSK symbols in these five received samples can be written in vector form as

$$\mathbf{C}' = (c_{k-2}, c_{k-1}, c_k, c_{k+1}, c_{k+2}) \qquad \text{(B.3)}$$

In the following, we use the same idea to determine a tight approximation to the variances and covariances in the correlation matrix of the five received samples. The approximation is influenced just by the five-symbol vector $\mathbf{C}'$.

Since we consider five received sample y_{k-2}, y_{k-1}, y_k, y_{k+1}, and y_{k+2} at the same time, we use y_m to represent m^{th} received sample, where $m \in \{k-2, k-1, k, k+1, k+2\}$. Then y_m can be written as

$$y_m = y(mT) = \sum_{p=m-8}^{m+7} x_p u_{pm} + n_m$$

$$= \sum_{p=k-3}^{k+2} x_p u_{pm} + \sum_{p=m-8 \& p \notin [k-3,k+2]}^{m+7} x_p u_{pm} + n_m \qquad \text{(B.4)}$$

where the transmitted QPSK symbol x_p is related to the data QPSK symbol c_p by (2.1). Thus the C''s is related to six transmitted QPSK symbols (x_{k-3}, x_{k-2}, x_{k-1}, x_k, x_{k+1}, x_{k+2}). Then the variance σ_m^2 of y_m is

$$\begin{aligned}
\sigma_m^2 &= \frac{1}{2} E[y_m y_m^*] \\
&= 1 + \sum_{p=k-3}^{k+2} \sum_{p=k-3}^{k+2} \phi_{m,m}(p,q) z_{p,q} + \sum_{p=k-3}^{k+2} \sum_{q=m-8 \& q \notin [k-3,k+2]}^{m+7} \phi_{m,m}(p,q) z_{p,q} \\
&\quad + \sum_{q=k-3}^{k+2} \sum_{p=m-8 \& p \notin [k-3,k+2]}^{m+7} \phi_{m,m}(q,p) z_{p,q} \\
&\quad + \sum_{p=m-8 \& p \notin [k-3,k+2]}^{m+7} \phi_{m,m}(p,p) + \sum_{p=m-8}^{m+7} \sum_{q=m-8 \& p,q \notin [k-3,k+2]}^{m+7} \phi_{m,m}(p,q) z_{p,q} \\
&= A_m + B_m \qquad \text{(B.5)}
\end{aligned}$$

where $\phi_{m,m}(p,q)$ and z_{pq} are given in (3.63) and (4.8) respectively. A_m and B_m are two parts of σ_m^2:

$$A_m = 1 + \sum_{p=k-3}^{k+2} \sum_{p=k-3}^{k+2} \phi_{m,m}(p,q) z_{p,q} + \sum_{p=m-8 \& p \notin [k-3,k+2]}^{m+7} \phi_{m,m}(p,p) \qquad \text{(B.6)}$$

$$\begin{aligned}
B_m &= \sum_{p=k-3}^{k+2} \sum_{q=m-8 \& q \notin [k-3,k+2]}^{m+7} \phi_{m,m}(p,q) z_{p,q} + \sum_{q=k-3}^{k+2} \sum_{p=m-8 \& p \notin [k-3,k+2]}^{m+7} \phi_{m,m}(q,p) z_{p,q} \\
&\quad + \sum_{p=m-8}^{m+7} \sum_{q=m-8 \& p,q \notin [k-3,k+2]}^{m+7} \phi_{m,m}(p,q) z_{p,q} \qquad \text{(B.7)}
\end{aligned}$$

Noting that each $z_{p,q}$ in A_m is the function of the elements only belonging to the

desired five-symbol vector $\mathbf{C}'$. The rest data QPSK symbols, not in $\mathbf{C}'$, are considered as ISI symbols at this moment. It is obvious that A_m is determined only by the desired data QPSK symbols while B_m is determined by both the desired and the ISI data QPSK symbols. Since $|\phi_{m,m}(p,q)|$ decays in terms of $\frac{1}{|m-p|^3|m-q|^3}$ and $m \in$ {k-2, k-1, k, k+1, k+2 } , A_m is the dominant part of σ_m^2. To show this, we give some numerical results below.

Examples:

Assuming that the channel conditions are: $\alpha = 1.0$, $\rho = 0.5$, $f_D T = 0.004$, symbol $SNR = 20dB$, and the data QPSK sequence $\mathbf{C}$ containing 20 symbols. The 9^{th} to 13^{th} are the desired data QPSK symbols. Set k=11.

Set the roll-off parameter of the raised-cosine pulse $\beta = 0.35$:

When $\mathbf{C}$ = {1, 1, 1, 1, 1, 1, 1, 1, 1, 1, 1, 1, 1, 1, 1, 1, 1, 1, 1, 1 }:

$\sigma_k^2 = 100.87$, $A_k = 103.69$;

When $\mathbf{C}$ = {1, j, -1, -j, 1, j, -1, -j, 1, 1, 1, 1, 1, j, -1, -j, 1, j, -1, -j }:

$\sigma_k^2 = 103.19$, $A_k = 103,69$;

When $\mathbf{C}$ = {1, j, -1, -j, 1, j, -1, -j, 1, j, -1, -j, 1, j, -1, -j, 1, j, -1, -j }:

$\sigma_k^2 = 51.0$, $A_k = 51.021$;

Set the roll-off parameter of the raised-cosine pulse $\beta = 1.0$:

When $\mathbf{C}$ = {1, j, -1, -j, 1, j, -1, -j, 1, j, -1, -j, 1, j, -1, -j, 1, j, -1, -j }:

$\sigma_k^2 = 51.0$, $A_k = 51.0$;

So we can see that the approximation (B.8) is a good approximation.

$$\sigma_m^2 \approx A_m \tag{B.8}$$

Similarly we can determine the approximation to the covariance $\sigma_{m,n}^2$ in the same way.

$$\begin{aligned}
\sigma_{m,n}^2 &= \frac{1}{2}E[y_m y_n^*] \\
&= \sum_{p=k-3}^{k+2}\sum_{p=k-3}^{k+2}\phi_{m,n}(p,q)z_{p,q} + \sum_{p=k-3}^{k+2}\sum_{q=n-8\&q\notin[k-3,k+2]}^{n+7}\phi_{m,n}(p,q)z_{p,q} \\
&\quad + \sum_{q=k-3}^{k+2}\sum_{p=m-8\&p\notin[k-3,k+2]}^{m+7}\phi_{m,n}(q,p)z_{p,q} \\
&\quad + \sum_{p=max(m-8,n-8)\&p\notin[k-3,k+2]}^{min(m+7,n+7)}\phi_{m,n}(p,p) + \sum_{p=m-8}^{m+7}\sum_{q=n-8\&p,q\notin[k-3,k+2]}^{n+7}\phi_{m,n}(p,q)z_{p,q} \\
&= C_{m,n} + D_{m,n}
\end{aligned} \tag{B.9}$$

where $\phi_{m,n}(p,q)$ and z_{pq} are given in (3.63) and (4.8) respectively. $C_{m,n}$ and $D_{m,n}$ are two parts of σ_m^2:

$$C_{m,n} = \sum_{p=k-3}^{k+2}\sum_{p=k-3}^{k+2}\phi_{m,n}(p,q)z_{p,q} + \sum_{p=max(m-8,n-8)\&p\notin[k-3,k+2]}^{min(m+7,n+7)}\phi_{m,n}(p,p) \tag{B.10}$$

$$\begin{aligned}
D_{m,n} &= \sum_{p=k-3}^{k+2}\sum_{q=n-8\&q\notin[k-3,k+2]}^{n+7}\phi_{m,n}(p,q)z_{p,q} + \sum_{q=k-3}^{k+2}\sum_{p=m-8\&p\notin[k-3,k+2]}^{m+7}\phi_{m,n}(q,p)z_{p,q} \\
&\quad + \sum_{p=m-8}^{m+7}\sum_{q=n-8\&p,q\notin[k-3,k+2]}^{n+7}\phi_{m,n}(p,q)z_{p,q}
\end{aligned} \tag{B.11}$$

For the same reasons, $C_{m,n}$ is the dominant part in $\sigma_{m,n}^2$ and is determined only by

the desired five-symbol vector $\mathbf{C}'$. We approximate $\sigma^2_{m,n}$ by $C_{m,n}$, ie.

$$\sigma^2_{m,n} \approx C_{m,n} \tag{B.12}$$

A few numerical results are given below to demonstrate how good (B.12) is.

Examples:

Assuming that the channel conditions are: $\alpha = 1.0$, $\rho = 0.5$, $f_D T = 0.004$, symbol $SNR = 20dB$, and the data QPSK sequence $\mathbf{C}$ containing 20 symbols. The 9^{th} to 13^{th} are the desired data QPSK symbols. Set k=11.

Set the roll-off parameter of the raised-cosine pulse $\beta = 0.35$:

When $\mathbf{C}$ = {1, j, -1, -j, 1, j, -1, -j, 1, j, -1, -j, 1, j, -1, -j, 1, j, -1, -j }:

$\sigma^2_{k,k-1} = -50.0030$, $C_{k,k-1} = -49.992$;

$\sigma^2_{k-2,k+2} = -130.63$, $C_{k-2,k+2} = 140.09$;

Set the roll-off parameter of the raised-cosine pulse $\beta = 1.0$:

When $\mathbf{C}$ = {1, j, -1, -j, 1, j, -1, -j, 1, j, -1, -j, 1, j, -1, -j, 1, j, -1, -j }:

$\sigma^2_{k,k-1} = -49.992$, $C_{k,k-1} = -49.992$;

$\sigma^2_{k-2,k+2} = -99.747$, $C_{k-2,k+2} = -99.747$;

Summerizing the above derivation, we obtain the approximation to the variances and covariances of the five received samples, which are functions of the desired data QPSK symbols in vector $\mathbf{C}'$. Mathematically, the correlation matrix $\Phi_{yy}(C)$ in Section 4.3 can be written as

$$\mathbf{\Phi_{yy}(C)} \approx \mathbf{\Phi_{yy}(C')} \tag{B.13}$$

Note that the length of $\mathbf{C}$ is 20 and the the length of $\mathbf{C'}$ is 5. This approximation makes the MSDD using square-root raised-cosine pulse become practical. See Section 4.3 for details.

However, we have to keep in mind that the correlation matrix $\mathbf{\Phi_{yy}(C')}$ results in a non-optimal metric. It is obvious that the approximation depends on the β: when $\beta = 1.0$, the approximation in (B.8) and (B.12) is very tight. The resulted decoding metrics are very close to optimal metrics. When $\beta = 0.35$, the approximation in (B.8) and (B.12) is looser. The effect of the approximation on the performance of MSDD is shown in Section 4.3.

Bibliography

[1] J. G. Proakis, "**Digital Communications**", *New York: McGraw Hill*, 1989.

[2] J. Cavers and P. Ho, "**Analysis of the Error Performance of Trellis Coded Modulations in Rayleigh Fading Channel**", *IEEE Transactions on Communication*, Vol 40, No. 1, pp 74-83, January, 1992

[3] P.J. Mclane, P.H. Wittke, P Ho, and C. Loo, "**The Performance of Trellis Codes for Mobile Satellite Communications**", *IEEE Transactions on communications*, Vol. 36, No. 9, pp 1242-1246, November 1988

[4] G. Ungerboeck, "**Channel Coding with Multilevel/phase Signals**", *IEEE transactions on Information Theory*, Vol. IT-28, No. 1, pp. 55-67, January 1982.

[5] T. Chan and P. Ho, "**Bit-Error Probability of Uncoded QPSK Transmitted Over a 2-Ray Frequency Selective Rayleigh Fading Channel**", *Proc., IEEE supercom / ICC 92* , pp. 312.5.1-5, Chicago, June 92.

[6] P. Ho and D. Fung, "**Error Performance of Multiple Symbol Differential Detection of PSK Signals Transmitted over Correlated Rayleigh Fading Channels**", *IEEE Trans. on Communications*, November 1992 pp 1566-1569

[7] P.A. Bello and B.C. Nelin, "**The Effect of Frequency Selective Fading on the Binary Probabilities of Incoherent and Differentially Coherent Matched Filter Receivers**", *IEEE Trans. on Communications Systems*, Vol. CS-11, June 1963, pp.170-186.

[8] P.A. Bello,"**Binary Error Probabilities Over Selectively Fading Channels Containing Specular Components**, *IEEE Trans. on Communications Technology*, Vol. Com-14, No. 4 June 1966 pp 400-406.

[9] C.C. Bailey and J.C. Lindenlaub, "**Further results concerning the effect of frequency-selective fading on differentially coherent matched filter**

receivers", *IEEE trans. Commun. Technol.*, vol. COM-16, pp. 749-751, Oct. 1968.

[10] F. D. Garber, and M. B. Pursley, "**Performance of Differentially Coherent Digital Communications Over Frequency-Selective Fading Channels**", *IEEE Transactions On Communications*, Vol 36. No. 1 pp. 21-31 January 1988

[11] P. A. Bello, "**Characterization of randomly time variant linear channels**", *IEEE trans. Commun. Syst.*, vol. CS-11, pp. 360-393, Dec. 1963.

[12] C-E. W. Sundberg, N. Seshadri, "**Digital Cellular Systems For North America**", *Proc., Globecom 90* , pp. 405.5.1-5, San Diego, December 2-5, 1990

[13] A. Zogg, "**Multipath Delay Spread in a Hilly Region at 210 MHz**", *IEEE Trans. on Veh. Tech*, Vol. VT-36, No. 4, November 1987, pp 184-191

[14] D. Noneaker, and M.Pursley, "**M-ary Differential Phase Shift Keying with Diversity Combining for Communications over a Doubly Selective Fading Channel**", *Proc. IEEE Supercom/ICC'92*, Chicago, June 92, pp. 302.5.1-5

[15] J. K. Cavers, "**Pilot Symbol Assisted Modulation and Differential Detection in Fading and Delay Spread**", submitted to IEEE on Communicaitons.

[16] J. F. Healey, "**Statistics**", *Wadsworth Publishing Company, Belmont, California*, 1984.

[17] A. Viterbi, J. Wolf, E. Zehavi, and R. Padovani, "**A Pragmatic Approach to Trellis-Coded Modulation**", *IEEE Communications Magazine* July 1989, pp.11-19

[18] D. Divsalar and M. Simon, "**Multiple-Symbol Differential Detection of MPSK**", *IEEE Transactions on Communications*, Vol. 38, No. 3, pp. 300-308, March 1990

[19] D. Makrakis, A. Yongancoglu, and K. Feher, "**A Sequential Decoder for Differentially Detection of Trellis Coded PSK Signals**", *Proc., IEEE ICC'88*, Philadelphia, June 1988, pp. 1433-1438.

[20] W. Liu, and P. Ho, "**Differential Detection of PSK Signals in a 2-Ray Frequency Selective Rayleigh Fading Channnel**", *Proc., IEEE Globecom' 92 pp 1802-1806*, Orlando, Florida, December, 1992.

[21] J. K. Cavers, "**On the validity of the slow and moderate fading models for matched filter detection of Rayleigh fading signals**", *Can. J. Elect. & Comp. Eng.*, Vol 17, No. 4, 1992.

[22] D. Borth, K. Baum, B. Mueller, "**A comparison of Nonlinear equalization Methods for the U.S. Digital Cellular System**", *Proc., IEEE supercom / ICC 92*, pp. 312.1.1-5, Chicago, June 92.

[23] Electroinic Industries Association EIA, "**Cellular System : Dual Mode Subscriber Equipment - Network Equipment Compatibility Specifications**", *EIA project 2215, IS-54*, December 1989.

[24] D. Makrakis, and P. Mathiopoulos, "**Optimal Decoding in Fading Channels : A Combined Envelope, Multiple Differential and Coherent Detection Approach**", *Proc., IEEE Globecom 89*, Dallas, November 1989, pp. 1551-1557.

[25] Osborne and Luntz, "**Coherent and Non-Coherent Detection of CPFSK**", *IEEE Trans. on Communications*, vol. COM-22, pp. 1023-1036, August 1974.

[26] Q. Dai, and E. Shwedyk, "**Detection of Bandlimited Signals Over Frequency Selective Rayleigh Fading Channels**", accepted by *IEEE Trans on Comm.*

[27] G. Ungerboeck, "**Trellis-Coded Modulation with Redundant Signal Sets Part I-II**", *IEEE Communication Magazine*, Vol. 2, pp. 5-21, February 1987.

[28] S. G. Wilson, J. Freebersyser, and C. Marshall, "**Multiple-symbol Detection of M-DPSK**", *Conference Proceedings, IEEE Globecom 89*, Dallas, November 1989, pp. 1692-1697